

RICE UNIVERSITY

**A Finite Element Approach Towards
Biomechanical Optimization of Prophylactic Vertebroplasty**

by

Kay Sun

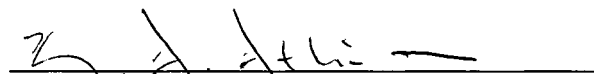
A THESIS SUBMITTED
IN PARTIAL FULFILMENT OF THE
REQUIREMENTS FOR THE DEGREE

Doctor of Philosophy

APPROVED, THESIS COMMITTEE:



Michael A.K. Liebschner
Assistant Professor of Bioengineering



Kyriacos A. Athanasiou
Karl F. Hasselmann Professor of Bioengineering

Antonios G. Mikos
John W. Cox Professor of Bioengineering and
Professor of Chemical and Biomolecular
Engineering

HOUSTON, TEXAS

May 2006

UMI Number: 3216786

INFORMATION TO USERS

The quality of this reproduction is dependent upon the quality of the copy submitted. Broken or indistinct print, colored or poor quality illustrations and photographs, print bleed-through, substandard margins, and improper alignment can adversely affect reproduction.

In the unlikely event that the author did not send a complete manuscript and there are missing pages, these will be noted. Also, if unauthorized copyright material had to be removed, a note will indicate the deletion.



UMI Microform 3216786

Copyright 2006 by ProQuest Information and Learning Company.
All rights reserved. This microform edition is protected against
unauthorized copying under Title 17, United States Code.

ProQuest Information and Learning Company
300 North Zeeb Road
P.O. Box 1346
Ann Arbor, MI 48106-1346

ABSTRACT

A Finite Element Approach Towards Biomechanical Optimization of Prophylactic Vertebroplasty

by

Kay Sun

Vertebroplasty has the potential to be a highly effective vertebral fracture prevention treatment, but the procedure must first be optimized for maximum benefit and minimal risk of safety to the patient. The procedure involves the percutaneous injection of a liquid bone cement into the vertebral body, which upon hardening provides instantaneous structural reinforcement. This research characterizes the effects of bone cement volume, material properties and distribution patterns on the global and internal vertebral biomechanics after prophylactic vertebroplasty in order to optimize these cement properties based on biomechanical efficacy and risk of complications which pose a threat to patient safety. In light of the many factors affecting the biomechanical outcome, a computational approach was employed since multiple analyses can be repeated on the same specimen. The accuracy of the models is assured by using realistic, image-based finite element models of human vertebral bodies that are specimen-specific, anatomically detailed and calibrated to experimental results. Prophylactic vertebroplasty was simulated on these models under various cement configurations and their biomechanical efficacies were evaluated based on the criteria for biomechanical success

developed in this research - maximum mechanical reinforcement to reach low fracture risk levels with minimal amount of cement and maintenance of intravertebral mechanical compatibility to retain the normal dynamics of the weight-bearing spine. The biomechanically optimal bone cement is determined as one that results in a spatially dispersed distribution when injected into the vertebral body. The higher vertebral reinforcements achieved with a dispersed cement fill may lower the risk of complications due to cement leakages since smaller cement volume would be just as biomechanically effective. Furthermore, the disperse fill results in minimal intravertebral stress concentrations that may reduce the risk of subsequent fractures in the adjacent untreated vertebrae. Now that the bone cements with spatially dispersed fill patterns is known to produce optimum biomechanical effects, the biochemistry of materials with this unique characteristic can be specifically tailored to include biodegradability and drug release capabilities for various applications that require the merger of fracture prevention, tissue engineering and drug delivery innovations into one without any concerns for adverse biomechanical affects.

ACKNOWLEDGEMENTS

I wish to express my appreciations to my advisor, Dr. Michael Liebschner, as well as members of my thesis committee, Drs. Kyriacos Athanasiou and Antonios Mikos, for their guidance.

I owe heartfelt thanks to my colleagues and friends in the Liebschner lab, Brandon Bucklen, Jeremy Lemoine, Wafa Tawackoli, Alistair Templeton and Matthew Wettergreen, for creating a lively and highly entertaining work environment. I have thoroughly enjoyed the years of laughter, raillery and daily debates as to what to have for lunch.

My parents deserve my gratitude for their support. I am also indebted to my brother for his help with computer programming and for his invaluable advice on all aspects of my life, from what computer science classes to take to how to do my taxes. Finally, I would like to thank my constant feline companion who has stood or more accurately slept beside me all these years while I toil away in my research.

TABLE OF CONTENTS

ABSTRACT	II
ACKNOWLEDGEMENTS.....	IV
LIST OF FIGURES	VII
LIST OF TABLES	XIII
CHAPTER 1 INTRODUCTION.....	1
1.1. MOTIVATION.....	2
1.2. OBJECTIVES	6
1.3. OVERVIEW	8
CHAPTER 2 BACKGROUND	10
2.1. PREVENTION OF VERTEBRAL FRACTURES.....	11
2.2. VERTEBROPLASTY	13
2.2.1. Procedure.....	13
2.2.2. Complications of Vertebroplasty	16
2.3. BIOMECHANICS OF VERTEBROPLASTY	21
2.3.1. Fracture Repair	21
2.3.2. Fracture Prevention	26
2.4. BIOMECHANICAL GOAL OF VERTEBROPLASTY	29
2.5. INJECTABLE BONE SUBSTITUTES FOR VERTEBROPLASTY	33
2.6. POTENTIAL OF VERTEBROPLASTY	35
CHAPTER 3 BIOMECHANICS OF VERTEBRAL REINFORCEMENT USING PMMA	37
3.1 INTRODUCTION	38
3.2 METHODS.....	40
3.2.1 QCT Scan	40
3.2.2 Mechanical Testing	41
3.2.3 Finite Element Modeling	43
3.2.4 Vertebroplasty Modeling.....	47
3.3 RESULTS	50
3.3.1 Effects of PMMA volume fill and placement.....	50
3.3.2 Effects of bone mineral density	52
3.3.3 Optimal PMMA volume.....	55
3.4 DISCUSSION	59
3.5 CONCLUSION.....	62
3.6 ACKNOWLEDGEMENTS.....	63
CHAPTER 4 OPTIMIZATION OF BONE CEMENT PROPERTIES FOR VERTEBRAL REINFORCEMENT	64
4.1 INTRODUCTION	65
4.2 METHODS.....	66
4.3 RESULTS	68
4.3.1. Effect of Cement Strength	68
4.3.2. Effect of Cement Modulus	69
4.3.3. Intervertebral Stresses and Strains.....	70
4.4 DISCUSSION	75

4.5 CONCLUSION.....	77
4.6 ACKNOWLEDGEMENTS.....	78
CHAPTER 5 PREMATURE ADJACENT VERTEBRAL FRACTURE AFTER VERTEBROPLASTY.....	79
5.1 INTRODUCTION	80
5.2 METHODS.....	83
5.2.1. Experimental Design	83
5.2.2. Specimen Preparation.....	84
5.2.3. Vertebroplasty	84
5.2.4. Mechanical Testing	85
5.2.5. Radiographic Imaging	88
5.3 RESULTS	88
5.4 DISCUSSION	91
5.5 CONCLUSION.....	94
CHAPTER 6 EFFECTS OF CEMENT AUGMENTATION DISTRIBUTION AND MATERIAL PROPERTIES ON VERTEBRAL BIOMECHANICS.....	95
6.1 INTRODUCTION	96
6.2 METHODS.....	98
6.2.1. QCT Image Processing.....	98
6.2.2. Voxel Model Generation	99
6.2.3. Material Properties	102
6.3 RESULTS	113
6.4 DISCUSSION	117
6.5 CONCLUSION.....	121
6.6 ACKNOWLEDGEMENTS.....	121
CHAPTER 7 CONCLUSIONS	122
REFERENCES	128
APPENDIX	138

LIST OF FIGURES

- Figure 1-1: Illustration of vertebroplasty. From left to right: Compression fracture of a vertebra within the spinal column²; A close-up view of the compression fracture; During vertebroplasty, a bone biopsy needle penetrates the pedicle and enters the body of the fractured vertebra. Bone cement is then injected to the fracture site through the needle; The bone cement fills the voids within the porous network of trabecular bone and upon hardening, stabilizes the disconnected trabeculae caused by fracture..... 4
- Figure 2-1: A photograph of the transverse section of a human torso at the L3 vertebral level from the Visible Human Project¹²⁰ with transpedicular and posterolateral vertebroplasty approaches depicted. The cannula enters the vertebral body via the pedicle with the transpedicular approach, while the posterolateral approach enters the vertebral body directly from the side of the body..... 14
- Figure 2-2: Microcomputed tomography scan of the superior view of the cross-section of a human thoracic vertebra with close-ups of cortical and trabecular bone. The posterior processes of the vertebra were removed at the pedicles. 15
- Figure 2-3: Microcomputed tomographic scan of the superior view of the cross-section of a human thoracic vertebra with posterior processes removed, which had been injected with PMMA (left) and its zoomed in view (right). 15
- Figure 2-4: Illustration of the three types of cement leakages: venous, epidural space and discal leaks (Adapted from Clemente²⁶). 17
- Figure 2-5: Finite element mesh of vertebral body with different placements of PMMA (shaded) cement. From left to right, bipediculär, unipediculär - left, unipediculär – right and posterolateral vertebroplasty⁷⁰ 26
- Figure 2-6: High angle of rotation in the sagittal plane (α) of the vertebral body after unipediculär vertebroplasty when loaded under pressure boundary conditions brings instability to the treated vertebra. 26

- Figure 2-7: Gradient-of-risk relationship between bone density and fracture risk. Bone density is plotted in T-score units relative to mean and standard deviations of healthy young adult population. World Health Organization's definitions of osteoporosis, osteopenia, and normal are intended to identify patients at high, intermediate, and low risks of fracture⁴¹ 30
- Figure 2-8: Risk of vertebral fragility fracture according to the strength of L3 vertebra. The high fracture risks is when vertebral strength is less than 3 kN and low fracture risks is when vertebral strength is greater than 5 kN (Adapted from Biggeman et al.¹⁹) 32
- Figure 3-1: A slice of the quantitative computed tomography (QCT) scans of the human vertebral bodies imaged with a liquid K₂HPO₄ phantom that was used to calibrate mineral densities⁶⁸. Finite element models were constructed from the high resolution images 41
- Figure 3-2: Uniaxial compression testing of vertebral body in a servohydraulic testing machine. Compression platens with lockable ball joint allow the top platen to rest flat on the specimen⁶⁸ 42
- Figure 3-3: The series of QCT scans of a vertebral body was stacked together and the three dimensional geometry of the vertebral body was contoured out. The surface mesh was then filled with brick elements to generate the volume mesh 43
- Figure 3-4: Sectioned normalized stress-strain curve of 8 mm diameter cylindrical samples of vertebral trabecular bone loaded beyond the ultimate point⁷¹. The yield point was determined from a 0.1% strain offset rule, which states that the yield point is the intersection between the stress-strain curve and the elastic loading line offset to 0.001 strain at zero stress. This offset elastic loading line provided the first linear region oa. By following the contour of the normalized stress-strain curve from yield point, linear regions ab, bc, cd and de were defined. The slopes (E_1/E_{zz} , E_2/E_{zz} , E_3/E_{zz} , E_4/E_{zz} , E_5/E_{zz}) as well as strain ranges (ϵ_{yield} , ϵ_{ab} , ϵ_{bc} , ϵ_{cd} and ϵ_{de}) of the five linear regions were calculated. The slope of each linear region represented the ratio of the elastic modulus of trabecular cylindrical samples over the on-axis modulus ($E_{zz} = E_1$). 45
- Figure 3-5: The predicted fracture loads using the average ϵ_{yield} and $\epsilon_{ultimate}$ of 1.21% and 2.57%, respectively, matched well with the experimentally determined values, validating the accuracy of the models⁷¹ 46
- Figure 3-6: The finalized vertebral body finite element model with added layers of cortical shell and endplates, along with the casting cement PMMA to duplicate experimental loading conditions. Each model consisted of 1816 elements, of which 1008 are trabecular⁶⁹ 47

- Figure 3-7: Finite-element mesh of a vertebral body with two PMMA capsules (shaded) simulating bipedicular vertebroplasty (left) and one PMMA capsule in the horizontal plane simulating posterolateral vertebroplasty (right). 48
- Figure 3-8: The compressive stress-strain curve of PMMA from which the post-yield properties were extracted from the six points along the curve ⁸² 49
- Figure 3-9: Effect of posterolateral and bipedicular placement and volume fill of PMMA on the (a) average normalized compressive stiffness increase; and (b) average normalized compressive strength increase of reinforced vertebral bodies. Stiffness and strength augmentations were linearly proportional to the PMMA volume fill for both approaches. 51
- Figure 3-10: Effect of initial vertebral QCT density and volume fill of bone cement PMMA on the relative compressive stiffness increase of reinforced vertebral bodies using (a) bipedicular; and (b) posterolateral cement placement. Greatest variations in stiffness increase for average QCT densities below 0.1 g/cm³ and PMMA volumes over 20%. For densities greater than 0.1 g/cm³, stiffness augmentations were less dependent on density. 53
- Figure 3-11: Effect of initial vertebral QCT density and volume fill of bone cement PMMA on the relative compressive strength increase of reinforced vertebral bodies using (a) bipedicular; and (b) posterolateral cement placement. Greatest variations in strength increase with average QCT densities when PMMA volumes were over 30%. 55
- Figure 3-12: Variations in ultimate compressive stress of reinforced vertebral bodies with initial vertebral QCT density at 0%, 5%, 10%, 15%, 20%, 30% and 35% volume fill with PMMA for (a) bipedicular; and (b) posterolateral vertebroplasty. The three fracture risk groups defined by Biggeman et al.¹⁹: high risk group with ultimate stress < 1.6 MPa and fracture risk of 100%, medium risk group with ultimate stress from 1.6 to 2.7 MPa, and low risk group with ultimate stress > 2.7 MPa and fracture risk near 0%. 58
- Figure 3-13: Biomechanically optimal poly(methylmethacrylate) (PMMA) volume fill relative to vertebral body volume required to reduce fracture risk to low levels for bipedicular and posterolateral prophylactic vertebroplasty (n = 8). 59
- Figure 4-1: Finite element mesh of a vertebral body with two bone cement capsules (shaded) simulating bipedicular vertebroplasty. 67

Figure 4-2:	Effect of bone cement compressive strength on the average normalized compressive vertebral stiffness increase (treated stiffness / initial stiffness) and vertebral strength increase (treated fracture load / initial fracture load).	69
Figure 4-3:	Effect of bone cement compressive elastic modulus on the average normalized compressive vertebral stiffness increase (treated stiffness / initial stiffness) and vertebral strength increase (treated fracture load / initial fracture load).....	70
Figure 4-4:	(a) Stress and (b) strain distributions within a frontal section of an osteoporotic vertebra before and after treatment with 20% volume fill of PMMA (shaded).....	73
Figure 4-5:	Illustration comparing the extent of endplate deflection in the adjacent vertebra before and after cement augmentation with an axial load applied. Note: Degree of deflection is exaggerated for illustration purposes.....	74
Figure 4-6:	Intravertebral stress profiles of the trabecular bone elements above the implanted bone cement at varying moduli. Only at very low bone cement modulus were the internal stresses comparable to the untreated model... ..	75
Figure 5-1:	The resultant compressive load from the action of muscles, ligaments and body weight follows the curvature of the spine, passing through the centers of rotation of each segment ⁹⁴	82
Figure 5-2:	Fluoroscopic X-ray of the sagittal view of a vertebral segment treated at the top and bottom vertebrae with PMMA.	85
Figure 5-3:	Experimental setup to apply unconstraint axial compression to the spinal segments using a 6-DOF robotic arm (left). A close-up view of the spinal segment (right).	86
Figure 5-4:	Illustrations of unconstraint axial compression where the sum of the shear forces (Fx and Fy) and bending moments (Tx, Ty and Tz) from the two load cells are minimized by displacing the top of the segment in x' and y' directions while applying load in the plane orthogonal to the top endplate (Fz').....	87
Figure 5-5:	Paired comparisons between the fracture strengths of the untreated lumbar spinal segments predicted from the fracture stress of the untreated thoracic segments of the same spines and the experimentally tested treated lumbar segments. 4.2% to 37.4% reductions in fracture strength were observed except for Specimen #3 which had a 14.4% increase.....	89

Figure 5-6:	X-rays of the (a) untreated thoracic and (b) treated lumbar spinal segments when unloaded (left) and after reaching the fracture point (right). Crush type fracture occurred in the untreated thoracic segment, while in the treated lumbar segment of the same spine, biconcave fracture was observed.....	90
Figure 6-1:	Quantitative computed tomography scans of vertebrae treated with PMMA and CORTOSS. The compact distribution of PMMA within vertebra (left) is distinctly different from the more dispersed distribution of CORTOSS (right).....	97
Figure 6-2:	A quantitative computed tomography scan before (left) and after rendering (right) by auto-thresholding using Analyze to remove the posterior elements and to set the extraneous non-bone tissue to zero pixel value... 99	
Figure 6-3:	Voxel mesh of the vertebral potted with PMMA at the top and bottom endplates and finally attached to two metalplates.....	101
Figure 6-4:	Effect of element size and hence mesh density on the predicted vertebra stiffness. Convergence is achieved with 14,886 bone elements with element size of 1.2x1.2x1 mm.....	102
Figure 6-5:	Material definitions of trabecular-marrow and trabecular-cement composites for 1.2x1.2x1 mm resolution QCT images. Elements with pixel value between 18,132 and 53,043 were defined as the trabecular-marrow composite where pixel value of 18,132 represented 100% bone marrow, while 53,043 pixel value represented densest trabecular bone. Trabecular-cement composite was defined with pixel values between 53,043 and 65,534 where 100% bone cement had a pixel value of 65,534.....	105
Figure 6-6:	The material definitions of the trabecular-marrow and trabecular-cement composites for 1.5x1.5x1 mm (left) and 2.1x2.1x2 mm resolution QCT images (right). The pixel value for the densest trabecular bone that separated the trabecular-marrow and trabecular-cement composites was 47,850 for the 1.5x1.5x1 mm image resolution. Reducing the resolution and hence the mesh density lowered the densest trabecular bone pixel value to 32,441, thereby enlarging the pixel spectrum for the trabecular-cement composite.....	106
Figure 6-7:	The intersection of the X-ray image projections (left) re-created the PMMA bolus injected into vertebra (right) ¹¹³	107

- Figure 6-8: QCT slice numbers 7 (left) and 12 (right) overlaid with the transverse images of the PMMA bolus (brighter silhouette) that had been repositioned to fit within the CORTOSS treated vertebral body (duller silhouette) and resized so that the total volume of PMMA was the same as CORTOSS..... 108
- Figure 6-9: The compact fill pattern of CORTOSS (left) and PMMA (right) within the vertebral body model. 109
- Figure 6-10: The accuracy of the calibrated coefficients for the first and second order correlations between bone element elastic modulus and bone tissue volume fraction to predict vertebral stiffness. 111
- Figure 6-11: The range of bone element elastic modulus predicted using the calibrated first and second order correlations to bone tissue volume fraction. The elastic modulus derived from the second order correlation when $\phi = 1$ is closer to the experimentally determined values for cortical bone than for the first order correlation. 112
- Figure 6-12: The increase in vertebral stiffness after treatment with CORTOSS was higher than with PMMA. 114
- Figure 6-13: The distributions of axial stress in the (a) untreated, treated with (b) CORTOSS and (c) PMMA models. Large areas of high compressive stress (darkest areas) were observed in the PMMA models compared to the untreated, but were less prominent in the CORTOSS models. 115
- Figure 6-14: Higher vertebral stiffness increase achieved with dispersed cement fill than with a compact one. 116
- Figure A-1: Simplified block models of half of a sagittal cross-section of a vertebral body, with area 2A and total height 4L, before and after implantation with a bone cement. A compression force of F was applied to both models.. 138

LIST OF TABLES

Table 2-1:	Comparison of the various osteoporosis drug treatments ^{5,8,11,25,40,74,102}	12
Table 2-2:	Summary of the <i>in-vitro</i> biomechanical studies on the effect of different cement types used in vertebroplasty for fracture repair.....	22
Table 2-3:	Summary of the <i>in-vitro</i> biomechanical studies on the effects of cement volume and placement on vertebroplasty for fracture repair.....	23
Table 2-4:	Summary of <i>in-vitro</i> biomechanical studies on vertebroplasty for fracture prevention.	28
Table 2-5:	World Health Organization diagnostic criteria for osteoporosis ^{44,76,81,105} ..	30
Table 3-1:	Physical and mechanical data on all 8 single vertebral bodies tested (F for female, M for male, SD for standard deviation, VB for vertebral body)....	42
Table 3-2:	Anisotropic elastic constants for human vertebral trabecular bone. The Young's moduli (E_{xx} and E_{yy}) and shear moduli (G_{xy} , G_{xz} , G_{yz}) are expressed as a factor of the longitudinal modulus, E_{zz} ¹¹⁶	44
Table 3-3:	Original and modified post-yield tissue properties of 8 mm cylindrical vertebral trabecular tissue ⁷¹	46
Table 4-1:	The nine different bone cement material properties (M1 to M9) investigated were based on the compressive elastic modulus and strength of PMMA....	67
Table 5-1:	Summary of the experimentally determined fracture strength, stress, type and bone density for all the tested spinal segments	90
Table 6-1:	Materials properties and element specifications.	112

Chapter 1

INTRODUCTION

Osteoporosis-related vertebral fragility fractures are an increasing public health problem affecting the growing elderly population. As a direct consequence, an escalating number of vertebral fractures have been repaired by vertebroplasty because of its minimal invasiveness and therefore quick recovery time, as well as its high success in alleviating pain brought on by the fracture. The treatment involves the percutaneous injection of a bone cement that hardens to stabilize the fracture site. The introduction of the bone cement into the vertebra also results in an almost instantaneous structural reinforcement of the vertebra, which makes vertebroplasty ideal as a highly effective fracture prevention treatment. However, the biomechanics of prophylactic vertebroplasty have yet to be fully investigated despite the huge potential for success. Even the effects of vertebroplasty for fracture repair on the biomechanics of the treated vertebra and of the entire spinal column are poorly understood, which is especially disconcerting since the repair treatment is performed thousands of times per year. This research focuses on evaluating the biomechanical efficacy of prophylactic vertebroplasty and optimizes the procedure by identifying aspects of bone cement properties that are critical to the biomechanical success of the treatment and that contribute to lower risk of complications which pose a threat to patient safety.

1.1. Motivation

Osteoporosis is a systemic skeletal disorder characterized by low bone mass and deterioration in bone tissue microarchitecture, caused by an imbalance between resorption and formation of bone. The reduced bone density and quality weaken the mechanical strength of the bone, a loss which increases bone fragility and fracture risk⁷. Osteoporosis can affect both men and women at any age, but it is more prevalent in older individuals, especially women after menopause. In fact, 80% of those affected by osteoporosis are women⁸⁸. In the United States alone, osteoporosis has become a major public health threat with more than 10 million people diagnosed with the bone disorder and 34 million more at a high risk of developing it⁸⁹. It is estimated that by the year 2020, 50% of Americans over the age of 50 will have or be at risk of developing osteoporosis, further aggravating the growing problem¹¹¹.

In the United States, approximately 700,000 out of over 1.5 million osteoporosis-related fragility fractures per year are vertebral fractures^{88,100}. Compared with fractures at other sites where up to 90% are due to falls, 58% of osteoporotic vertebral fractures occur spontaneously during routine activities²⁸. Fractures caused by little or no trauma are sustained when the amount of bone available for mechanical support falls below each individual's own fracture threshold. The lifetime fracture risk of the vertebrae from age 50 years onwards is estimated to be almost 16% in white women and 5% in white men⁸³. Women with lower bone mass than the mean of the population have a 7-fold increased risk and a 25-fold risk increase in women with both lowered bone mass and a history of previous vertebral fractures¹⁰³.

The estimated annual cost of medical treatments related to osteoporotic fractures in the United States is over \$17 billion (\$46 million each day)⁸⁹ and is expected to rise. Specifically for vertebral osteoporotic fractures, the total direct cost was estimated at \$746 million in 1995⁹⁹. These alarming statistics demonstrate a growing health and economic problem, which may have a devastating effect on the healthcare system, as osteoporotic fractures are expected to increase 4-fold over the next 50 years due to the continued increase in the size of the aging population¹⁰⁰. Therefore, better fracture repair and prevention measures are in dire need as costs associated with osteoporosis-related fractures will more than double, even triple, in the next 30 years¹¹⁵.

A relatively new procedure, called vertebroplasty, has the potential to serve as both a fracture repair and prevention treatment. The procedure involves simply the injection of an acrylic bone cement, poly(methylmethacrylate) (PMMA), into the vertebral fracture site. The liquid cement hardens within 10 to 20 minutes, thereby stabilizing the defects (Figure 1-1). The PMMA cement being stiffer and stronger than the native bone within the vertebrae also results in strengthening of the entire treated vertebra. The instantaneous reinforcement feature of the procedure makes it a highly effective fracture prevention treatment as well, especially when compared to current fracture prevention drug treatments that take years before any appreciable bone mass increase is observed. Furthermore, the recovery time for patient is greatly reduced since only a small incision to the skin on the back is needed to introduce the cement to the vertebra through a long needle, thereby enabling vertebroplasty to be performed as an outpatient procedure.

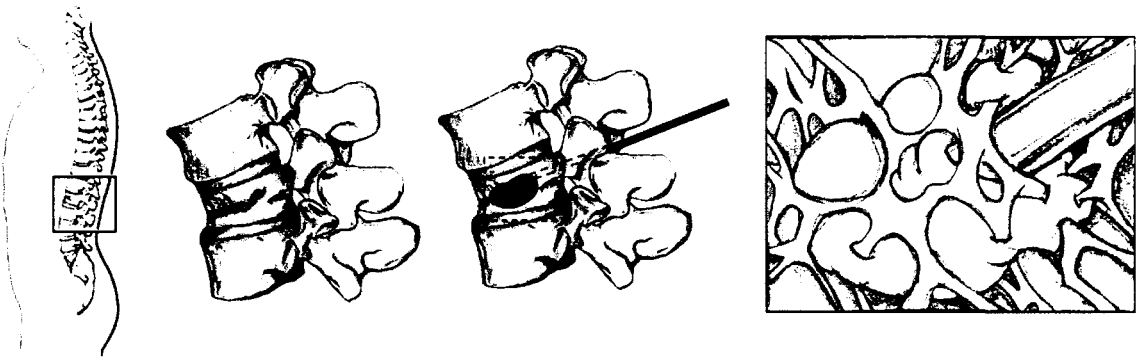


Figure 1-1: Illustration of vertebroplasty. From left to right: Compression fracture of a vertebra within the spinal column²; A close-up view of the compression fracture; During vertebroplasty, a bone biopsy needle penetrates the pedicle and enters the body of the fractured vertebra. Bone cement is then injected to the fracture site through the needle; The bone cement fills the voids within the porous network of trabecular bone and upon hardening, stabilizes the disconnected trabeculae caused by fracture.

The clinical aim of vertebroplasty for repair is to achieve rapid analgesic effect through the stabilization of the fractured vertebrae in patients experiencing back pain⁸⁰. The biomechanical goal of vertebroplasty for both fracture repair and prevention is to regain mechanical strength of the vertebra to “normal” levels. Unfortunately, information is limited on the effects of introducing a stiff material into a vertebra on the biomechanics of the treated vertebra itself and of the entire vertebral column. Such knowledge will permit the refinement of the procedure for both repair and prevention, specifically with regards to cement volume, distribution patterns and material properties for biomechanical efficacy and patient safety. This research focuses on elucidating the effects of these factors on vertebral biomechanics for fracture prevention.

A full investigation into the biomechanics of vertebroplasty would traditionally require *in-vitro* mechanical testing of cadaveric specimens. However, due to the many parameters affecting the biomechanical effectiveness of the procedure, namely volume,

placement and material properties of the injected bone cement, as well as the bone density of the vertebra, an unrealistically large number of specimens would be needed to demonstrate a statistical distinction in mechanical enhancements with one variable over another for each parameter. The large number of samples required is due to biological variability in the cadaveric specimens, which can be eliminated using computational approach since multiple analyses can be repeated on the same specimen. Another benefit of computer modeling is in the simulation of vertebroplasty, where the volume and distribution of the bone cements can be controlled in an exact and precise manner not possible in cadaveric studies. This feature enables any discrepancies in mechanical enhancements to be attributed solely on the parameter being investigated. As a result, the total number of variables that actually needs to be studied *in-vitro* can be significantly reduced with computer modeling, leaving only the optimal parameters for verification with cadaveric testing. Lastly, additional information into the biomechanical effects of vertebroplasty on the internal stresses and strains can be easily accessed and visualized in the computer models. The detection of the stresses and strains in the interior of vertebrae are not feasible in cadaveric experiments without resorting to destroying the structural integrity of the vertebrae just to position measurement devices. In this research, finite element simulations of prophylactic vertebroplasty on vertebral models were used to evaluate both the global and internal vertebral biomechanics.

The finite element method, developed in the 1950s to design airplanes, breaks complex geometric problems into finite elements of simple shapes like tetrahedrons or hexahedrons. The simplified solutions to the constitutive differential equations of the problem are then extended to the entire geometry using linear algebraic relationships.

Vertebral geometry and non-uniform bone density distribution within the vertebra itself are unique to each individual, therefore factoring in both these features will improve vertebral model predictions. Faulkner et al.³⁹ in 1991 was the first to duplicate the exact vertebral geometry and heterogeneity within the vertebra in patient-specific computer models by defining the material properties of each building block or finite element in the models based on the corresponding pixel value derived from quantitative computed tomography (QCT) scans. For better accuracy and realism, this research also utilizes each individual's QCT scans to construct patient-specific finite element models of human vertebrae, which were used to simulate and thereby evaluate the biomechanics of prophylactic vertebroplasty.

1.2. Objectives

This research characterizes the effects of bone cement volume, material properties and distribution patterns on the global and internal vertebral biomechanics after prophylactic vertebroplasty in order to optimize these cement properties based on biomechanical efficacy and risk of complications. First, the biomechanical efficacy of the current bone cement PMMA for use in prophylactic vertebroplasty was evaluated. Second, in an attempt to achieve the desired biomechanical goal of vertebroplasty, the material properties of the bone cement were varied to determine the optimal cement properties. The significance of maintaining the internal mechanical compatibility of the treated vertebrae was subsequently confirmed experimentally. Last, the effect of bone cement distribution patterns within the vertebrae on both global and internal biomechanics was evaluated.

Specifically, the objectives were:

- To determine the efficacy of prophylactic vertebroplasty with PMMA on intact vertebral bodies with respect to biomechanical recovery and fracture risk reduction using finite element modeling. The dependency of vertebral body compressive stiffness and strength augmentations on bone cement volumes, placement positions and bone mineral densities were evaluated to establish an optimal configuration to provide mechanical enhancements beyond the fracture risk levels.
- To characterize the effects of bone cement material properties on the global and internal biomechanics of the treated vertebrae finite element models and ultimately establish the biomechanically optimal cement material properties for vertebral reinforcement.
- To experimentally determine the biomechanical effects of prophylactic vertebroplasty on fracture strength of untreated adjacent vertebrae. The effects and thereby the existence of stress concentrations observed in the vertebroplasty models were explored using vertebroplasty treated cadaveric three-level spinal segments.
- To evaluate the effects of cement augmentation distribution and its material properties on vertebral biomechanics after prophylactic vertebroplasty by using finite element modeling. Both features of the cement are critical in reducing the risk of complications from vertebroplasty, including cement leakages and adjacent vertebral fractures.

1.3. Overview

The remainder of this thesis describes the process of optimizing cement properties, including volume, placement, material properties and spatial distribution patterns, based on the desired global structural reinforcement with the least affect on the internal vertebral mechanics.

Chapter 2 describes the limitations of current fracture prevention drug treatments, along with details of the vertebroplasty procedure and its complications. The current research on vertebroplasty biomechanics for fracture repair and prevention is reviewed. The chapter also explores alternative bone cements that have additional tissue engineering properties which can be exploited for even greater benefits to patients.

Chapter 3 evaluates the efficacy of PMMA to regain vertebral strength lost to osteoporosis in eight finite element vertebral models of different bone densities by varying cement volume and placement.

In the fourth chapter, the material properties of PMMA were varied so as to identify the optimal properties that would provide the maximum vertebral strength increase while maintaining the mechanical compatibility within the vertebral models.

In order to experimentally confirm the significance of mechanical compatibility of PMMA and intravertebral trabecular bone on the global vertebral biomechanics, Chapter 5 investigates whether vertebroplasty lowered the fracture strength of adjacent untreated vertebrae under physiological loading conditions caused by stress concentrations built up in the trabecular bone around the PMMA in the treated vertebrae.

In Chapter 6, dispersed and compact distribution patterns of two bone cements, CORTOSS and PMMA, were recreated in finite element models of the same vertebra.

The effects of cement fill patterns as well as its material properties on the global and internal vertebral biomechanics after vertebroplasty were evaluated.

Conclusions are presented in the final chapter, in addition to future directions.

Chapter 2

BACKGROUND

Vertebroplasty is a highly effective and efficient vertebral fracture repair treatment, with great promise as a prophylactic fracture prevention treatment. However, the current vertebroplasty procedure with poly(methylmethacrylate) (PMMA) has limitations and complications that could potentially have adverse affects on the patient's well-being. Some of these obstacles are a result of bio-incompatibilities of the injected bone cement with bone tissue, while others are a direct consequence of the lack of information on the biomechanics of the procedure. This research characterizes the biomechanical effects of various bone cement properties on the tissue and whole bone levels, thereby optimizing prophylactic vertebroplasty for biomechanical efficacy and patient safety.

A significant portion of this chapter is published in Liebschner, M. and Sun, K., "Biomechanical Efficacy of Vertebroplasty and Kyphoplasty" in Advances in Spinal Fusion - Molecular Science, Biomechanics and Clinical Management, editors Lewandrowski, Yaszemski, White III, Wise, Trantolo, Marcel Dekker NY, pages 463 - 488, 2003.

2.1. Prevention of Vertebral Fractures

Current fracture prevention treatments involve drug therapies, which focus on inhibiting further bone loss and restoring bone mass already lost by stimulating bone formation, thereby strengthening bone and reducing risk of fracture. Estrogen, selective estrogen receptor modulators (SERMs), bisphosphonates, calcitonin and other anti-resorptive supplements, like calcium and vitamin D, interfere with bone resorption by impeding osteoclast activity. Bone stimulating agents help to increase bone mass density by encouraging osteoblast activity, thereby increasing bone formation. Fluoride, parathyroid hormone and growth hormone are some of the promising anabolic agents being used outside the United States. Both anti-resorptive and anabolic drugs have serious side effects, and are generally not associated with dramatic increases in bone mass, requiring 6 months to 1 year to achieve efficacy (Table 2-1). During this one year period, up to 19% of osteoporotic patients may sustain a subsequent fracture after the onset of treatment⁷⁴. The need for a more effective preventive measure that can offer immediate fracture risk reductions can be easily filled by vertebroplasty. The only requirement is simply a better understanding of the biomechanics of the procedure to bring about maximum benefit to the patient while minimizing potential risks. This research therefore optimizes the vertebroplasty procedure for use as a prophylaxis, making it biomechanically effective and safer by lowering risks of complications.

Table 2-1: Comparison of the various osteoporosis drug treatments^{5,8,11,25,40,74,102}.

Treatment Modality	Bone gain (%/yr)	Reduction fracture risk (%)	Advantages	Disadvantages
Estrogen	1 - 2	20 - 50	FDA approved, Effect does not decrease over time with long term use	Risk of breast and uterine cancer, Does not promote remineralization of bone, Low long term compliance rate
SERMs	0.7 - 1	30	Reduced risk of breast cancer	Risk of thromboembolism
Bisphosphonates	1 - 3.5	30 - 50	FDA approved	Gastrointestinal side effects
Calcitonin	0.5	36	FDA approved	Low efficacy, Side effects occur in 15-20% of patients, including nausea and flushing
Fluoride	5 - 9	-	Significant bone mass increase in lumbar spine	Only trabecular bone density increase, cortical bone density decrease, no change in vertebral fracture rates
Parathyroid Hormone	0.7 - 4	20	Benefits may persist even after injections have stopped	May increase trabecular bone mass at expense of cortical bone
Growth Hormone	< 1.6	-		Low efficacy
Calcium Supplements & Vitamin D	0.8 - 1	25 - 50	Up to 2000 mg daily can reduce the rate of bone loss after menopause.	Role of vitamin D alone in persons without vitamin D deficiency is unknown.

FDA = Food and Drug Administration

SERMS = selective estrogen receptor modulators

2.2. Vertebroplasty

The vertebroplasty procedure and its complications are discussed.

2.2.1. Procedure

The skin, subcutaneous soft tissue, and pedicular periosteum are anesthetized prior to a small skin incision that allows easy passage of the vertebroplasty needle, which consists of a trocar with a cannula that ranges in size from 11 to 13 gauge. The cannula advancement is guided using standard fluoroscopy ^{30,36}, computed tomography (CT) guidance ²³, or CT fluoroscopy. The preferred placement of the cannula is via the transpedicular approach to the posterior quarter of the vertebral body in order to avoid cement leaking into the intervertebral foramen ⁶⁰ (Figure 2-1). The foramen contains the spinal cord and blood vessels that feed into each vertebra and is enclosed by the pedicles, lamina and vertebral body. The cannula enters the trabecular cortex of the vertebral body by boring through the pedicle either by a slight back-and-forth twisting motion or gentle tapping on the needle handle. Frequent fluoroscopic checks are made as the cannula traverses the pedicle to ensure proper alignment ⁶⁰. In the event there is inadequate visualization under fluoroscopic guidance due to osteolysis involvement at the pedicles, transpedicular access is not possible. A posterolateral approach maybe used instead, but the risk of pneumothorax associated with this route is relatively high ³⁰ (Figure 2-1). In Chapter 3, the differences in biomechanical efficacy of prophylactic vertebroplasty between the transpedicular (also known as bipedicular when both pedicles are used) and posterolateral approaches are determined.

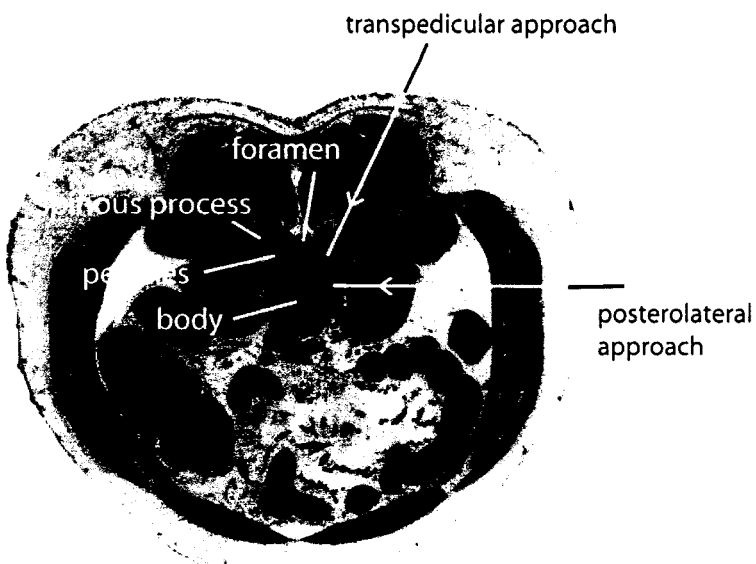


Figure 2-1: A photograph of the transverse section of a human torso at the L3 vertebral level from the Visible Human Project¹²⁰ with transpedicular and posterolateral vertebroplasty approaches depicted. The cannula enters the vertebral body via the pedicle with the transpedicular approach, while the posterolateral approach enters the vertebral body directly from the side of the body.

The vertebral body consists of an inner highly porous (30% to over 90%), irregular latticework of trabeculae bone tissue⁵². The voids between the trabeculae bone tissue are filled with red bone marrow that produces red blood cells. The trabecular core is surrounded by a thin, 0.35 mm average thickness, layer of compact bone tissue called cortical bone¹⁰⁷ (Figure 2-2). With less than 30% porosity, the cortical bone is much denser and therefore much stronger than trabecular bone, providing protection and support as it forms an external layer around the weaker trabecular bone⁵². During vertebroplasty, the flow of PMMA within the vertebral body is monitored under fluoroscopy as the injection of the bone cement into the vertebral body displaces the bone marrow back in the blood vessels, taking its place in the voids of the trabecular bone

(Figure 2-3). In this research, finite element models of the major load bearing vertebral bodies were constructed to simulate prophylactic vertebroplasty.

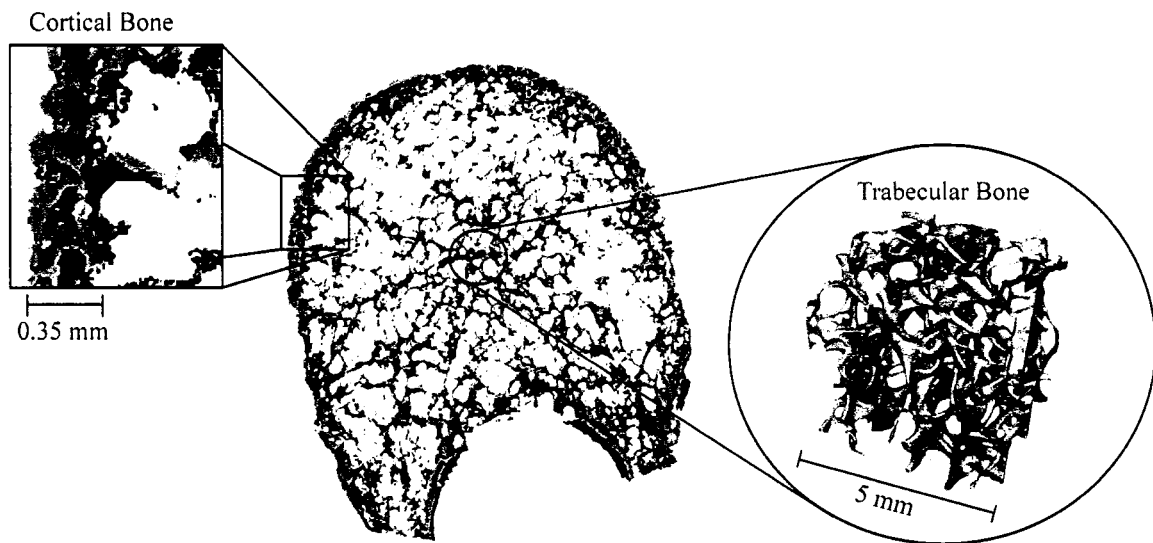


Figure 2-2: Microcomputed tomography scan of the superior view of the cross-section of a human thoracic vertebra with close-ups of cortical and trabecular bone. The posterior processes of the vertebra where removed at the pedicles.

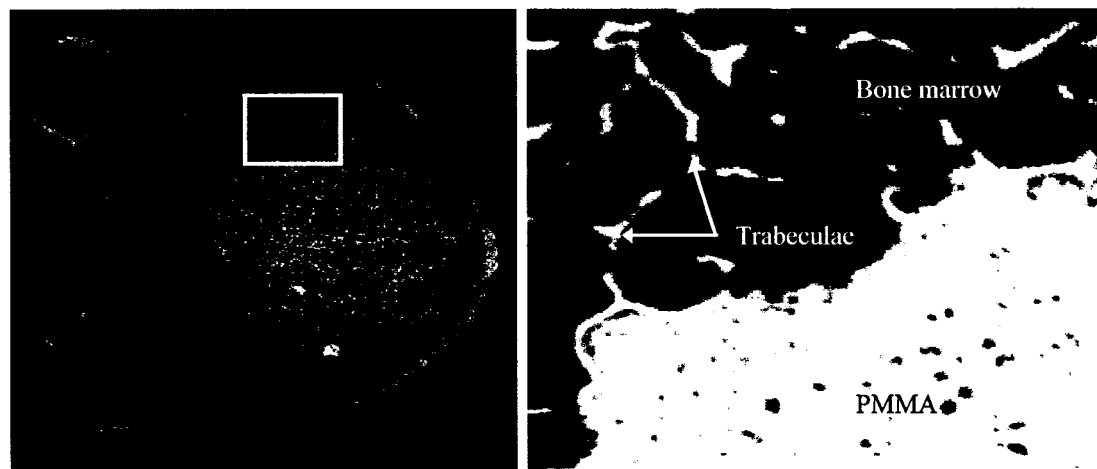


Figure 2-3: Microcomputed tomographic scan of the superior view of the cross-section of a human thoracic vertebra with posterior processes removed, which had been injected with PMMA (left) and its zoomed in view (right).

The injection of cement is stopped immediately whenever the cement begins to flow to untoward locations, such as intervertebral disc space, the posterior vertebral wall, or when it approaches the paravertebral veins at the posterior quarter of the vertebral body, which may result in extravasations^{36,60}. Injection is also terminated when sufficient vertebral filling is attained. The average PMMA volume injected into a vertebral body is 4 - 6 cm³, up to a maximum of 8 - 12 cm³^{53,87}.

2.2.2. Complications of Vertebroplasty

Complications brought about by leakages of cement and possible heightened risks of fracture to the untreated adjacent vertebrae are the major side-effects of vertebroplasty.

Cement Leakages

The cause of most procedural complications is leakage of PMMA into adjacent structures as a result of vertebral cortical destruction or fracture, inadvertent injection of cement into the vertebral venous plexus, or excess vertebral filling. Cement leaks have been reported in 30 - 67% of patients who underwent vertebroplasty⁷³. The majority of PMMA leakages have no clinical consequence, but when they do, the consequences are severe, and at times even fatal. There are three types of cement leakages (Figure 2-4):

1. Venous extravasations that occur in the perivertebral or epidural veins are common in more than 10% of vertebroplasty cases, but are only symptomatic in less than 3% of patients⁸⁰. Venous leaks can lead to compression of the spinal cord and nerve roots, as well as pulmonary embolism^{29,31,36,78}.

2. Soft tissue leakages occur around the spine, in the epidural space or along the needle track. They are rarely symptomatic, but if leakage occurs in the epidural space or intervertebral foramina, there is a high risk of nerve root or spinal cord compression

³⁷

3. Leaks into an intervertebral disc from a disc herniation are frequent and mostly asymptomatic. However, the presence of bone cement in the disc may alter the biomechanics of the vertebral column, perhaps even provoking fractures in the adjacent vertebrae, particularly in osteoporotic patients with higher risk of secondary vertebral collapse³⁶.

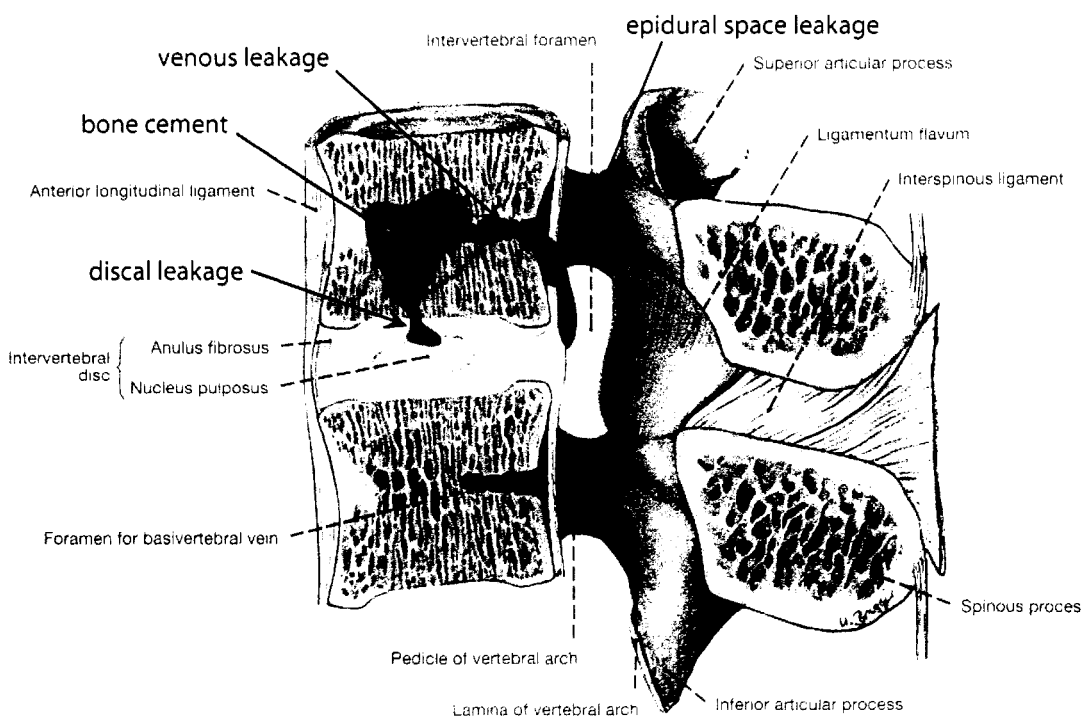


Figure 2-4: Illustration of the three types of cement leakages: venous, epidural space and discal leaks (Adapted from Clemente²⁶).

The risk of cement extravasations may be minimized by performing intraosseous venography prior to the vertebroplasty procedure. The contrast material, iohexol, is

injected into the vertebral body, which outlines the perivertebral venous drainages and fracture lines. This visualization allows the trabecular space to be evaluated so that the needle can be positioned safely away from the venous plexus so as to avoid venous leakages and potential leaks along the fracture lines^{36,37,60}. Unfortunately, due to the different flow characteristics of the contrast material and bone cement, it is difficult to ascertain whether there is accurate correlation between the flow paths of the two agents. In other words, venography is unable to accurately predict the final casting of PMMA and the cement may still leak into the vertebral veins. Additionally, there is the danger of the contrast material leaking into the intervertebral disc in the event that fractures have affected the endplates and can subsequently interfere with the detection of similar leaks with PMMA. The usefulness of venography is still debatable especially when the complication rates are typically no different in vertebroplasty cases with or without venography^{30,36,42,79}. This research optimizes the prophylactic vertebroplasty to require less cement volume while still able to achieve the desired level of mechanical reinforcement, thereby minimizing risk of cement leakages and subsequent complications. Although the rheology of the bone cement through the porous network of trabeculae also influences the risk of leakages, this research focuses on vertebral biomechanics once the cement has hardened.

Adjacent Vertebral Fractures

Recent studies have suggested that PMMA filling may promote fractures in the adjacent vertebrae due to the sharp increase in stiffness of the augmented vertebra^{50,121}. It is hypothesized that drastic changes in the mechanical dynamics and kinematics of the

vertebral column lead to an increase in mechanical demands on the neighboring vertebrae, thereby increasing the risk of fracture. A similar phenomenon is seen in spinal fusion, where increase risk for disc degeneration in vertebrae adjacent to a fusion is observed. However, there is limited information on this phenomenon. Retrospective reviews of vertebroplasty clinical studies are inconclusive. Jensen and Dion's⁶⁰ review of vertebroplasty cases found that vertebrae adjacent to the site of cement injection are at no higher risk of fracture than any other vertebrae as fractures might occur in any patient at all vertebral levels due to the progression osteoporosis, especially since existing fractures are strong independent predictors of the risk of future vertebral fracture¹⁰³. On the other hand, the retrospective studies by Grados et al.⁴⁶ and Uppin et al.¹¹⁷ observed higher incidences of vertebral compression fractures adjacent to a cemented vertebra than to an uncemented vertebra. Due to the contradictory results of different retrospective studies, an alternative approach with direct analysis of the biomechanical consequences of vertebroplasty on the whole vertebral column may yield additional insight.

A biomechanical investigation on the failure of adjacent vertebrae by Berlemann et al.¹⁸ showed a 19% lower ultimate failure load for treated intact vertebrae compared to the untreated control. Tohmeh et al.¹¹⁴ had first suggested that the mechanism for such failure may be due to the alteration of the biomechanics of load transfer to the adjacent vertebrae due to the presence of stress concentrations or “stress-risers” within the treated vertebra. In order to investigate the possible “stress-riser” effect, the changes in stress and strain distributions within a vertebral body before and after vertebroplasty need to be determined and finite element models are ideal to study intravertebral biomechanics.

Previous studies by Baroud et al.¹² and Polikeit et al.⁹⁶ had used finite element analysis to elucidate the effect of vertebral reinforcement with PMMA on load transfer in the intervertebral disc within an osteoporotic functional spinal unit. For both models, geometric details of the spinal units were extracted from quantitative computed tomography (QCT) scans and homogenous trabecular bone material properties were assigned. Baroud et al.¹² had modeled the L4-L5 lumbar segment without any posterior processes under step-wise displacement controlled compressed, while Polikeit et al.⁹⁶ had duplicated the L2-L3 segment with the posterior processes left intact and a compressive force of 1000 N under was applied with flexion and lateral bending. Despite these differences, both models showed high stress concentration in the areas above and below the cement of the treated vertebra. High pressures within the intervertebral discs were also observed, brought on by the cement inhibiting the inward deflection of the endplates of the treated vertebrae during compression. As a result, the incompressible discs force the endplate of the adjacent vertebrae to deflect inward as noted by the 12 to 20% displacement of the endplates. The resultant increase in endplate deflection from vertebroplasty may consequently lead to fractures in the adjacent vertebrae. To confirm the vertebroplasty-induced endplate failure mechanism, a controlled cadaveric experiment was performed in Chapter 5 to detect differences in fracture pattern and fracture loads with and without vertebroplasty, thereby verifying the effects and hence the existences of these stress concentrations.

2.3. Biomechanics of Vertebroplasty

Vertebroplasty for vertebral fracture repair was introduced in the United States in 1993, while the first paper that dealt with the biomechanics of procedure was published six years later. The high success rate of pain relief, between 80 to 90%, seems to have led to an overconfidence in the procedure, without a full understanding of its biomechanical ramifications^{30,31,36,61,78,122}. Even to this day, there have been only a handful of studies on vertebroplasty biomechanics for both fracture repair and prevention. This research fills this information void by characterizing the effects of bone cement volume, material properties and distribution patterns on the global and internal vertebral biomechanics after prophylactic vertebroplasty so as to optimize the procedure based on biomechanical efficacy and risk of complications.

2.3.1. Fracture Repair

Most of studies conducted on the biomechanics of vertebroplasty for fracture repair have been *in-vitro* cadaveric experiments (Tables 2-2 and 2-3). The experimental procedure for these studies are generally the same, involving the creation of the fracture, which provided data on the intact vertebral properties, and the subsequent cement repair and mechanical retesting of the treated specimens to determine if the initial mechanical properties were recovered. However, due to differences in the testing conditions, severity of fractures, vertebral levels, cement volume and type, it is difficult to make direct comparisons across all studies.

Table 2-2: Summary of the *in-vitro* biomechanical studies on the effect of different cement types used in vertebroplasty for fracture repair.

Authors	Specimen levels	Cement Material	Volume (mL)	Procedure	Number of specimens	Bone density (t-score)	Bone density (g/cm ²)	Testing method
Bai et al. 1999 ¹⁰	Single VB T8-L3	Simplex P Cap	1.5 1.5	BP	16			Uniaxial compression
Belkoff et al. 1999 ¹³	Single VB L1-L5	PMMA Cranioplastic Osteobond	8 8	BP	33	Mean = -2.3 0.7 to -6.9		Uniaxial compression
Belkoff et al. 2000 ¹⁴	Single VB L1-L5	Orthocomp Simplex P	8 8	BP	20	Mean = -5.0 -3.4 to -6.4		Uniaxial compression
Belkoff et al. 2001 ¹⁷	Single VB T8-T10	Simplex P Modified Simplex P BoneSource Simplex P Modified Simplex P BoneSource	4 4 6 6 6	BP BP	59	-3.8 ± 1.1	0.75 ± 0.15	Uniaxial compression
Belkoff et al. 2002 ¹⁵	Single VB T8-T10	Cranioplastic BoneSource BoneSource Cranioplastic BoneSource BoneSource	4 4 6 6 6 8	BP	60	-4.9 ± 1.4	0.61 ± 0.19	Uniaxial compression
Lim et al. 2002 ¹²	Single VB T2-L1	Simplex P BoneSource	6.0 ± 3.4 4.8 ± 2.0	BP	10		0.56 to 0.89	Uniaxial compression
Wilson et al. 2000 ¹²³	3-LS T7-T9 T10-T12	Cranioplastic Simplex P	10 5	BP/KYP	16	-2.61 ± 0.98 -3.04 ± 1.16		Flexion extension
Hitchon et al. 2001 ⁵⁵	5-LS T9-L1	Simplex P BoneSource	7 to 10	BP	20	0.52 to 0.91 0.53 to 1.08	Flexion Extension	

VB = vertebral body; LS = level segment; BP = bipedicular vertebroplasty. KYP = kyphoplasty

Table 2-3: Summary of the *in-vitro* biomechanical studies on the effects of cement volume and placement on vertebroplasty for fracture repair.

Authors	Specimen levels	Cement Material	Volume (mL)	Procedure	Number of specimens	Bone density (t-score)	Bone density (g/cm ²)
<u>Effect of Cement Volume</u>							
Belkoff et al. 2001 ¹⁶	Single VB T6-L5	Orthocomp	2	BP	144	Mean = -5.2 -3.5 to -7.7	
			4				
			6				
			8				
Molly et al. 2003 ⁸⁴	Single VB T6-L5	Simplex 30	2	BP	120	-2.6 to -6.2	0.42 to 0.93
			4				
			6				
			8				
<u>Effect of Cement Placement</u>							
Tohmeh et al. 1999 ¹¹⁴	Single VB L2-L5	Simplex	10	BP	40	Mean = -5.5 -3.7 to -8.8	
Higgins et al. 2003 ⁵⁴	Single VB T1-T6	PMMA	6	UP			
	T10-L5		10% fill	UP	61	0.15 to 0.9	
			20% fill				

VB = vertebral body; BP = bipedicular vertebroplasty; UP = unipedicular vertebroplasty

Effect of Cement Types

Most of the *in-vitro* studies evaluated the biomechanical efficacies of different bone cements, such as hydroxyapatite (HA)^{15,17,72}, Orthocomp¹⁴, calcium phosphate (CaP)¹⁰ and different types of PMMA¹³, on single vertebral bodies. All these bone cements are able to either increase or restore vertebral strength, but only Orthocomp and CaP are able to also restore vertebral stiffness. Multi-leveled vertebrae have also been used to show reduction of compliance in flexion-extension after repair with PMMA¹²³, and similar flexibility with PMMA and HA cements⁵⁵.

Effect of Cement Volume

The effect of cement volume was first determined by Belkoff et al.¹⁶, who had recommended PMMA (Simplex P) and Orthocomp volumes needed to restore strength and stiffness for thoracic and lumbar vertebrae. Since the size of vertebral bodies vary greatly from patient to patient, the study was revisited by the same research group to determine the cement volume effects based on percent vertebral body fill⁸⁴. They reported weak correlations between strength and stiffness restoration and percent volume fill. The poor correlations are due to wide scatter of the data, which is a result of bone density variability in vertebral specimens manifested by pooling data from different donor spines of different bone density as each specimen can only be destructively tested once. This biological variability problem is eliminated when computer models are used. In the study by Liebschner et al.⁷⁰, a finite element model of a L1 vertebral body was used to simulate vertebroplasty using different volumes of PMMA⁷⁰. To replicate damage of the vertebral body model caused by fracture, the elastic modulus of the

trabecular bone were reduced based on initial strain during reloading. The properties of the trabecular bone elements were replaced with that of PMMA at specific locations within the vertebral body to duplicate the shape of the PMMA bolus after vertebroplasty. The predicted vertebral stiffness from the uniaxial compression of the repaired model was found to increase with PMMA volume fill. The same method of simulating vertebroplasty was also used in finite element models in Chapters 3 and 4, where vertebral strengths were predicted in addition to stiffness.

Effect of Cement Placement

The damaged vertebral body model from Liebschner et al.⁷⁰ was also used to evaluate the biomechanical efficacy of the various placements of PMMA, including unipedicular, bipediculär and posterolateral (Figure 2-5). The vertebral stiffness increases predicted for the four different PMMA placements were found to be comparable to each other at each cement volume under displacement controlled uniaxial compression. However, when a uniform compressive pressure load was applied, medial-lateral bending motion or “toggle” towards the untreated side of unipedicular vertebroplasty was observed (Figure 2-6). As the stress boundary condition is more realistic to *in-vivo* loading conditions, the instability with unipedicular vertebroplasty may actually occur. Due to this probability and the unpopularity of unipedicular vertebroplasty, unipedicular placement of bone cements is not explored further in this research.

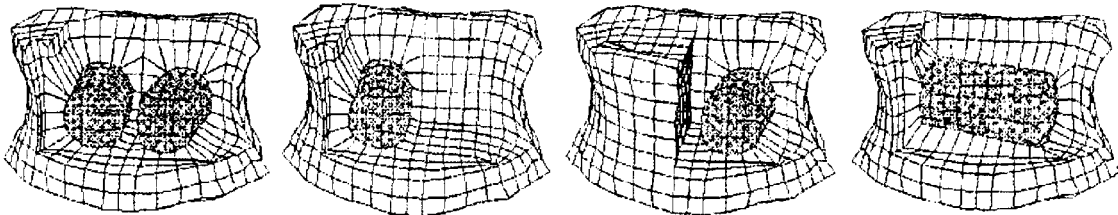


Figure 2-5: Finite element mesh of vertebral body with different placements of PMMA (shaded) cement. From left to right, bipedicular, unipedicular - left, unipedicular – right and posterolateral vertebroplasty⁷⁰.

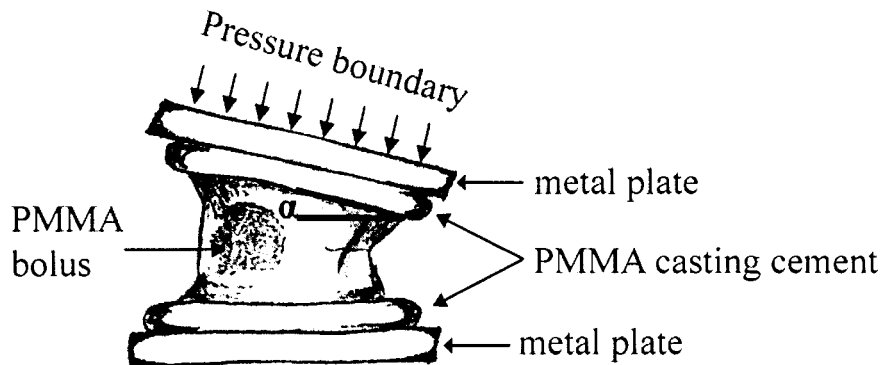


Figure 2-6: High angle of rotation in the sagittal plane (α) of the vertebral body after unipedicular vertebroplasty when loaded under pressure boundary conditions brings instability to the treated vertebra.

2.3.2. Fracture Prevention

Some *in-vitro* studies have focused on the strength augmentation ability of vertebroplasty using different forms of CaP^{10,53,58,72} and PMMA^{10,35,53,54} (Table 2-4). Regardless of bone cement, all of the studies showed increases in mechanical vertebral stiffness and strength after treatment. No significant differences in mechanical enhancements were observed with CaP and PMMA by Bai et al.¹⁰ and Lim et al.⁷², while Heini et al.⁵³ noticed higher reinforcements with PMMA than CaP. The discrepancy could be because of the different types of CaP used. Another reason,

discovered by Heini et al.⁵³ and Ikeuchi et al.⁵⁸, is that higher vertebral strength increase is achieved with larger volume of cement and lower initial bone density. Therefore, even though the vertebral specimens may have been randomly distributed into the experimental design groups, any bone density bias of the specimens will skew the results. Due to large biological variability in the cadaveric specimens, this research favors the computational approach, which allows multiple analyses to be performed on the same model, thereby providing direct proof of the cause-and-effect of cement volume, placement and material properties on vertebral mechanics.

Table 2-4: Summary of *in-vitro* biomechanical studies on vertebroplasty for fracture prevention.

Authors	Specimen levels	Cement Material	Volume (mL)	Procedure	Number of specimens	Bone density (g/cm ²)
Bai et al. 1999 ¹⁰	Single VB T8-L3	CaP PMMA	1.5 1.5	BP	24	
Dean et al. 1999 ³⁵	Single VB L1-L4	CMW 3	1 to 8	UP	36	
Heini et al. 2001 ⁵³	Single VB T2-L4	PMMA EBC	6.1 to 12.9	BP	75	0.53 to 1.35
Ikeuchi et al. 2001 ⁵⁸	Single VB T9-L5	CaP	Half of VB Whole VB	BP	45	0.45 ± 0.11 0.51 ± 0.15
Lim et al. 2002 ⁷²	Single VB T2-L1	Simplex P BoneSource	6.0 ± 3.4 4.8 ± 2.0	BP	20	0.56 to 0.89

VB = vertebral body; BP = bipedicular vertebroplasty; UP = unipedicular vertebroplasty

2.4. Biomechanical Goal of Vertebroplasty

Previous biomechanical studies had considered the repair of a collapsed vertebra successful when vertebral stiffness or strength is restored to pre-fractured values^{16,70}. By increasing vertebral strengths to pre-fracture levels, additional fractures could, theoretically, be prevented if the spine were loaded to the same magnitude that caused the initial fracture. This criterion was used as a basis to provide guidance as to the volume of cement needed for vertebroplasty so as to minimize risk of extravasations^{16,70}. Unfortunately, since 58% of osteoporotic vertebral fractures occur spontaneously during routine activities²⁸, the loads experienced in subsequent fractures can easily equal or exceed that of the initial collapse. As a result, the fractured vertebrae need to be strengthened to levels that enable sufficient support of normal weight-bearing dynamics¹¹⁴. The aim of prophylactic vertebroplasty therefore should be geared towards fracture prevention through enhancement of the mechanical integrity of the compromised vertebrae to low fracture risk levels.

Much of the abstruseness of the ultimate biomechanical goal of vertebroplasty stems from the highly debated issue of what comprises fracture risk. Newton-John and Morgan⁹⁰ suggested that a fracture threshold is reached when bone mass falls 2.5 standard deviations below the mean of normal young population. Since this is a relatively easily monitored value in a clinical setting, it has been adopted as the most common technique for vertebral risk assessment. The World Health Organization's criterion for diagnosis of osteoporosis (Table 2-5) is also based on epidemiological data relating bone mineral density to fracture risks (Figure 2-7).

Table 2-5: World Health Organization diagnostic criteria for osteoporosis ^{44,76,81,105}.

Population Group	Diagnostic Criterion	Spinal BMD (g/cm^2)	
		Women	Men
Normal	BMD within 1 SD of mean peak bone mass	> 1.059	> 1.13
Osteopenia	BMD 1 to 2.5 SD below mean peak bone mass	0.80 – 0.95	0.86 – 1.13
Osteoporosis	BMD 2.5 or more SD below mean peak bone mass	< 0.80	< 0.86
Severe Osteoporosis	Osteoporosis with one or more fragility fractures	< 0.80	< 0.86

BMD = bone mass density

SD = standard deviation

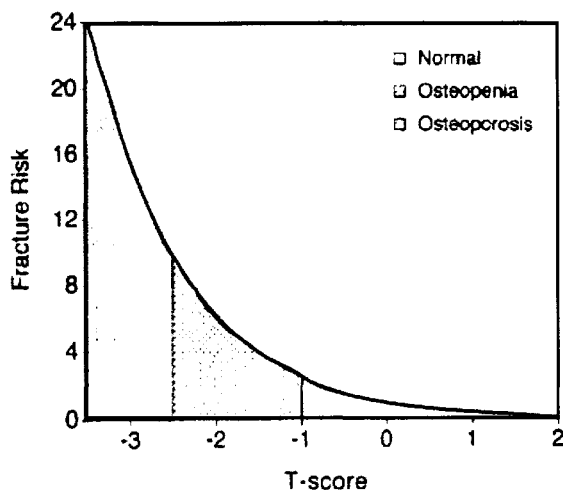


Figure 2-7: Gradient-of-risk relationship between bone density and fracture risk. Bone density is plotted in T-score units relative to mean and standard deviations of healthy young adult population. World Health Organization's definitions of osteoporosis, osteopenia, and normal are intended to identify patients at high, intermediate, and low risks of fracture ⁴¹.

However, Riggs et al.¹⁰¹ found that bone mineral density values in patients with and without vertebral fractures overlap widely, demonstrating a low sensitivity of the criterion. A stronger basis for fracture risk maybe with vertebral strength since risk of fracture is a measure of the probability of a mechanical overload in bone. Vertebral strength predictions have been shown to be of significantly higher accuracy if, in addition to bone density, geometry of the bone specifically endplate area is also accounted for ($r = 0.80$, standard error of estimate = 1.06 kN), compared to with bone density alone ($r = 0.62$, standard error of estimate = 1.40 kN)²¹.

Biggemann et al.¹⁹ later used this improved strength prediction correlation to quantify the “normal” vertebral strength values needed to sustain spinal load during regular daily activities. The L3 vertebral strength of 75 patients (53 females and 22 males) were estimated from the regression and related to the risk of vertebral fracture determined from the percentage of spines with at least one fractured vertebra between T10 and L5. Two clearly defined strength groups were noted: 100% fracture risk for strengths less than 3 kN (high risk) and 0% risk for strengths greater than 5 kN (low risk). Strengths between 3 and 5 kN were at an intermediate risk group. As such, the “normal” or low fracture risk level for the L3 vertebra is when its compressive strength is at least 5 kN (Figure 2-8). By normalizing the strength levels by total endplate area, the same definitions can be applied to other vertebral levels.

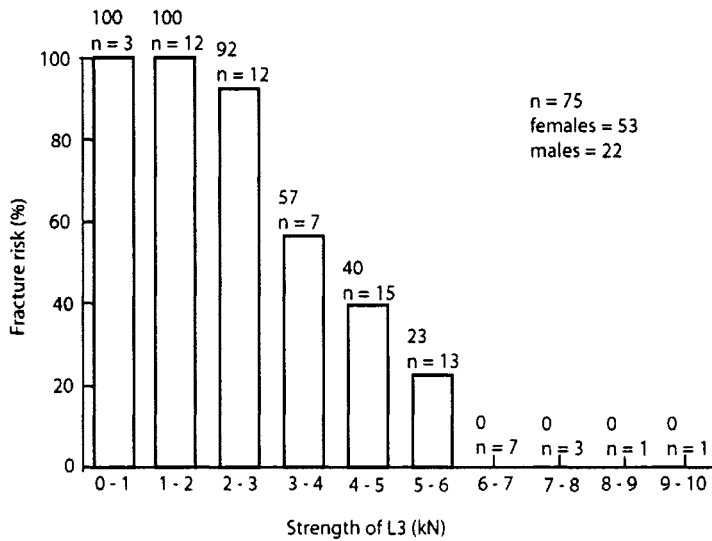


Figure 2-8: Risk of vertebral fragility fracture according to the strength of L3 vertebra. The high fracture risks is when vertebral strength is less than 3 kN and low fracture risks is when vertebral strength is greater than 5 kN (Adapted from Biggeman et al. ¹⁹).

The same definitions can be applied to other vertebral levels by normalizing strength levels by total endplate area of the L3 vertebra ($\sim 14 \text{ cm}^2$). The new definitions of the three fracture risk groups are: high risk group with stress less than 2.2 MPa and fracture risk of 100%, medium risk group with stress from 2.2 to 3.6 MPa, and low risk group with stress greater than 3.6 MPa and fracture risk near 0%. Therefore, the biomechanical goal of vertebroplasty for both fracture repair and prevention is to increase compressive stress of the vertebral body to beyond fracture risk levels ($> 3.6 \text{ MPa}$) so as to prevent further fractures. This new biomechanical goal for vertebroplasty was used to evaluate the biomechanical efficacy of PMMA in Chapter 3.

2.5. Injectable Bone Substitutes for Vertebroplasty

The focus of most previous biomechanical studies of vertebroplasty was in comparing the biomechanical efficacy of new cements with PMMA. The shift towards evaluating alternative cements indicates problems with the current PMMA bone cement. In 2003, the Food and Drug Administration issued a warning about the numerous side effects of PMMA linked to the high incidence of PMMA leakage in the treatment of spinal fractures⁴. Although reported complication rates are low, ranging from 1% to 10%⁶⁰, such leakage can result in compression of the spinal cord and nerve roots, as well as pulmonary embolism^{29,31,36}. Another concern with PMMA recently speculated involves the provocation of fractures in the vertebrae adjacent to the treated vertebra due to the stress concentrations with the treated vertebra, which alter the transfer of load to the adjacent vertebrae^{18,46,117}. There is also temperature elevations of up to 70°C generated during the exothermic polymerization reaction of PMMA, which may cause damage to the surrounding nerve and bone tissue^{38,104}, in addition to the tissue damage caused by the neurotoxic methylmethacrylate monomer^{20,33,34}. The high curing temperature of PMMA in combination with its neurotoxic effect may contribute to the marked pain relief experienced by patients, but they also inhibit the natural bone healing response of the body.

The biochemical disadvantages of PMMA, including high curing temperature, toxic monomer and non-biocompatibility, can be overcome by the development of new injectable bone cements with tissue engineering ideology. All of the new bone cements that were biomechanically evaluated against PMMA in previous *in-vitro* studies were biocompatible¹⁴ and/or biodegradable^{10,15,17,53,55,58,72}. Theoretically, the biodegradable

material injected into the vertebrae will increase the vertebral strength temporarily. As the material slowly degrades, its osteoconductive properties stimulate new bone growth at the fracture site, resulting in repair. This strategy can also be used as a prophylactic treatment, to prevent fractures by reinforcing osteoporotic vertebrae in the short-term while stimulating bone growth in order to strengthen the vertebrae in the long-run. The procedure can be repeated as many times as needed until repair is complete or fracture risk is sufficiently lowered. The front runner of biodegradable materials is CaP, with its biodegradability, biocompatibility, absence of exotherm and osteoconductive properties^{10,58}, but the durability of repair after the biodegradable cement has been resorbed and remodeling has occurred is unknown. No long-term study of vertebroplasty using biodegradable cements has ever been published.

The remaining disadvantages of vertebroplasty using PMMA, cement leakages and high incidences of adjacent fractures, are a direct result of the lack of knowledge of the biomechanics of the procedure. Since no biomechanical studies have been conducted to optimize vertebroplasty based on the need to strengthen the vertebra so that it is no longer at risk for fracture, most surgeons simply inject an excessive amount of cement in hopes of gaining the maximum mechanical enhancement, thereby increasing the risk of leakages. This research rectifies this lack of information by offering guidelines as to the optimal PMMA volume and placement required to prevent any future fractures. Additionally, the controversy that vertebroplasty with PMMA is the reason behind the increasing incidences of fractures to the untreated adjacent vertebrae is resolved in Chapter 5 by experimentally testing the vertebroplasty-induced fracture mechanism put forth by numerical studies^{12,96}. A computational study, subsequently conducted in

Chapter 6, determines if the distribution patterns of bone cement can mitigate the stress concentrations within the treated vertebra that are believed to be the cause of adjacent vertebral fractures. In the end, the optimizations of vertebroplasty for fracture repair and prevention have to be tackled at both biochemical and biomechanical fronts. This research focuses on the optimizing biomechanical aspect of prophylactic vertebroplasty.

2.6. Potential of Vertebroplasty

Vertebroplasty is a highly effective fracture repair treatment due to its ability to rapidly relieve pain once the liquid cement hardens to stabilize the fracture site and its quick recovery time for the patient. The minimally invasive procedure is also an extremely promising fracture prevention treatment that provides immediate strength enhancements to osteoporotic vertebrae at risk of failing at any time. This new prophylactic treatment is a significant improvement upon current drug therapies that require at least a year before enough new bone has grown for fracture risks to even begin to diminish. However, there are efficacy and patient safety issues that require more in-depth investigations into how the biochemistry and biomechanics of the bone cement affect the vertebrae on both the tissue and whole bone level. A good starting point for the investigations is with the current PMMA bone cement. The efficacy of PMMA for prophylactic vertebroplasty to achieve the new biomechanical goal of increasing vertebral strength to beyond fracture risk levels has to be first evaluated. The question of whether different surgical techniques for cement placement using safe volumes of PMMA are able to meet the new biomechanical goal needs to be answered. Also, how does changing the materials properties of the cement and even the way the cement is spatially distributed

within the vertebral body affect the overall vertebral and internal mechanics? The solution to these basic questions will provide the ideal biomechanical characteristics of bone cements that can be specially engineered and developed to also have desirable biochemical properties, such as biocompatibility, biodegradability and osteoconductivity, which would stimulate the reinforcement of the vertebra with natural native bone. The optimization of the bone cements both biomechanically and biochemically will ultimately bring about maximum benefit to the patient with minimal risks of complications.

Chapter 3

BIOMECHANICS OF VERTEBRAL REINFORCEMENT USING PMMA

This study determines the efficacy of prophylactic vertebroplasty using poly(methylmethacrylate) (PMMA) on intact vertebral bodies with respect to biomechanical recovery and fracture risk reduction. Vertebroplasty is a potentially effective fracture prevention treatment, but the risk of complications due to cement leakage must be minimized. Therefore, the least amount of bone cement required to improve vertebral strengths to low fracture risk levels was ascertained. Six different PMMA volumes were virtually implanted into previously validated vertebral body finite element models following bipedicular and posterolateral vertebroplasty. Stiffness and fracture load of the treated and untreated vertebral body models under uniaxial compression were predicted. The results show that prophylactic vertebroplasty can be an effective in reducing fracture risk, but the large PMMA volume required for the successful reinforcements of high risk vertebral bodies indicates a high risk of cement leakage and its associated complications. Therefore, alternative materials have to be developed for prophylactic vertebroplasty.

3.1 Introduction

Osteoporotic vertebral fractures are an increasing public health problem affecting the growing elderly population, occurring at a frequency of 700,000 per year in the United States alone¹⁰⁰ and in more than 25% of women over the age of 70²⁷. Current therapy for vertebral fractures emphasizes merely on pain control using narcotic or anti-inflammatory medications and immobilization⁹⁸. Bone mass conservation drugs are also prescribed to prevent further fractures since the risk for subsequent fractures is about a 25-fold risk increase in women with low bone mass and a single fracture¹⁰³. Unfortunately, these osteoporotic medications often require 6 months to 1 year to achieve efficacy^{11,25,102} during that time up to 19% of osteoporotic patients may sustain a subsequent fracture⁷⁵. There is therefore a dire need for a more effective preventive measure that can reduce fracture risk, and ultimately decrease the incidence of subsequent vertebral fractures.

A potential intervention recently proposed, vertebroplasty, involves the percutaneous injection of PMMA bone cement into the osteoporotic vertebral body to achieve mechanical reinforcement and thereby minimize fracture risk²⁰. This procedure is mainly known for its current application towards the treatment of vertebral fractures, with the aim to relieve pain by vertebral stabilization. Despite clinical success in pain relief and improvements in the structural behavior of the treated vertebral bodies, 30 to 67% of patients who underwent vertebroplasty experienced cement leakages outside the vertebral body⁷³, and into the perivertebral or epidural veins, soft tissue around the spine, epidural space or along the needle track, and intervertebral disc³⁷. Although reported complication rates are low, ranging from 1% to 10%⁶⁰, such leakages can result in

compression of the spinal cord and nerve roots, as well as pulmonary embolism^{29,31,36,78}.

The high incidences of cement leakage are attributed to overly aggressive filling of the vertebral body. Therefore, to minimize the risk of complications for prophylactic vertebroplasty, the least amount of bone cement required to improve vertebral strength from high to low fracture risk levels must be determined. This knowledge requires an understanding of all the factors that affect vertebral reinforcement, which is believed to depend on bone cement placement and volume as well as the initial bone properties of the vertebral body.

The goal of this study was to determine the efficacy of prophylactic vertebroplasty on intact vertebral bodies with respect to biomechanical recovery and fracture risk reduction. In order to minimize biological variability, specimen-specific finite element models of human vertebral bodies were developed from quantitative computed tomography (QCT) scans and were used to simulate two different surgical vertebroplasty approaches (bipedicular and posterolateral) using a range of cement volumes. The specific aims were to: 1) determine the dependency of vertebral body compressive stiffness and strength augmentations on bone cement volumes and placement positions; 2) quantify the effectiveness of stiffness and strength reinforcements with respect to bone mineral densities of the vertebral bodies; and 3) determine the optimal configuration to provide mechanical enhancements beyond a fracture risk group.

3.2 Methods

3.2.1 QCT Scan

Eight fresh, radiographically normal, whole vertebral bodies (L1-L4) were isolated from eight cadavers whose ages ranged from 49 to 82 years (mean = 71.1 ± 10.7 , 6 females, 2 males). Posterior elements (pedicles and lamina) of the vertebral bodies were removed using an autopsy saw and intervertebral disc material was dissected from both endplates using scalpels. Eighteen to twenty-four QCT scans of 1.5 mm thick transverse cross-sections were obtained for each vertebral body using a clinical scanner (GE9800, General Electric, Milwaukee, WI) at scan settings of 140 kV, 70 mA (0.25 mm/pixel in plane resolution, 512 x 512 pixel field of view). During scanning, the vertebral bodies were held in place using an acrylic fixture and submerged in water in a container of about the same size as the human torso in order to mimic the human body. A liquid K_2HPO_4 phantom (Mindways Software, Inc., San Francisco, CA) was included in each scan to correct for scanner drift and to convert CT numbers in Hounsfield units to bone mineral density in g/cm^3 ⁶⁸ (Figure 3-1). The average QCT densities of the vertebral bodies ranged from 0.0384 to 0.127 g/cm^3 , with a mean QCT density of $0.091 \pm 0.03 g/cm^3$ for all 8 specimens. The preparation and scanning of the vertebral bodies were performed in a previous study by Kopperdahl et al.⁶⁸.

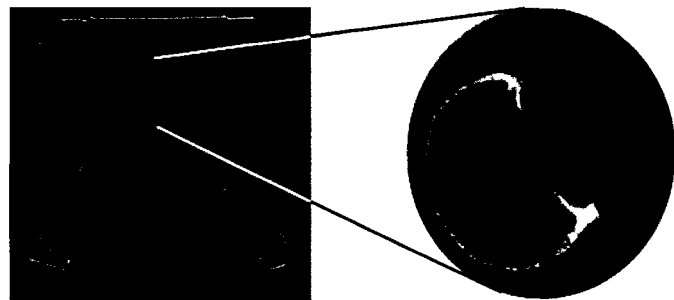


Figure 3-1: A slice of the quantitative computed tomography (QCT) scans of the human vertebral bodies imaged with a liquid K₂HPO₄ phantom that was used to calibrate mineral densities ⁶⁸. Finite element models were constructed from the high resolution images.

3.2.2 Mechanical Testing

Mechanical testing of the specimens was also performed in the previous study by Kopperdahl et al. ⁶⁸. After QCT scanning, PMMA was molded to the concave endplates using a fixture that ensured plano-parallel ends. Compression tests were performed between steel platens on a screw-driven load frame (Instron Corporation, Model 5583, Canton, MA). The upper platen was attached to a ball joint, which was locked in place after applying a pre-load of 50N (Figure 3-2). After preconditioning, specimens were loaded monotonically in displacement control at a rate of 0.15 mm/sec (~0.5 % strain per second) to a randomly selected strain level. Strains were based on the initial height of each specimen including PMMA, measured using calipers, and recorded using a two-inch extensometer spanning the platens. The load-deformation curve recorded was used to derive the compressive stiffness and fracture strength of the vertebral bodies (Table 3-1). The experimentally determined vertebral stiffness was derived from the slope of the first linear portion of the load-deformation curve. The stiffness was matched subsequently in the calibration of the specimen-specific finite element vertebral body models by adjusting

the vertebral shell modulus. The maximum compressive load applied during the experiment was used to verify the predicted vertebral fracture strength.

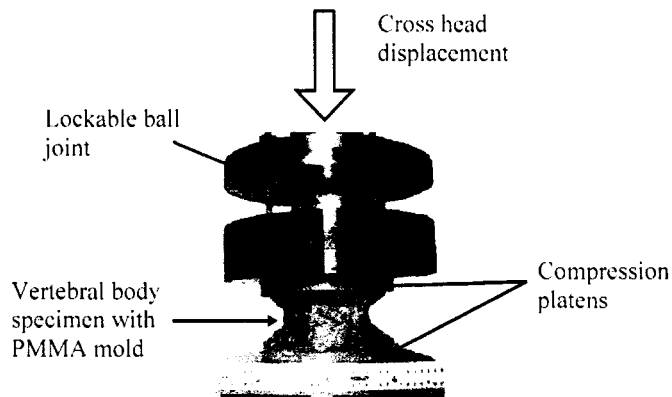


Figure 3-2: Uniaxial compression testing of vertebral body in a servohydraulic testing machine. Compression platens with lockable ball joint allow the top platen to rest flat on the specimen⁶⁸.

Table 3-1: Physical and mechanical data on all 8 single vertebral bodies tested (F for female, M for male, SD for standard deviation, VB for vertebral body).

Specimen number	Donor age	Sex	Spine level	Average (SD) QCT density [g/cm ³]	Min/max QCT density [g/cm ³]	Whole VB stiffness [N/mm]	Fracture strength [kN]
1	49	F	L3	0.0912 (0.0132)	0.0713/0.1089	17363	6.123
2	76	F	L3	0.0762 (0.0157)	0.0630/0.1047	8340	2.417
3	66	F	L4	0.1244 (0.0173)	0.1021/0.1519	12300	4.418
4	80	F	L4	0.0384 (0.0069)	0.0298/0.0502	7200	2.571
5	82	M	L3	0.1269 (0.0268)	0.0918/0.1765	29876	9.553
6	66	F	L4	0.0805 (0.0150)	0.0585/0.1045	8280	2.779
7	73	F	L1	0.0743 (0.0178)	0.0499/0.0996	8242	2.793
8	77	M	L2	0.1133 (0.0227)	0.0694/0.1408	14650	6.626

3.2.3 Finite Element Modeling

A custom written contouring algorithm was used to extract the bone geometry from the QCT scans⁶⁹. By stacking the QCT images, a three dimensional geometry of the vertebral body was reconstructed (XYZ Scientific Applications Inc., Livermore, CA). The trabecular tissue of the vertebral body interior was paved with 20-noded brick elements of about 3 mm in size (Figure 3-3). Each trabecular element was assigned an elastic modulus in the superior to inferior direction (E_{zz}) based on the following relation⁶⁶:

$$E_{zz} \text{ (MPa)} = 3850 \rho_{\text{QCT}} \text{ (g/cm}^3) - 81.9 \quad r^2 = 0.76, n = 76 \quad (3.1)$$

where ρ_{QCT} is the QCT mineral density. The other elastic constants (Young's modulus: E_{xx}, E_{yy} ; Poisson's ratio: $\nu_{xy}, \nu_{xz}, \nu_{yz}$; Shear modulus: G_{xy}, G_{xz}, G_{yz}) were derived from ratios obtained by Ulrich et al.¹¹⁶ (Table 3-2).

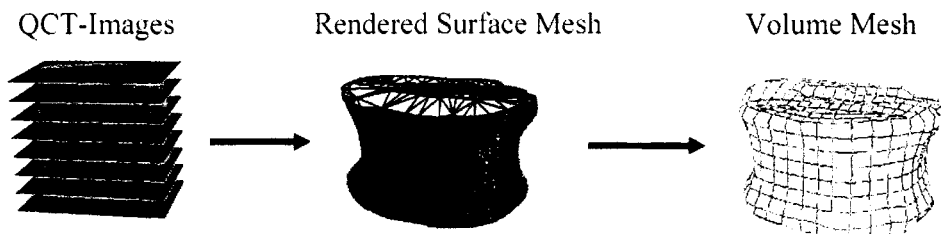


Figure 3-3: The series of QCT scans of a vertebral body was stacked together and the three dimensional geometry of the vertebral body was contoured out. The surface mesh was then filled with brick elements to generate the volume mesh.

Table 3-2: Anisotropic elastic constants for human vertebral trabecular bone. The Young's moduli (E_{xx} and E_{yy}) and shear moduli (G_{xy} , G_{xz} , G_{yz}) are expressed as a factor of the longitudinal modulus, E_{zz} ¹¹⁶.

Ratio	Value	Poisson's Ratio	Value
E_{xx}/E_{zz}	0.42	ν_{xy}	0.381
E_{yy}/E_{zz}	0.287	ν_{xz}	0.095
E_{zz}	1	ν_{yx}	0.260
G_{xy}/E_{zz}	0.153	ν_{yz}	0.115
G_{xz}/E_{zz}	0.192	ν_{zx}	0.226
G_{yz}/E_{zz}	0.129	ν_{zy}	0.399

The plastic material definitions of the trabecular elements were based on post-yield trabecular tissue properties determined from five points defined along the normalized (stress divided by modulus) stress-strain curve measured empirically from 22 8 mm diameter cylindrical vertebral trabecular cores loaded to failure under compression in the longitudinal direction (z-direction)⁶⁷ (Figure 3-4). The strain ranges of the five linear regions (ε_{yield} , ε_{ab} , ε_{bc} , ε_{cd} and ε_{de}) were calibrated to the 8 vertebral body models such that the compressive behavior of the anterior vertebral bodies matched the experimental results. Perfectly plastic behavior was assumed for the cortical elements with ultimate strain at 1.4%⁶⁶. The calibrated post-yield trabecular tissue properties were previously proven successful in accurately predicting ultimate vertebral fracture load⁷¹ (Table 3-3). The predicted compressive behavior of the untreated vertebral bodies closely matched the experimentally determined behavior and the predicted fracture loads were strongly correlated with the measured values ($r^2 = 0.94$, average relative error of 12.7%) (Figure 3-5). The higher modified bone properties indicate that the 8 mm trabecular core is too large for use at this resolution of finite element models since higher strains and stresses are experienced at smaller scales of trabecular bone due to its heterogeneity⁸⁵.

However, the smaller the trabecular bone size, the more difficulty it is to accurately measured the bone's mechanical properties as the disruption of the random network of interconnected trabeculae at the ends during machining results in large experimental errors ⁶⁴. Therefore, the modification of the post-yield properties is warranted. Furthermore, as no data is currently available on the nonlinear compressive behavior of vertebral bone in the transverse direction, the same post-yield properties were assumed for all three direction normalized by directional modulus. This assumption is valid as the models showed insensitivity to variations in material properties in the transverse direction for the loading conditions applied.

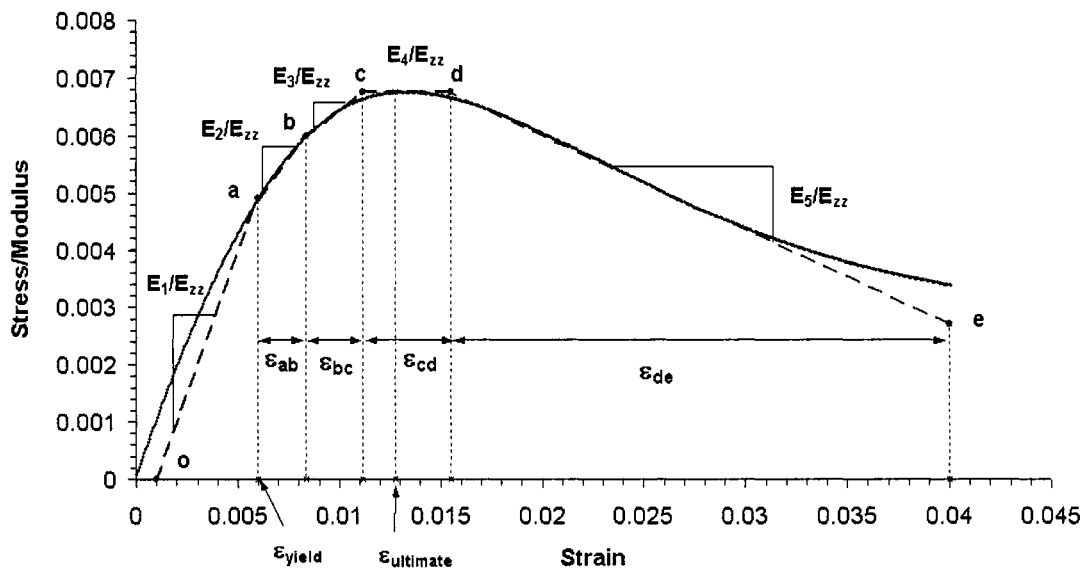


Figure 3-4: Sectioned normalized stress-strain curve of 8 mm diameter cylindrical samples of vertebral trabecular bone loaded beyond the ultimate point ⁷¹. The yield point was determined from a 0.1% strain offset rule, which states that the yield point is the intersection between the stress-strain curve and the elastic loading line offset to 0.001 strain at zero stress. This offset elastic loading line provided the first linear region oa. By following the contour of the normalized stress-strain curve from yield point, linear regions ab, bc, cd and de were defined. The slopes (E_1/E_{zz} , E_2/E_{zz} , E_3/E_{zz} , E_4/E_{zz} , E_5/E_{zz}) as well as strain ranges (ϵ_{yield} , ϵ_{ab} , ϵ_{bc} , ϵ_{cd} and ϵ_{de}) of the five linear regions were calculated. The slope of each linear region represented the ratio of the elastic modulus of trabecular cylindrical samples over the on-axis modulus ($E_{zz} = E_1$).

Table 3-3: Original and modified post-yield tissue properties of 8 mm cylindrical vertebral trabecular tissue⁷¹.

Original		Modified			
Strain	Value	Strain	Value	Slope	Value
ϵ_{yield}	0.00602	ϵ_{yield}	0.0121	E_1/E_{zz}	1.000
$\epsilon_{ultimate}$	0.0128	$\epsilon_{ultimate}$	0.0257	E_2/E_{zz}	0.480
ϵ_{ab}	0.00232	ϵ_{ab}	0.0467	E_3/E_{zz}	0.275
ϵ_{bc}	0.00284	ϵ_{bc}	0.00572	E_4/E_{zz}	-0.00235
ϵ_{cd}	0.00424	ϵ_{cd}	0.00853	E_5/E_{zz}	-0.170
ϵ_{de}	0.0245	ϵ_{de}	0.0493		

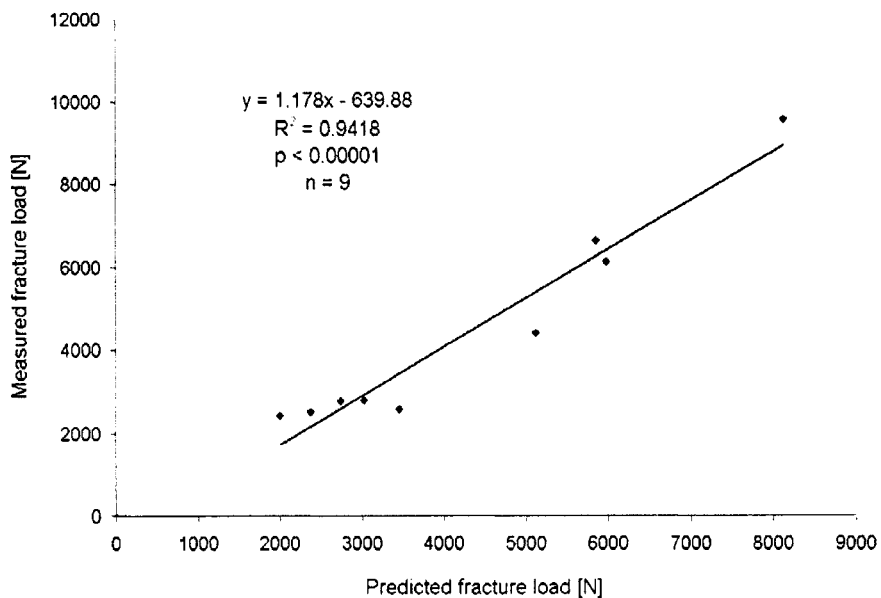


Figure 3-5: The predicted fracture loads using the average ϵ_{yield} and $\epsilon_{ultimate}$ of 1.21% and 2.57%, respectively, matched well with the experimentally determined values, validating the accuracy of the models⁷¹.

The cortical shell and endplates were assumed to have a nominal thickness of 0.35 mm¹⁰⁷ and were also paved with 20-noded brick elements. Cortical bone was assumed to be isotropic, with Poisson's ratio of 0.3¹¹⁸ and ultimate strain of 1.4%⁶⁶. Since elastic modulus of the cortical bone was not dependent on vertebral stiffness, the cortical

modulus of each vertebral body was calibrated by varying the modulus until the structural stiffness calculated matched the stiffness determined from experimental loading⁶⁹. The calibrated cortical modulus ranged from 15 to 3400 MPa, with a mean value of 732 MPa. PMMA, with a modulus of 2500 MPa and Poisson's ratio of 0.3, was modeled at both endplates of each vertebral body in order to simulate the parallel loading surfaces in the experimental test conditions⁶⁸. The final meshes were verified and adjusted in order to prevent element distortion⁶⁹ (Figure 3-6). The experimentally calibrated finite element models were subsequently used to simulate vertebroplasty.

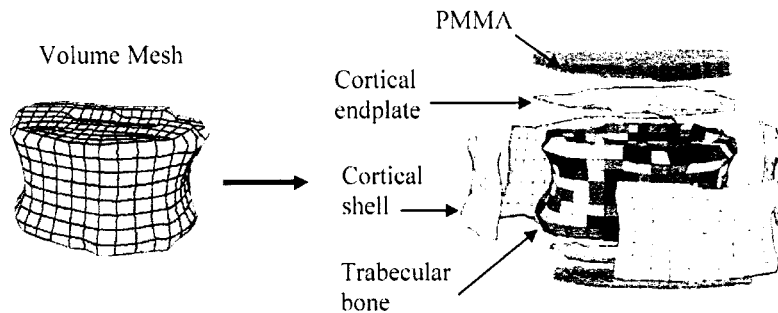


Figure 3-6: The finalized vertebral body finite element model with added layers of cortical shell and endplates, along with the casting cement PMMA to duplicate experimental loading conditions. Each model consisted of 1816 elements, of which 1008 are trabecular⁶⁹.

3.2.4 Vertebroplasty Modeling

The procedures used in simulating vertebroplasty followed those described in Liebschner et al.⁷⁰. In that study, it was demonstrated that vertebral body instability may occur due to asymmetric cement placement, in the form of a medial-lateral toggle motion towards the untreated side when a compressive pressure load was applied. As a result, only symmetric cement placements, bipedicular and posterolateral vertebroplasty

approaches, are recommended and therefore, simulated in this study using the vertebral body finite element models (Figure 3-7). Symmetric cement filling was achieved by modeling equal volumes of PMMA in each side of the vertebral body, centered along the sagittal plane of the vertebral body and at central height. For each vertebroplasty simulation, six different PMMA volumes ($1, 2.5, 3.5, 5, 7.5$ and 9 cm^3) were virtually implanted, corresponding to approximately 5%, 10%, 15%, 20%, 30% and 35% fill of PMMA to whole vertebral body volume. Considering the high porosity and weaker material properties of trabecular bone, the mechanical contribution of trabecular bone, within the relatively large size of each trabecular element (about 3 mm), is insignificant compared to PMMA. Therefore, for areas where PMMA were positioned, the material properties of the whole trabecular bone elements were replaced with that of PMMA. The plastic material definitions of PMMA were derived using the same method as for trabecular bone by specifying six points along the post-yield compressive behavior of the bone cement⁸² (Figure 3-8).

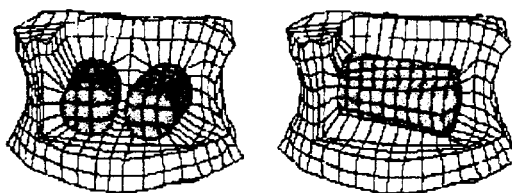


Figure 3-7: Finite-element mesh of a vertebral body with two PMMA capsules (shaded) simulating bipedicular vertebroplasty (left) and one PMMA capsule in the horizontal plane simulating posterolateral vertebroplasty (right).

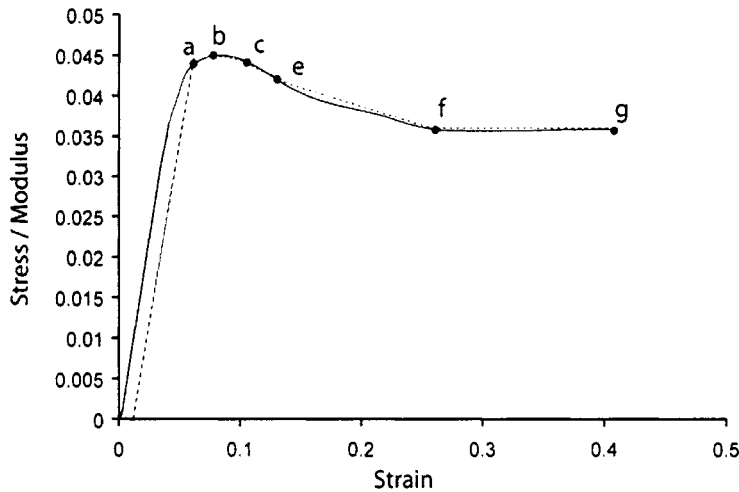


Figure 3-8: The compressive stress-strain curve of PMMA from which the post-yield properties were extracted from the six points along the curve⁸².

A total of 104 simulations, 13 cases (12 treated by vertebroplasty + 1 untreated) per vertebral body, were analyzed. A uniform compressive displacement was applied to the top layer of PMMA at the superior endplate of the vertebral body model in order to duplicate experimental loading conditions. The finite element solver ABAQUS version 5.8 (Hibbit, Karlsson and Sorenson, Inc., Pawtucket, RI) was used to perform non-linear analysis simulating uniaxial compression to predict the stiffness and fracture load of the treated and untreated vertebral body models. Fracture load of the treated model was obtained from the first peak of the computer predicted load-deformation curve, which was attributed to failure of the weaker trabecular bone. Subsequent peak was due to failure of the stronger PMMA cement. Vertebral stiffness was determined from the slope of the first linear portion of the predicted load-deformation curve. The variations of vertebral compressive stiffness and strength reinforcements with bone cement and initial trabecular bone densities for both bipedicular and posterolateral approaches were scrutinized.

3.3 Results

3.3.1 Effects of PMMA volume fill and placement

Stiffness

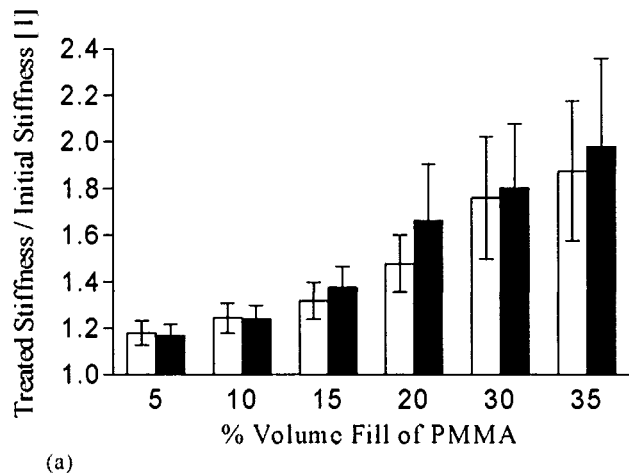
As expected, stiffness augmentations were influenced strongly by volume fraction of PMMA, with greater stiffness increase at higher PMMA volume fill. For both bipedicular and posterolateral vertebroplasty simulations, low amounts of PMMA showed similar average stiffness enhancements at about 17% increase and only 4.5% standard deviation for 5% PMMA fill. For 10% PMMA fill, about 24% increase in stiffness with 5.2% standard deviation was observed. As the volume of PMMA fill increased, the average stiffness increases rose linearly, with a steeper incline for the bipedicular approach (slope = 2.78 for bipedicular; slope = 2.45 for posterolateral). At 35% PMMA fill, average stiffness increase was 98% for the bipedicular case compared to only 88% for the posterolateral, and percent standard deviations of 19% and 16%, respectively (Figure 3-9a).

Fracture strength

Similar observations were noted for compressive strength augmentation, where average strength augmentations increased linearly with increasing PMMA volume fill. The average strength increases for the two approaches were comparable to each other at low amounts of PMMA fill. About 9% strength increase and standard deviations of only 3.0% were observed at 5% PMMA fill, and at 10% PMMA fill, strength was increased on average by 12% with 4.2% deviations. Increasing PMMA volume fill to 35% fill demonstrated a greater increase in strength for bipedicular cement placement versus

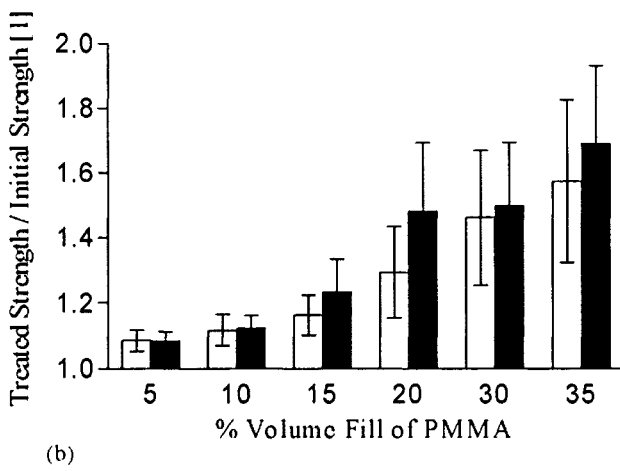
posterolateral. Strength increase of 69% and 14% standard deviation was determined for the bipedicular approach while the posterolateral approach resulted in only a 54% strength increase and 16% standard deviation (Figure 3-9b).

Posteriorlateral $y = 2.4526x + 1.0062, r^2 = 0.984, n = 8$
 Bipedicular $y = 2.7764x + 1.0062, r^2 = 0.969, n = 8$



(a)

Posteriorlateral $y = 1.619x + 0.9673, r^2 = 0.978, n = 8$
 Bipedicular $y = 1.9974x + 0.9695, r^2 = 0.924, n = 8$



(b)

Figure 3-9: Effect of posterolateral and bipedicular placement and volume fill of PMMA on the (a) average normalized compressive stiffness increase; and (b) average normalized compressive strength increase of reinforced vertebral bodies. Stiffness and strength augmentations were linearly proportional to the PMMA volume fill for both approaches.

3.3.2 Effects of bone mineral density

Stiffness

Greatest variations in stiffness were evident for average QCT densities below 0.1 g/cm³ and PMMA volumes over 20%. As the average bone density decreased from 0.1 g/cm³, stiffness enhancements increased, with steeper inclines for higher PMMA volumes. For PMMA volumes less than 20%, the variation in stiffness reinforcement with bone density in both vertebroplasty cases ranged from 14% to 52% (difference of 38%). Increasing the volume of PMMA to 35% fill increased the variation of stiffness enhancements with bone density to a range of 70% to 180% (difference of 110%). For average QCT densities above 0.1 g/cm³, stiffness increases remained less dependent on density (Figures 3-10a and b). These results agree closely with previous *in-vitro* vertebral augmentation studies on single vertebral bodies, which were mechanically tested under uniaxial compression after injection with calcium phosphate ⁵⁸, PMMA or experimental brushite cement ⁵³. In those studies, greater augmentation effect at lower initial bone mineral density was also observed.

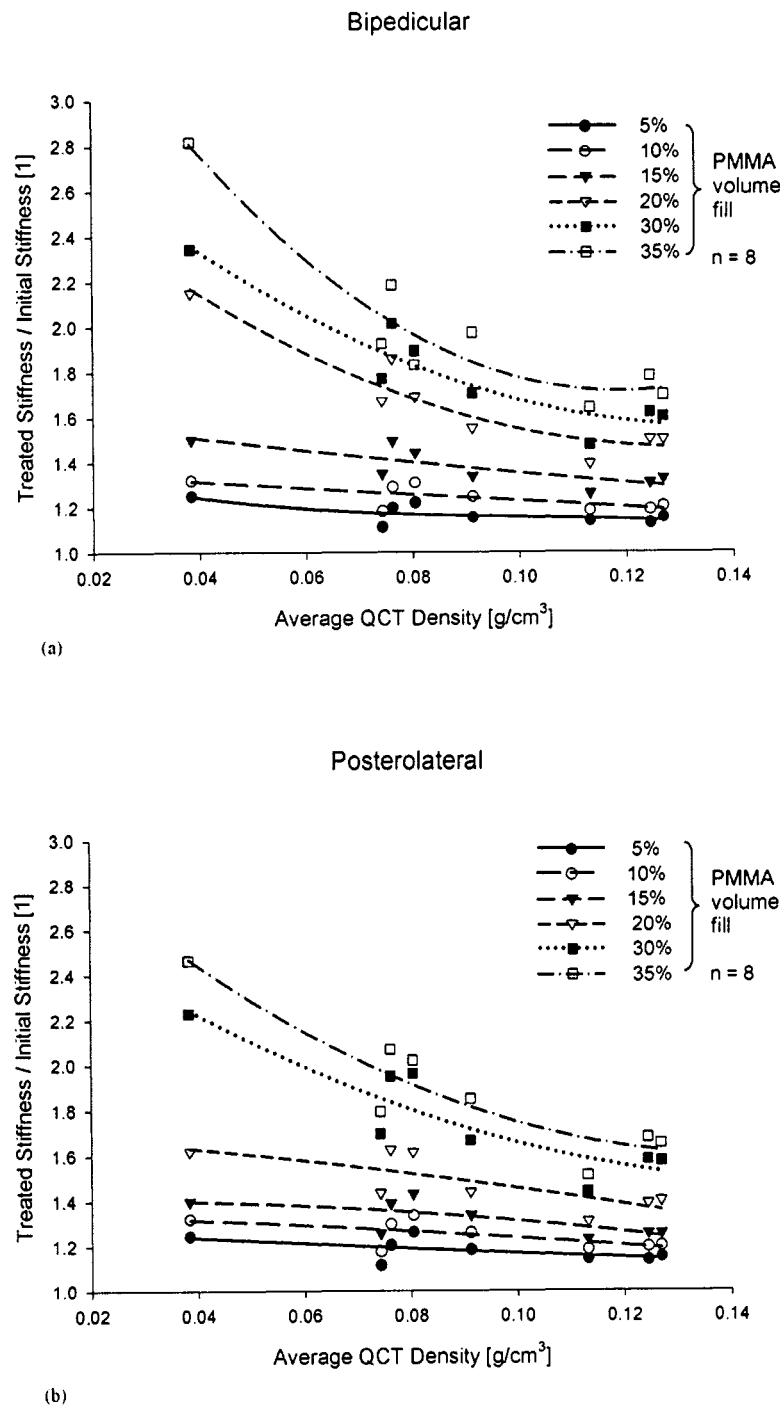
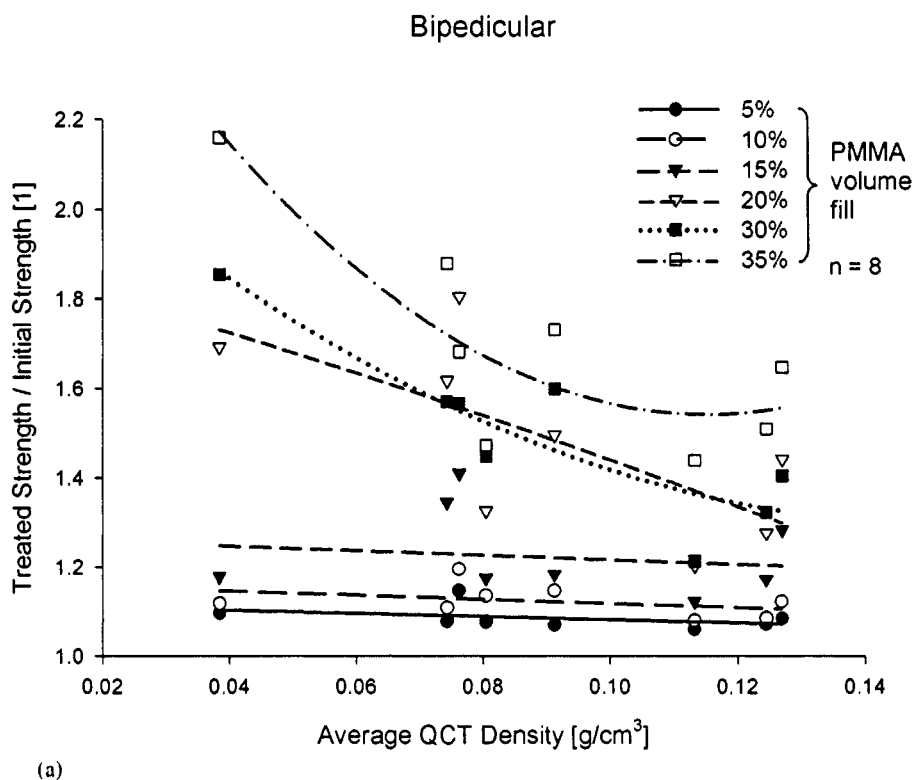


Figure 3-10: Effect of initial vertebral QCT density and volume fill of bone cement PMMA on the relative compressive stiffness increase of reinforced vertebral bodies using (a) bipedicular; and (b) posterolateral cement placement. Greatest variations in stiffness increase for average QCT densities below 0.1 g/cm^3 and PMMA volumes over 20%. For densities greater than 0.1 g/cm^3 , stiffness augmentations were less dependent on density.

Fracture strength

Bone density had only an effect on strength at high amounts of PMMA fill. The variation in strength increase was never greater than 18% (ranging from 7% to 25% increase) at PMMA volumes less than 15% fill for the bipedicular approach and less than 20% fill for the posterolateral case. At volumes higher than those values, the strength increase ranged from 25% to 115% (difference of 80%) for both simulations (Figures 3-11a and b).



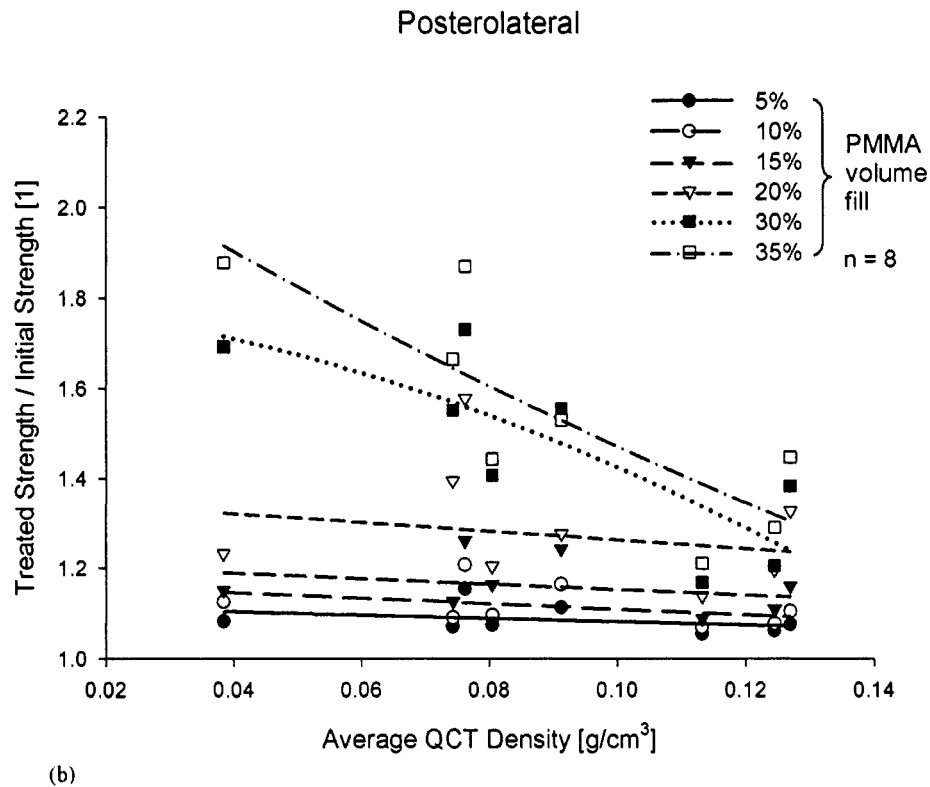
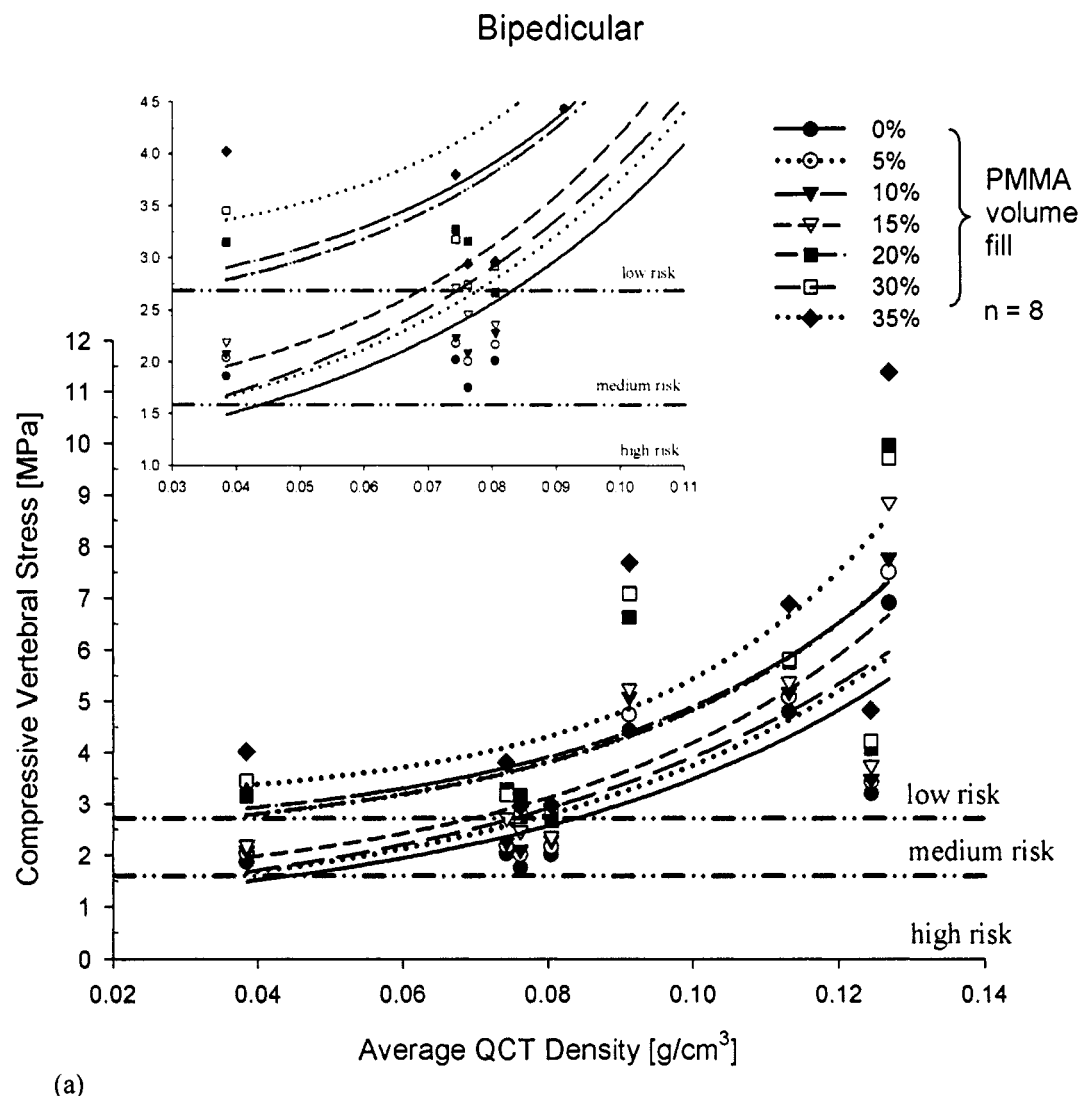


Figure 3-11: Effect of initial vertebral QCT density and volume fill of bone cement PMMA on the relative compressive strength increase of reinforced vertebral bodies using (a) bipedicular; and (b) posterolateral cement placement. Greatest variations in strength increase with average QCT densities when PMMA volumes were over 30%.

3.3.3 Optimal PMMA volume

Following Biggeman et al.'s ¹⁹ definition of fracture risk based on vertebral strength for the L3 vertebra, the proposed strength levels were normalized by endplate area in order to apply the same definitions to other vertebral levels. The absence of posterior elements in the finite element models was also corrected for by accounting for the 26% load bearing contribution of the facets under axial compression when still attached within the continuum of a spinal segment ^{9,124}. The new definition of the three

fracture risk groups are: high risk group with ultimate stress less than 1.6 MPa and fracture risk of 100%, medium risk group with ultimate stress from 1.6 to 2.7 MPa, and low risk group with stress greater than 2.7 MPa and fracture risk near 0%. For posterolateral vertebroplasty approaches, reinforcement of vertebral bodies, with average QCT densities below 0.048 g/cm^3 require about 30% PMMA volume fill in order to achieve success in improving vertebral stress from high fracture risk levels to over 2.7 MPa, into the low risk zone, while only 20% PMMA fill was needed for bipedicular case. For medium fracture risk vertebral bodies, higher PMMA volume (20 to 30%) was needed for lower trabecular densities (0.048 to 0.068 g/cm^3), while only 5 to 15% PMMA volume fill was required for trabecular densities greater than 0.068 g/cm^3 . If trabecular densities were above 0.083 g/cm^3 , the vertebral bodies would already be in the low risk zone and prophylactic reinforcement would not be necessary (Figures 3-12 and 3-13).



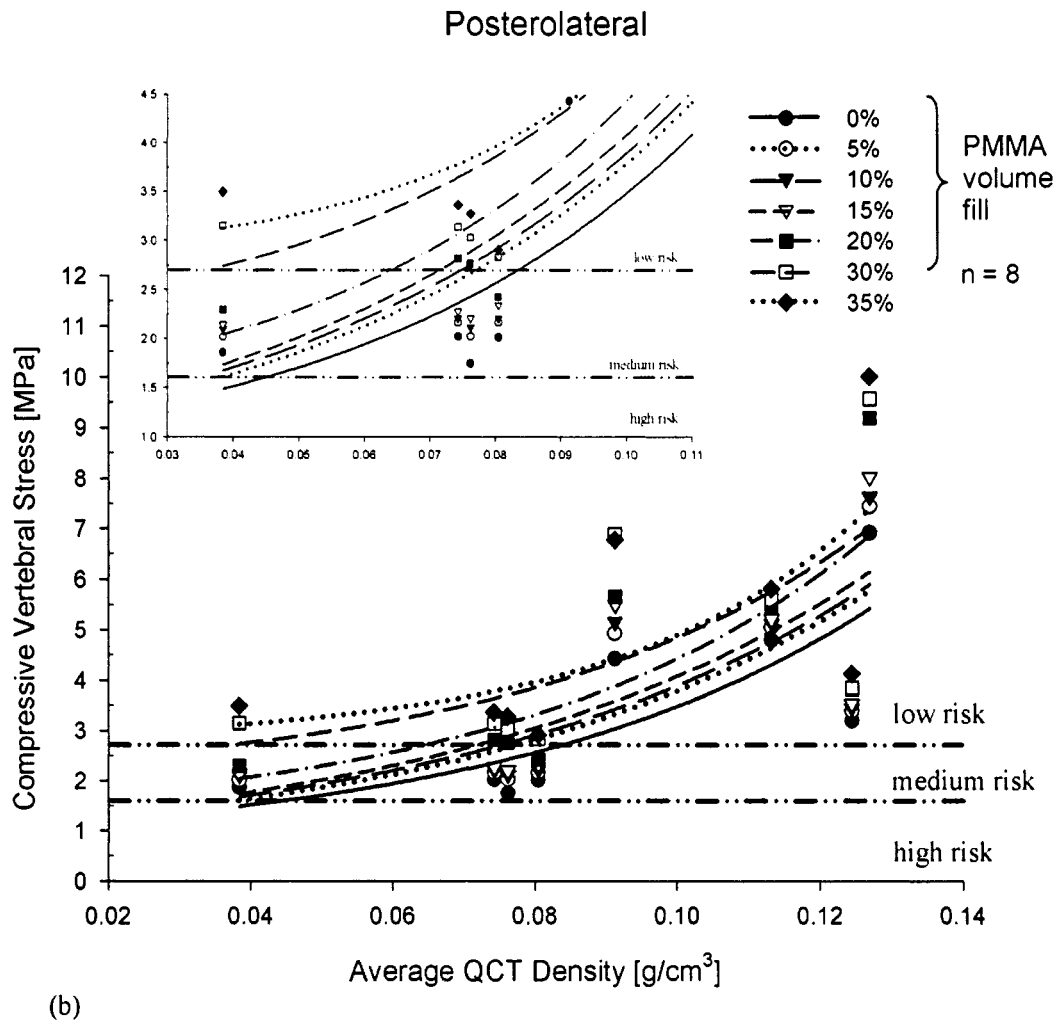


Figure 3-12: Variations in ultimate compressive stress of reinforced vertebral bodies with initial vertebral QCT density at 0%, 5%, 10%, 15%, 20%, 30% and 35% volume fill with PMMA for (a) bipedicular; and (b) posterolateral vertebroplasty. The three fracture risk groups defined by Biggeman et al.¹⁹: high risk group with ultimate stress < 1.6 MPa and fracture risk of 100%, medium risk group with ultimate stress from 1.6 to 2.7 MPa, and low risk group with ultimate stress > 2.7 MPa and fracture risk near 0%.

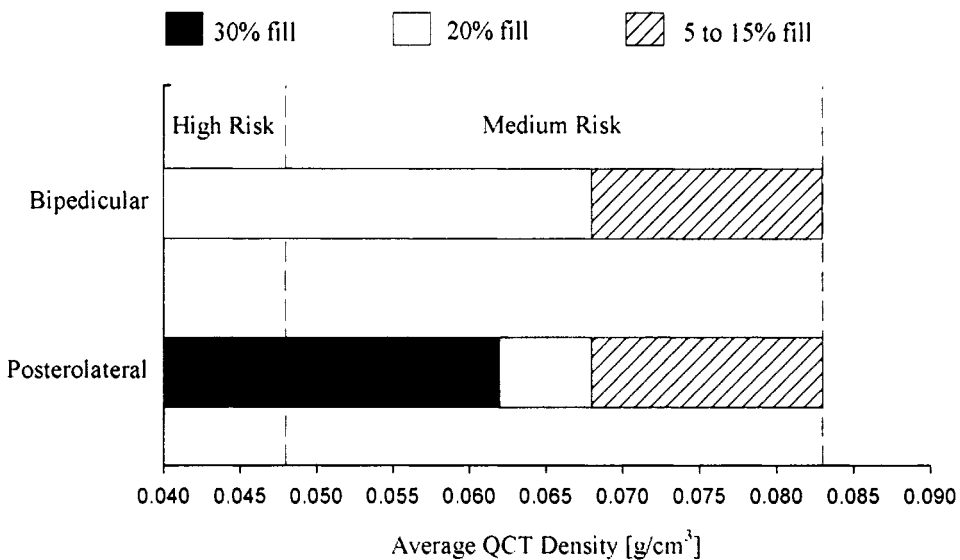


Figure 3-13: Biomechanically optimal poly(methylmethacrylate) (PMMA) volume fill relative to vertebral body volume required to reduce fracture risk to low levels for bipedicular and posterolateral prophylactic vertebroplasty ($n = 8$).

3.4 Discussion

The purpose of this study was to determine the effects of bone cement (PMMA) volume and placement, and initial bone density on prophylactic vertebroplasty of intact vertebral bodies. Vertebral stiffness and strength augmentation after virtual prophylactic vertebroplasty are influenced strongly by both bone density and volume fraction of the implanted cement, and least affected by the placement of PMMA. The stiffness and strength increases are directly proportional to PMMA filler volume. Greater augmentation effects were also observed for vertebral bodies with average QCT densities below 0.1 g/cm^3 , with even more pronounced effects as the bone densities decreased. For densities above 0.1 g/cm^3 , the mechanical augmentations are less dependent on bone density. These results agree closely with the *in-vitro* vertebral augmentation study performed previously^{53,58}, which also noted greater augmentation effect at lower initial

bone mineral density. In addition, for PMMA volumes higher than 20%, the stiffening and strengthening effects are greater for the bipedicular approach versus posterolateral. No significant differences were noted for lower cement volumes. Based on the results of this efficacy study, further information is furnished for developing guidelines as to the minimum volume of PMMA bone cement needed to improve the mechanical integrity of vertebral bodies at risk for fracture to low fracture risk levels. Vertebral bodies at high risk of fracture required at least 20% volume fill of PMMA for augmentation, while lower PMMA volumes are needed for the medium risk vertebral bodies. Between 5 to 15% and 20 to 30% fill are successful in achieving the desired strength improvements for vertebral bodies in the low and high spectrum of the medium risk range, respectively.

The findings of this study are plausible and realistic for a number of reasons. First, the use of finite element modeling allows the volume and distribution of bone cement to be controlled in an exact and precise manner not possible in cadaveric studies. In addition, the combined experimental and computational approach allows multiple analyses to be repeated on the same specimen, thereby eliminating biological variations. Second, the vertebral bodies were modeled using anisotropic elastic constants. Since bone is an orthotropic material with strong dependency of trabecular bone material properties on both mineral density and orientation⁴⁵, a more accurate model of bone behavior would be achieved if anisotropic material properties⁷¹ were used rather than isotropic material properties⁷⁷. Third, the specimen-specific finite element models were calibrated so that the predicted vertebral stiffness and strength corresponded to the experimentally determined values. This procedure provides a more accurate post-yield predictions compared to other models that assumed perfectly plastic yield properties for

trabecular bone⁷⁷ and that determined the cortical bone material properties from elastic modulus-density relationships^{39,56,106}. Finally, the definitions of fracture risk are based on vertebral strength values, rather than bone density. Although bone density has been adopted as the most common technique for vertebral risk assessment, studies have reported a substantial overlap in bone density measurements of individuals with and without osteoporotic fractures^{3,43,47,101}, demonstrating a low sensitivity of the criterion. Biggemann et al.¹⁹ found that fracture risk derived from density risk groups (normal, slightly osteoporosis, modest osteoporosis and severe osteoporosis) exhibits a wide overlap between the neighboring groups, while strength dependent fracture risk shows two clearly defined strength groups. High fracture risk (100% risk) when vertebral strengths are less than 3 kN and low risk (0% risk) when vertebral strengths are greater than 5 kN. Vertebral strengths between 3 and 5 kN are at an intermediate risk group. Therefore, based on a more precise definition of fracture risk, more accurate cement volume recommendations can be made.

A limitation in this study is that only the response of the reinforced vertebral bodies to monotonic, uniaxial compressive load is addressed. Vertebral bodies *in-vivo* experience more complex loading conditions (compression, shear and bending), which can lead to different types of fractures and fracture behavior. However, given the complexity of the system and that almost all of the experimental studies performed on vertebroplasty tested the augmented vertebrae specimens under uniaxial compression, the uniform compressive loading condition simulated is considered adequate for the purpose of providing insight into the biomechanics behind the procedure.

Optimization of vertebroplasty is vital for the technique to be both safe and biomechanically effective, especially when the procedure is to be redirected as a prophylactic treatment for osteoporotic vertebral bodies at risk for fracture. The results of this study offer some possible improvements to the current clinical procedure, which is based solely on the discretion of the orthopedic surgeon. This study suggests that although PMMA is able to provide sufficient strengthening effect to reduce the fracture risk of vertebral bodies from high to low, at least 20% PMMA fill is required to reinforce high risk vertebral bodies. Since this volume is typically the amount used clinically, the risk of complications will be as high as that for current vertebroplasty procedure for fracture repair. Therefore, alternative materials have to be investigated for use on vertebral bodies at high risk of fracture. However, since there are no immediate suitable substitutes available, PMMA may still be used for vertebral bodies at the low spectrum of the medium fracture risk zone since only 5 to 15% fill of PMMA is needed, which is less than the current volumes used clinically. With regards to cement placement, bipedicular vertebroplasty is biomechanically more efficient due to its higher strengthening effect and safer due to easier surgical access than the posterolateral case.

3.5 Conclusion

Prophylactic vertebroplasty is able to reduce vertebral fracture risk from high to low using at least the same volume of PMMA that is currently used for fracture repair, which has up to 67% incidence cement leakages^{37,73}. Since this procedure is intended as a preventative treatment before fractures occur, the danger to patients from complications arising from the cement leakages is too high. Stronger bone cements was therefore

modeled in the next Chapter to determine if greater mechanical enhancements could be achieved, which could mean smaller and safer PMMA volumes.

3.6 Acknowledgements

Financial support for this work was provided by the Whitaker Foundation. The authors thank David Kopperdahl, PhD, for providing the experimental data; Tony M. Keaveny, PhD and W.S. Rosenberg, MD for their contributions; and Elizabeth Leister for helping to write some of the computer programs.

Chapter 4

OPTIMIZATION OF BONE CEMENT PROPERTIES FOR VERTEBRAL REINFORCEMENT

Finite element models of whole vertebral bodies were used in this study to ascertain the mechanical augmentation effects of bone cement material properties on vertebrae at risk for fracture and ultimately determine the biomechanically optimal cement material properties for vertebral reinforcement. Greater vertebral strength reinforcement than that provided by poly(methylmethacrylate) (PMMA) is needed to reach low fracture risk levels with reduced volumes of bone cement. However, the amount of vertebral strength enhancement achieved is limited to that of PMMA. Also, at the maximum achievable vertebral strength increase, high stress concentrations in the trabecular bone areas immediately above and below the cement are created. These stress concentrations lead to an increase risk of fracture within the treated vertebra itself and possibly to the untreated adjacent vertebrae as hypothesized in previous numerical studies^{12,96}. Therefore, both maximum vertebral strength augmentation and minimal intravertebral stress concentrations can not be achieved simultaneously with any bone cement material properties using the current cement placement. In light of this new information, additional variables such as distribution patterns of bone cements within the vertebra need to be explored.

4.1 Introduction

Vertebroplasty is a minimally invasive, radiographic procedure involving the percutaneous injection of a bone cement into either a collapsed vertebral body for fracture repair to achieve pain relief through mechanical stabilization or intact osteoporotic vertebrae to reduce fracture risk as a means of reinforcement. Currently, PMMA is the only available cement with reports of clinical application in spinal repair and reinforcement, though not approved by the Food and Drug Administration (FDA) for this procedure. The FDA even issued a warning recently about the numerous side effects, such as nerve root compression and pulmonary embolism, linked to the high incidence of PMMA leakage in the treatment of spinal fractures ⁴. These concerns, along with other PMMA shortcomings, including non-biodegradability, barrier to bone remodeling, damage to neighboring tissue due to drastic temperature increase from polymerization ^{38,104}, and possible provocation of fractures in the adjacent vertebrae ^{12,18,46,96,117}, make the acrylic cement unsuitable for use in vertebroplasty, especially as a prophylactic treatment. As a result, alternative bone substitutes to replace PMMA need to be investigated.

The success of the bone strengthening technique relies heavily on the mechanical properties of the augmentation material. The injected cement must have sufficient strengthening effect to increase the strength of the augmented vertebrae to low fracture risk levels in order to prevent future fractures (results from Chapter 3). Additionally, the risk of adjacent vertebral fractures must also be minimized. It is believed that the PMMA bone cement causes alterations to the distribution of forces to the adjacent vertebrae, which result in increased risk of fracture in the neighboring vertebrae ^{12,96,114}. So as to

prevent fractures in adjacent vertebrae, load transfers as indicated by high stress concentrations must be kept to a minimal. Therefore, the aim of vertebral reinforcement for fracture prevention is to achieve maximum strength augmentation, while minimizing stress concentrations within the vertebra.

The goal of this study was to determine the effects of bone cement material properties on the global and internal biomechanics of the treated vertebrae and ultimately establish the biomechanically optimal cement material properties for vertebral reinforcement. Experimentally validated and anatomically detailed, specimen-specific computer models developed from quantitative computed tomography (QCT) scans were used in order to minimize biological variability. Bipedicular vertebroplasty was simulated using 20% volume fill of cement with a wide range of material properties. The differences in the overall structural behavior of the vertebral body models virtually implanted with bone cements of varying compressive elastic moduli and strengths were evaluated. Optimal cement properties were determined when goal of vertebral reinforcement was reached, i.e. maximum vertebral strength increase and minimum intravertebral stress concentrations.

4.2 Methods

Eight specimen-specific finite element models of human vertebral bodies (L1-L4; mean age = 71.1 ± 10.7 ; 6 females, 2 males; mean QCT density = $0.091 \pm 0.03 \text{ g/cm}^3$) that had previously been calibrated to experimental results⁷¹ and were used in Chapter 3 were used again in this study. Bipedicular vertebroplasty was modeled since it is the most commonly performed vertebroplasty approached due to its ease of access to the anterior

vertebral body through the pedicles (Figure 4-1). This approach has also been shown to offer greater mechanical augmentation (results from Chapter 3) and stability⁷⁰ than other approaches. The average volume of cement used clinically, 5 cm³ corresponding to approximately 20% fill of cement to whole vertebral body volume, were virtually implanted¹⁶. Nine different material properties of bone cement, based on 1%, 10%, 50%, 100% and 150% of the compressive elastic modulus and strength of PMMA, were investigated (Table 4-1). The plastic material definitions of the 9 cements were identical to that for PMMA, which were derived from six points specified along the post-yield compressive behavior of PMMA⁸² (Figure 3-8).

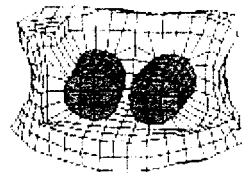


Figure 4-1: Finite element mesh of a vertebral body with two bone cement capsules (shaded) simulating bipedicular vertebroplasty.

Table 4-1: The nine different bone cement material properties (M1 to M9) investigated were based on the compressive elastic modulus and strength of PMMA.

Modulus (MPa)	Strength (MPa)	1.13 (1%)	11.3 (10%)	56.5 (50%)	113 (100%)	170 (150%)
25 (1%)					M6	
250 (10%)					M7	
1250 (50%)					M8	
2500 (100%)	M1	M2	M3	M4 (PMMA)	M5	
3750 (150%)				M9		

A total of 80 simulations, 10 cases (1 untreated + 9 treated with defined cement properties) per vertebral body, were analyzed. A uniform compressive displacement was applied to the top of the vertebral body model in order to duplicate experimental loading conditions. The finite element solver ABAQUS version 5.8 (Hibbit, Karlsson and Sorenson, Inc., Pawtucket, RI) was used to perform non-linear analysis simulating uniaxial compression to predict the stiffness and fracture load of the treated and untreated vertebral body models. Vertebral stiffness was determined from the slope of the first linear portion of the predicted load-deformation curve, while fracture load was obtained from the peak of the curve. The variations of vertebral compressive stiffness and strength reinforcements with bone cement elastic modulus and strengths were scrutinized. The internal stress and strain within the each vertebral body model when applied with the simulated ultimate load of the untreated vertebral body before and after treatment were compared. Optimal cement properties were determined when maximum vertebral strength increase and minimum intravertebral stress concentrations were achieved.

4.3 Results

4.3.1. Effect of Cement Strength

Strength of bone cement had no influence on vertebral stiffness, but it did have an augmenting effect on vertebral fracture load (Figure 4-2). For cement strengths below 5 MPa (equivalent to strength of the surrounding trabecular bone), the treated vertebral fracture loads fell below that of the untreated since the bone cement was weaker than the trabecular bone. As the strength of the bone cement rose from 5 MPa to 30 MPa, the treated vertebral fracture loads were amplified to levels exceeding that of the initial

fracture load. Any increase in cement strength above 30 MPa resulted in no changes in the increase in vertebral fracture loads, which remained at an average of 46%. At that cement strength level, the bone cement was stronger than the trabecular bone, and as such failure always occurred in the same weakest area of the trabecular bone.

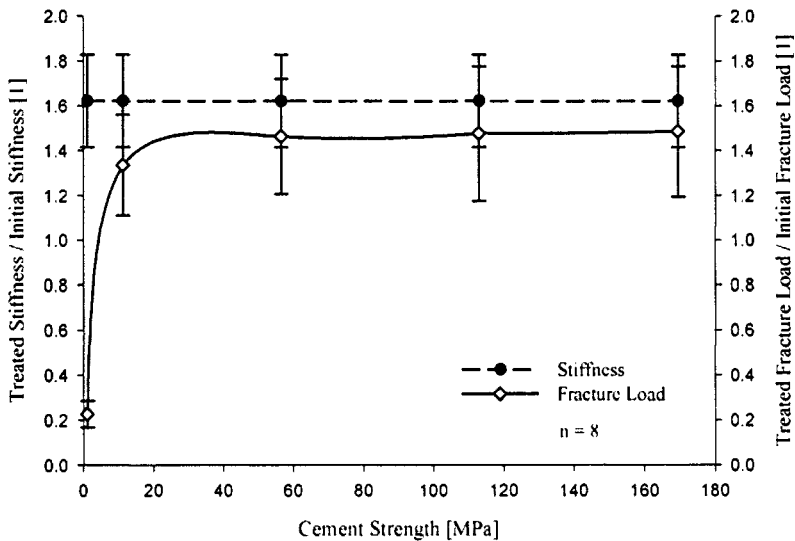


Figure 4-2: Effect of bone cement compressive strength on the average normalized compressive vertebral stiffness increase (treated stiffness / initial stiffness) and vertebral strength increase (treated fracture load / initial fracture load).

4.3.2. Effect of Cement Modulus

Both vertebral stiffness and fracture load were affected by the elastic modulus of the virtually implanted bone cement (Figure 4-3). When the bone cement modulus dropped below that of the surrounding trabecular bone (< 300 MPa), the treated vertebral stiffness was reduced to lower than the initial stiffness. As the cement modulus rose above 300 MPa, a gradual increase in vertebral stiffness was observed. This behavior is due to a shift of the load applied towards the stiffer cement and away from the softer trabecular bone, resulting in an increase in vertebral stiffness (see Appendix). In addition,

the shift in load distribution contributed to the increase in vertebral fracture load as the stronger bone cement now bear a majority of the applied load. A maximum of 44% average increase in fracture load was reached with cement modulus greater than 1300 MPa. The plateau attained in fracture load augmentation was again attributed to failure always occurring at the same weakest area of the trabecular bone.

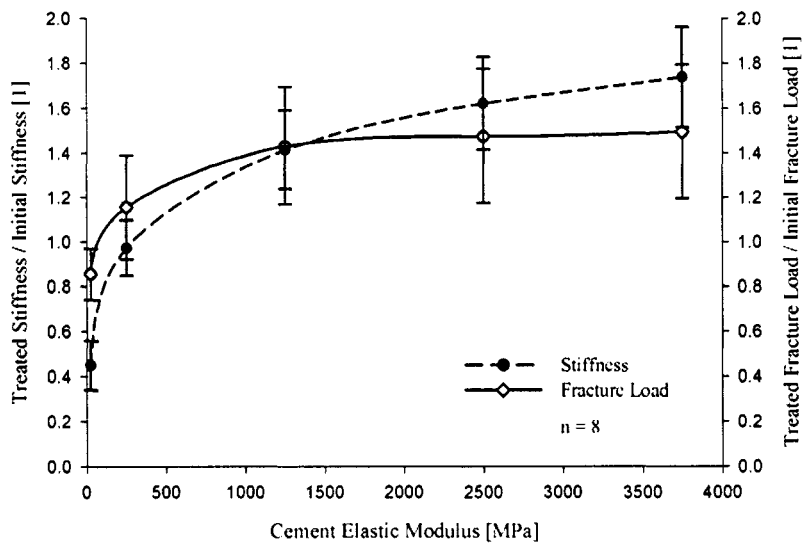
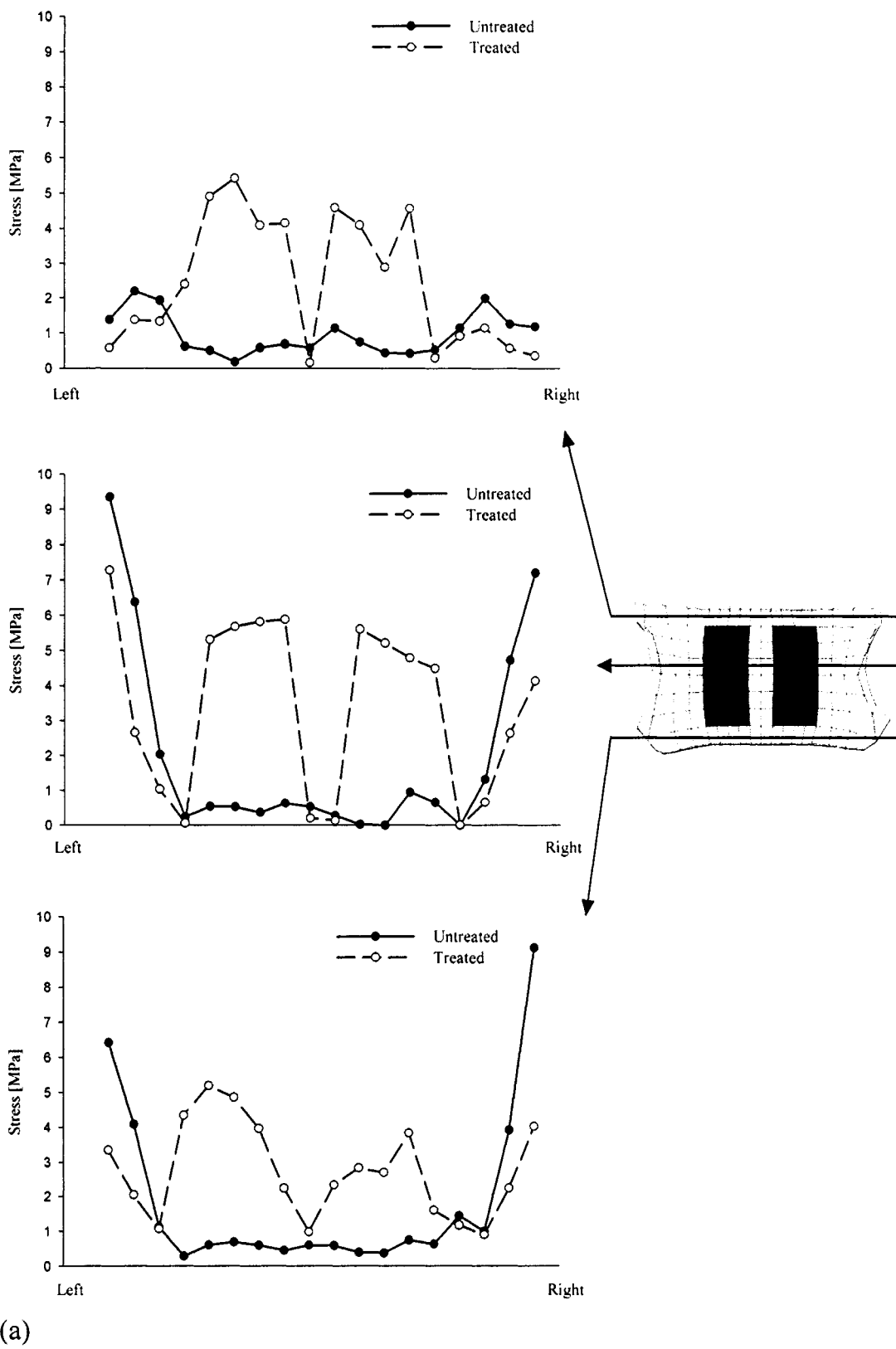


Figure 4-3: Effect of bone cement compressive elastic modulus on the average normalized compressive vertebral stiffness increase (treated stiffness / initial stiffness) and vertebral strength increase (treated fracture load / initial fracture load).

4.3.3. Intervertebral Stresses and Strains

For all of the treated models with the same material properties as PMMA, regions of high strains were found to be localized in areas above and below the virtually implanted PMMA within the reinforced vertebral bodies (Figure 4-4). These peaks were absent for the untreated models at the same locations, although sharp spikes in strains were noted at the areas where the PMMA would have been implanted, which implied damage in the un-reinforced areas. These results indicate that there was a shift in the

applied load towards to the stiffer PMMA regions, away from the surrounding trabecular bone. As such, the load was centered along the longitudinal axes of the injected PMMA, creating a stress concentration in the areas above and below the cement (Figure 4-4). This behavior confirmed previous findings where the rigid PMMA cement appeared to act as an “upright pillar”¹², which amplified the stress applied in their locale. The cement inhibited the deflection of the endplates inwards into the treated vertebrae during compression. The incompressible intervertebral discs were therefore forced into the adjacent vertebrae, resulting in a significant inward bulge of the endplate of the adjacent vertebra^{12,96}. Thus, the chain of events stemming from the shift in load distribution due to the PMMA cement may ultimately lead to the adjacent vertebral fractures (Figure 4-5).



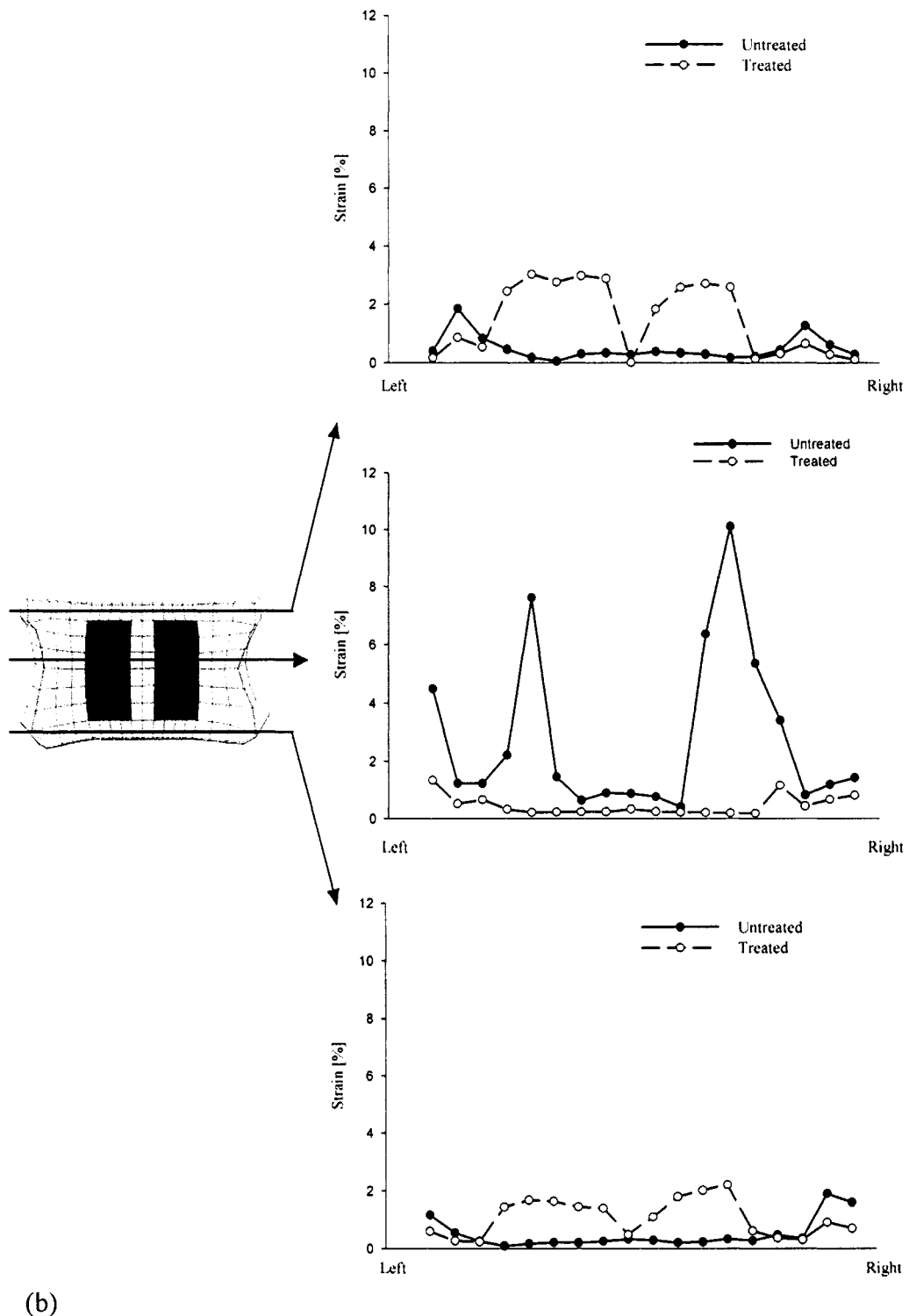


Figure 4-4: (a) Stress and (b) strain distributions within a frontal section of an osteoporotic vertebra before and after treatment with 20% volume fill of PMMA (shaded).

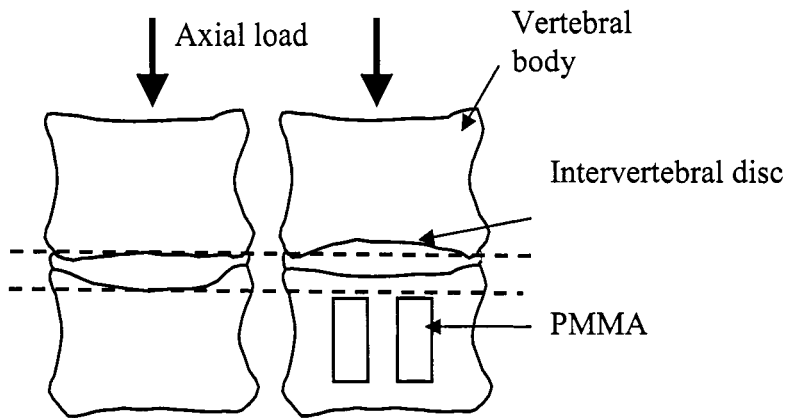


Figure 4-5: Illustration comparing the extent of endplate deflection in the adjacent vertebra before and after cement augmentation with an axial load applied. Note: Degree of deflection is exaggerated for illustration purposes.

The intravertebral stress concentrations were only eliminated with cement modulus at 25 MPa (Figure 4-6). However, at such a low modulus, the treated vertebral strength actually dropped below that of untreated. Therefore using current methods of cement placement, it is impossible to achieve both desired strength increase and intravertebral mechanical compatibility.

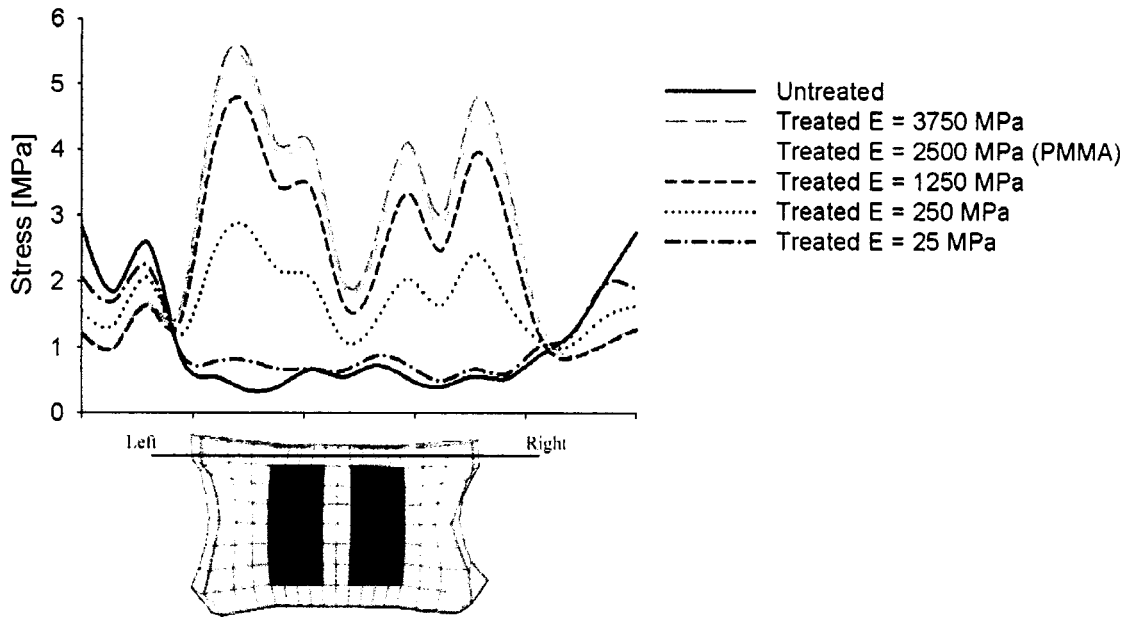


Figure 4-6: Intravertebral stress profiles of the trabecular bone elements above the implanted bone cement at varying moduli. Only at very low bone cement modulus were the internal stresses comparable to the untreated model.

4.4 Discussion

The objective of this study was to determine the biomechanically optimal bone cement material properties that can achieve the biomechanical goal of prophylactic vertebral reinforcement by reaching maximum vertebral strength increase and minimum intravertebral stress concentrations. This fortification criterion aims to prevent subsequent fractures by reducing the risk of fracture to the treated and the adjacent vertebrae. Unfortunately, no bone cement material properties are able to achieve the desired biomechanical goal. The vertebral strength increase topped out at only 30 MPa cement strength and 1300 MPa cement stiffness, which is at the same level of increase as PMMA cement. However, according to the results from the previous study in Chapter 3, greater vertebral strength enhancement is needed for 20% volume fill of cement than that from

PMMA so that less cement volume is required to reduce fracture risk to low levels, thereby lowering risk of cement leakages. Furthermore, cement properties that results in maximum vertebral strength increase also causes high intravertebral stress concentrations. Only at low cement stiffness of 25 MPa were these internal stress concentrations eliminated. The limited vertebral strength augmentation and presence of intravertebral stress concentrations make it impossible to determine optimal cement material properties. In light of this new information, additional variable such as distribution patterns of bone cements within the vertebra need to be explored.

Previous attempts at determining the most suitable bone cement for vertebroplasty consisted of *in-vitro* studies that only examined the differences in mechanical augmentations of vertebrae injected with a new bone cement compared to one filled with PMMA^{10,15,17,55,72}. For these studies, at least 20 specimens were required to demonstrate a statistical distinction between augmentations with the two cements. To investigate the differences between more cements of varying material properties, an even larger number of specimens would be needed. The large number of samples required for testing is due to biological variability in cadaveric specimens, which can be eliminated using computational approach since multiple analyses can be repeated on the same specimen. Another benefit of computer modeling is that the volume and distribution of the bone cements could be controlled in an exact and precise manner not possible in cadaveric studies. This feature enabled any discrepancies in mechanical augmentations to be attributed solely on the different material properties of the implanted bone cements.

In addition to cement material properties, volume and placement, the effectiveness of the vertebroplasty treatment is also influenced by the bone mineral

density of the vertebrae with greater augmentation effect at lower bone density^{53,58,109}.

With the wide variation of mean bone density in the vertebral body models, ranging from 0.038 to 0.127 g/cm³, it is not surprising to note the relatively high standard deviations, approximately 17%, in the results of this study.

The finite element modeling technique employed generated accurate virtual replications of the actual vertebral bodies, which produces plausible and realistic results. The models were developed based on QCT scans of the vertebral bodies, thereby incorporating the specific geometry and bone density distribution of each specimen. Since the density distribution within a vertebral body is not uniform, there are localized regions of low density and hence low strength, which are more susceptible to failure than other higher density areas. By defining the material property of each trabecular element in the finite element models based on the corresponding pixel value derived from the QCT scans, the exactly heterogeneity within the vertebral body is duplicated. The calibration of the trabecular bone and cortical shell and endplate material properties against experimental data also further improves the predictability of the models.

4.5 Conclusion

Higher degree of vertebral strength reinforcement than that reached with PMMA can not be achieved by increasing cement material properties alone. Cement modulus that results in maximum vertebral strength increase also leads to high intravertebral stress concentrations, which are believed to cause fractures to the untreated adjacent vertebra by endplate failure. This vertebroplasty-induced endplate failure mechanism was tested experimentally in the next chapter by determining whether vertebrae adjacent to treated

ones fracture at their endplates and at a lower compressive load compared to the untreated vertebrae. The importance of the intravertebral stress concentrations as a criterion for biomechanical success of vertebroplasty was evaluated based on the results from the subsequent *in-vitro* cadaveric experiment.

4.6 Acknowledgements

Financial support for this work was provided by the Whitaker Foundation. The authors thank David Kopperdahl, PhD, for providing the experimental data; Tony M. Keaveny, PhD and W.S. Rosenberg, MD for their technical contributions; and Elizabeth Leister for writing some of the computer programs.

Chapter 5

PREMATURE ADJACENT VERTEBRAL FRACTURE AFTER VERTEBROPLASTY

This cadaveric study experimentally determines whether vertebroplasty lowered the fracture strength of adjacent untreated vertebrae under physiological loading conditions. There are increasing incidences of fractures in the untreated adjacent vertebrae after vertebroplasty. These secondary fractures have been hypothesized to be the end result of high stresses generated within the treated vertebra. The stress concentrations are believed to lead to the inward endplate deflection of the adjacent vertebrae, which increases their risk for fracture. Others believed that the fractures are simply due to the progression of osteoporosis. To investigate this possible effect of vertebroplasty, untreated and PMMA treated three-level spinal segments from six spines were tested under unconstrained axial compression where shear forces and bending moments were minimized using a 6 Degrees-Of-Freedom robotic arm. Fracture strengths of the spinal segments before and after treatment were compared and radiographic X-rays were taken at every 600N increments to record the development of fracture. Five of the six treated segments experienced reductions in fracture strengths. Biconcave fractures produced by failures at the endplates were observed in the treated specimens as predicted by the hypothesized vertebroplasty-induced fracture mechanism, while wedge fractures were mostly seen in untreated controls. The increase risk of fracture to the untreated adjacent vertebrae after vertebroplasty using PMMA is therefore demonstrated.

5.1 Introduction

Vertebroplasty is a minimally invasive treatment for osteoporotic vertebral fractures involving the injection of an acrylic bone cement, PMMA, into a collapse vertebral body. The procedure has been gaining popularity due to its success in alleviating pain and restoring mobility^{30,31,37,62,78,122}. It is believed that the hardening of the injected cement inhibits the painful micromotion at the fracture site, thereby stabilizing the microfractures^{13,14,38,114}. However, despite the clinical success, up to 20% of patients with repaired vertebrae are expected to sustain further fractures^{75,117}, with approximately 67% of the new fractures occurring in the vertebrae adjacent to the one that was treated¹¹⁷.

The cause of adjacent vertebral fractures is still controversial. Some researchers have attributed the treatment itself to be the cause since the introduction of a much stiffer material into the vertebral body would altered distribution of forces along the spinal column, especially to the nearby vertebrae¹¹⁴. Others credited the increased risk of collapse simply to the progression of osteoporosis, with the adjacent bone being the next weak link, in addition to an increase in patient activity level after a pain-relieving vertebroplasty. Retrospective reviews of vertebroplasty clinical studies have some studies showing higher incidences of fractures in the adjacent vertebrae^{32,46,117,125}, while others demonstrated no statistical difference between patients who experienced fractures with and without vertebroplasty^{51,60}.

Biomechanical analyses into the effects of vertebroplasty have also yet to offer a conclusive explanation. Through finite element analyses of vertebroplasty, a fracture mechanism was proposed where a shift in the applied load towards to the stiffer PMMA

regions, away from the surrounding trabecular bone, creates high stress concentrations in the areas above and below the cement of the treated vertebra^{12,65,96,110}. The presence of the cement inhibits the inward deflection of the endplates of the treated vertebrae during compression. As a result, the incompressible discs bulge inwards into the endplate of the adjacent vertebrae, which may increase its risk of fracture. However, this mechanism was opposed by another finite element analysis, which reported to have found no significant increase in strains in the adjacent vertebra¹¹⁹. There have been also *in-vitro* studies that had shown that fracture strength and cortical strains of adjacent vertebrae was lowered¹⁸ and higher⁶³ respectively, after vertebroplasty.

Despite the conflicting results, all the biomechanical studies had one common thread – the uniaxial compression and/or flexion loading conditions applied were not physiological. The vertebrae *in-vivo* is kept upright via an intricate system of muscles, tendons and ligaments attached to each vertebra, which is primarily subjected to compressive forces, with superimposed bending in the sagittal plane and torsion around the vertical axis of the spine in order to maintain equilibrium⁴⁸. Since these ligamentous forces all act about the centers of rotation located within each intervertebral disc to maintain balance, the resultant axial compression force always acts orthogonal to the transverse plane of each vertebra, tracing out the curvature of the spine⁹³⁻⁹⁵ (Figure 5-1). Although the traditional uniaxial compression is also applied perpendicular to the transverse plane, extra shear forces and bending moments are generated as a result of the asymmetrical and non-uniform bone density distribution of the vertebrae. Due to the fixation of the specimen in the compression device that only permits movement in one axis, the vertebrae is unable to react to these additional forces, thereby constrained. Such

restrictions do not exist *in-vivo* and the vertebrae plus its surrounding muscles and ligaments are free to counter the extra forces. In order to duplicate the *in-vivo* loading conditions, unconstrained axial compression was provided by a six degrees-of-freedom (DOF) industrial robotic that is free to move in all directions independently¹¹².

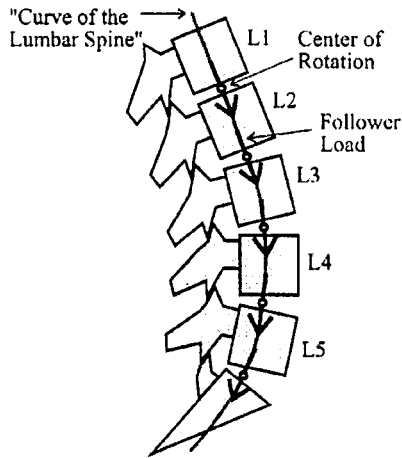


Figure 5-1: The resultant compressive load from the action of muscles, ligaments and body weight follows the curvature of the spine, passing through the centers of rotation of each segment⁹⁴.

The objective of this study was to determine whether vertebroplasty contributed to the reduction in fracture strength of adjacent untreated vertebrae under physiological loading conditions. A unique “worse-case-scenario” vertebroplasty case was generated by treating the top and bottom vertebrae of a three vertebral level segment, while leaving the middle vertebra untreated. This so-called “pincher effect” is expected to have the greatest affect on the adjacent vertebra. The treated and untreated control spinal segments were loaded incrementally stepwise under unconstrained axial compression and radiographic X-rays were taken at specific load intervals. Fracture strengths of pre-treated lumbar segments were predicted by assuming constant fracture stress along the spinal column

and were compared to post-treatment values, along with the fractures types from the X-rays.

5.2 Methods

5.2.1. Experimental Design

Twelve three-level spinal segments were prepared from the lumbar and thoracic regions of six human spines (mean age = 73.3 ± 3.2 , all male). The segments were divided into 2 groups, treated and untreated, such that no two segments from the same donor shared the same group. This type of grouping allows the differences in fracture load before and after vertebroplasty on the same vertebra to be calculated by testing it only once. Within the same spine, the compressive strength of lumbar vertebra increases caudally from the thoracic region to the lumbar region, but the ultimate stress throughout the spinal column remains relatively constant as the ultimate loads are normalized by endplate cross-sectional area ¹⁰⁸. Bone density also affects vertebral strength although they vary little within the same spine ¹⁹. The compressive stress and thereby strength of the vertebra at any level can be predicted once the strength of another vertebra in the same spine is known. Therefore for each spine, the strength of the middle vertebra in the treated group prior to vertebroplasty was estimated and subsequently compared to the experimentally measured strength of the same vertebra after vertebroplasty. Furthermore, all of the six L1-L3 segments were assigned to the treated group while the six T10-T12 segments were in the untreated control group. Since the strength of lumbar vertebra is higher than thoracic, any adverse effect of vertebroplasty will be clearly indicated by fracture strengths similar to or lower than that of the untreated thoracic segments.

Additionally, by exclusively treating only the lumbar vertebrae with the same volume of bone cement, the percent volume fill of PMMA will stay relatively constant, thereby eliminating the effect of cement volume.

5.2.2. Specimen Preparation

Six cadaveric spines were scanned with quantitative computed tomography (QCT) using a clinical scanner to ensure that there were no signs of radiographic abnormalities and also to provide a means to accurately calculate endplate areas. A K₂HPO₄ phantom (Mindways Software, Inc., San Francisco, CA) was included in each scan to convert CT numbers in Hounsfield units to bone mineral density in g/cm³. In preparation for vertebroplasty, the specimens were thawed overnight at room temperature and muscular and fatty tissues were detached from the vertebrae. The ligamentous structures, facet joints, transverse and posterior processes were left intact.

5.2.3. Vertebroplasty

To elucidate the maximum effect of vertebroplasty on adjacent bone strength reduction, the top and bottom vertebrae of specimens in the treated group were injected with 10 cm³ of PMMA (Simplex P; Stryker-Howmedica-Osteonics, Kalamazoo, MI) using a direct injection approach (Figure 5-2). This procedure created a “pincher effect” on the middle vertebra. In this bilateral, transpedicular approach, a 11-gauge vertebroplasty needle was placed into the center of each pedicle and advanced halfway into the vertebral body. The cement while fluid was poured into syringes attached to the

vertebroplasty needle and injected into each pedicle. The flow of PMMA within the vertebral body was monitored under fluoroscopy.



Figure 5-2: Fluoroscopic X-ray of the sagittal view of a vertebral segment treated at the top and bottom vertebrae with PMMA.

5.2.4. Mechanical Testing

After allowing the PMMA to cure for 24 hours in a 4 °C cooler, the spinal segments were permanently mounted, rostrally and caudally, in casting cement to secure its position with the horizontal alignment of the middle vertebra. Encasing the top and bottom vertebrae in cement also prevented any radial expansion through Poisson's effect, ensuring fracture only in the middle vertebra. After another 24 hour curing time, the entire assembly was positioned such that the top vertebra was mounted to a 6 DOF Force/Torque transducer (Omega-160, ATI Industrial Automation), which in turn was attached to the end of a 6 DOF industrial robotic arm (KUKA-150, KUKA Robotics Corporation) using a custom made connector. The bottom vertebra was rigidly fixed to another 6 DOF Force/Torque transducer¹¹² (Figure 5-3).

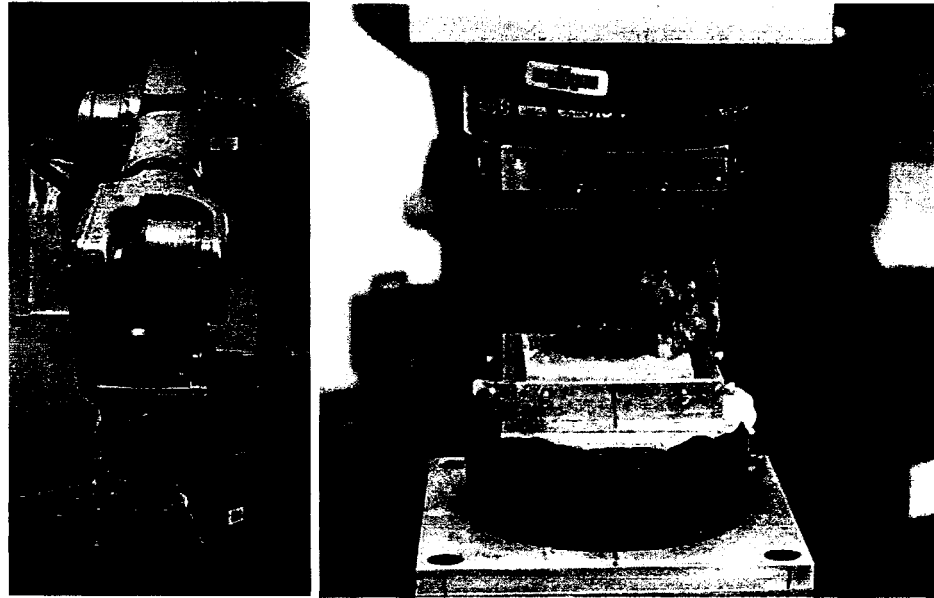


Figure 5-3: Experimental setup to apply unconstraint axial compression to the spinal segments using a 6-DOF robotic arm (left). A close-up view of the spinal segment (right).

The KUKA-150 is a six-axis electromechanical industrial robot with six articulated kinematics joints for all point-to-point and continuous path controlled tasks. The wrist is provided with a mounting flange for the attachment of end-effectors. Each axis is driven by a transistor-controlled, low-inertia servomotor. The system has a linear displacement resolution of 0.005 mm (with position repeatability of 0.2 mm) and angular displacement resolution of 0.1° under maximum payload of 5600 N. The force/torque transducers are capable of measuring the forces and moments in all three axis with forces up to 45,000 N in vertical axis and 15,000 N in transverse directions (with resolution of 0.005 N). The maximum allowable torque of each transducer is 1500 Nm with resolution of 0.01 Nm in all three orthogonal axes.

In order to manipulate the forces acting only on the middle vertebra, the coordinate system of the robotic arm was transformed from the robot base to a virtual coordinate (neutral position) approximately at center height and 2/3 posterior of the

anterior centrum of the middle vertebral body. Each specimen was loaded stepwise at 100 N compressive vertical load increments. At each step, both shear forces (F_x and F_y) and moments (T_x , T_y , T_z) summed from the two load cells were minimized (~zero) by displacing the top of the vertebrae in x' and y' -directions and tilting in their planes (Figure 5-4). Load data were directly acquired from the transducers for every step using NI-PXI 1010 system (National Instruments, Austin, TX) and Matlab software (Mathworks version 6.5, Natick, MA). Linear and rotational displacements, based on the assigned virtual coordinate system of the robotic arm, were also recorded throughout the experiment. The fracture strengths for the treated and untreated spinal segments of the same spine were compared.

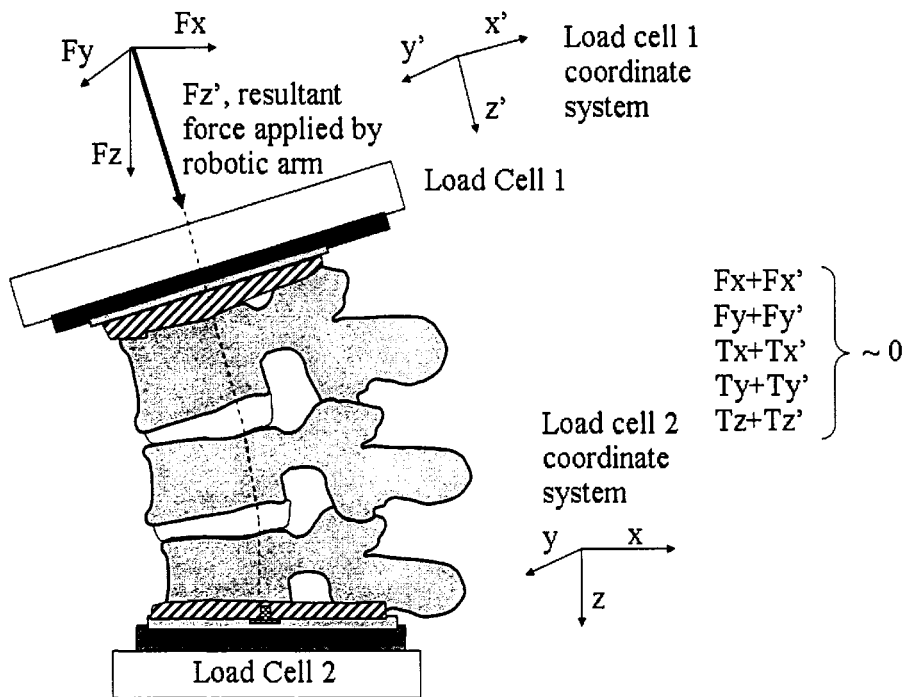


Figure 5-4: Illustrations of unconstraint axial compression where the sum of the shear forces (F_x and F_y) and bending moments (T_x , T_y and T_z) from the two load cells are minimized by displacing the top of the segment in x' and y' directions while applying load in the plane orthogonal to the top endplate (F_z').

5.2.5. Radiographic Imaging

Radiographs (X-ray) were taken during the compression test from sagittal plane of the spinal segments at every 600 N intervals using a Bowie portable X-ray unit (Bowie MFG. Inc., Lake City, Iowa). The alignment of the radiographic film and the distance to each segment were kept constant in order to maintain the same image resolution for all segments at all load intervals. The identification of the fracture types of each segment were made through examinations of the X-rays.

5.3 Results

The fracture strengths of the middle vertebra of the spinal segments were determined at the sharpest decrease in compressive load in the vertical axial load displacement curves. Prior to adjusting for the larger size of the lumbar vertebrae compared to the thoracic, four of the six treated lumbar segments had fracture strengths less than the untreated thoracic segment from the corresponding spine. Taking the different vertebral size into account by assuming constant fracture stress throughout the spinal column, the fracture strengths of the lumbar segments prior to treatment were predicted and subsequently compared to the treated group. Of the six segments that were treated, five of them showed reductions in fracture strengths ranging from 4.2% to 37.4% (Figure 5-5). Only one segment demonstrated an increase in fracture strength of 14.4%. Fracture strength reductions were statistically significant with 95% confidence using a paired T-test. Furthermore, within each of the six spines, the trabecular bone QCT densities of the thoracic and lumbar segments were comparable to each other (mean difference = 1.78%; range of difference = -10.6% to 13.7%). Therefore, bone density is

not a significant contributing factor for the reductions in fracture strengths after vertebroplasty.

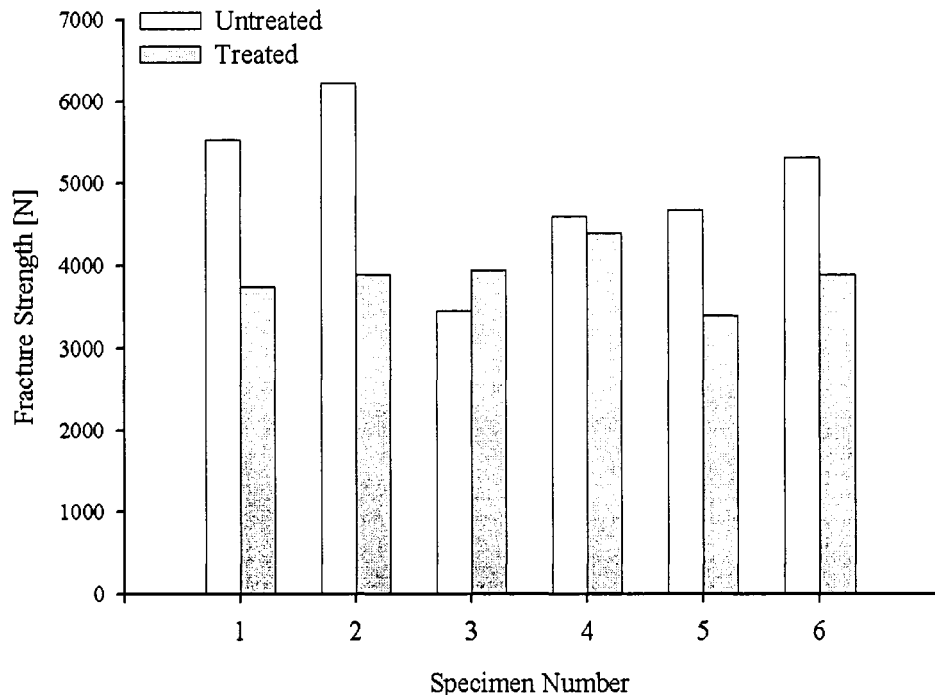


Figure 5-5: Paired comparisons between the fracture strengths of the untreated lumbar spinal segments predicted from the fracture stress of the untreated thoracic segments of the same spines and the experimentally tested treated lumbar segments. 4.2% to 37.4% reductions in fracture strength were observed except for Specimen #3 which had a 14.4% increase.

The untreated thoracic segments experienced all of the three main types of fractures. Three of them had wedge fractures, two had biconcave fractures and crush fracture was observed in one of them (Figure 5-6a). Five of the treated lumbar segments showed biconcave fractures, while no visible fractures were apparent at the X-ray resolution in one specimen (Figure 5-6b). The fracture strength, stress (strength normalized by endplate cross-sectional area), fracture types and QCT densities of all 12 spinal segments are tabulated in Table 5-1.

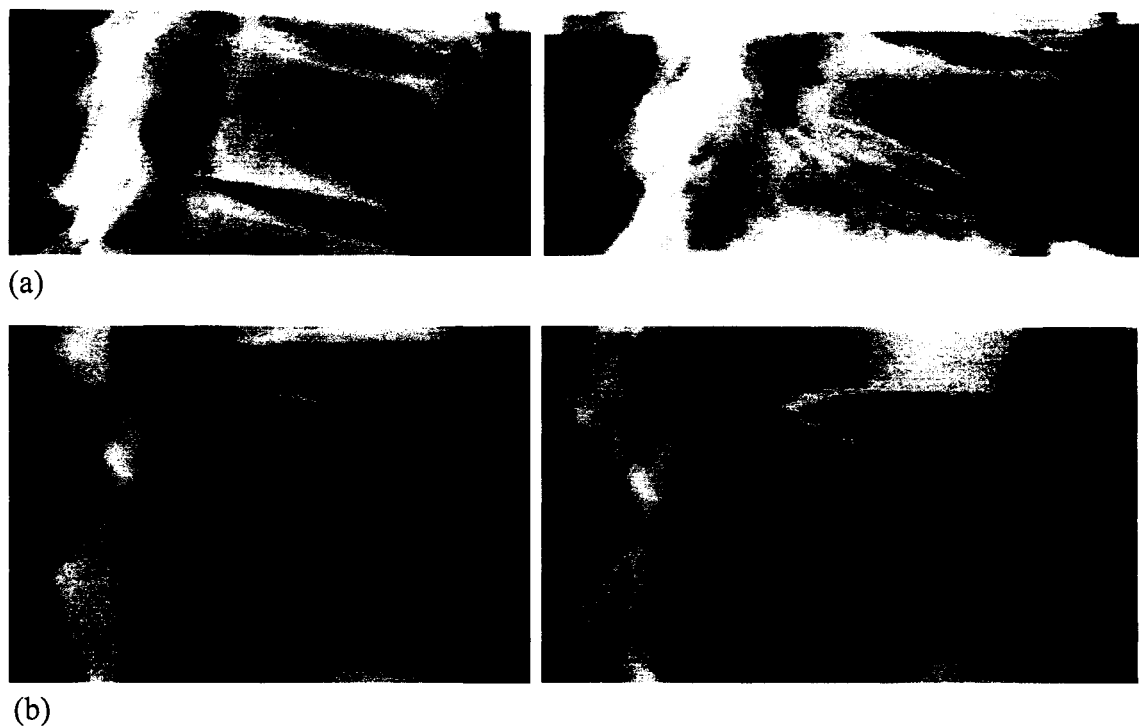


Figure 5-6: X-rays of the (a) untreated thoracic and (b) treated lumbar spinal segments when unloaded (left) and after reaching the fracture point (right). Crush type fracture occurred in the untreated thoracic segment, while in the treated lumbar segment of the same spine, biconcave fracture was observed.

Table 5-1: Summary of the experimentally determined fracture strength, stress, type and bone density for all the tested spinal segments

Specimen number	Spinal level	Group	Average QCT density [g/cm ³]	Fracture strength [N]	Fracture stress [MPa]	Fracture type
1	T10 – T12	Untreated	0.0822	3910	3.97	crush
2	T10 – T12	Untreated	0.0190	3908	2.43	biconcave
3	T10 – T12	Untreated	0.0863	3408	2.66	wedge
4	T10 – T12	Untreated	0.0963	3585	2.68	wedge
5	T10 – T12	Untreated	0.1071	3523	2.82	wedge
6	T10 – T12	Untreated	0.0075	3885	3.48	biconcave
1	L1 – L3	Treated	0.0844	3742	2.69	biconcave
2	L1 – L3	Treated	0.0164	3894	1.52	NV
3	L1 – L3	Treated	0.0884	3942	3.04	biconcave
4	L1 – L3	Treated	0.0947	4400	2.56	biconcave
5	L1 – L3	Treated	0.0952	3394	2.04	biconcave
6	L1 – L3	Treated	0.0083	3888	2.55	biconcave

NV = none visible

5.4 Discussion

The objective of this study was to determine whether vertebroplasty contributed to the reduction in fracture strength of the adjacent untreated vertebrae under physiological loading conditions. Five of the six spinal segments demonstrated reductions in fracture strengths after vertebroplasty. Additionally, the untreated segments experienced mainly wedge fractures with some biconcave and crush fractures, while only biconcave fractures were observed in the treated segments. Wedge, biconcave and crush fractures occur in all levels of the vertebral column, with wedge fractures being the most common and crush the least ⁵⁹. Therefore, the exclusivity of biconcave fractures in the treated segments and the more common wedge type fractures in only the untreated segments are indicative of the effect of vertebroplasty. This change in fracture pattern concurs with endplate deflection fracture mechanism proposed by Baroud et al. ¹² and Polikeit et al. ⁹⁶. Finite element models of two level spinal segments from the two previous studies showed that the presence of PMMA bone cement, with elastic modulus 30 times that of the surrounding apparent level trabecular bone, in the treated vertebra inhibits the inward deflection of the endplates during compression. As a result, the incompressible intervertebral disc pushes the adjacent vertebra endplate further inwards. The inward deflection of the adjacent vertebral endplate would appear as biconcave fractures if the top and bottom vertebrae were treated as shown in the present study.

Furthermore, Polikeit et al. ⁹⁶ noticed changes in the craniocaudal displacement of the spinal segment before and after vertebroplasty increased with increase of PMMA volume. This observation means that as the volume of PMMA increases, more trabecular bone near the endplates are replaced with PMMA, thereby further inhibiting endplate

deflection of the treated vertebra and restricting displacement during compression. The endplate of the adjacent vertebra, on the other hand, experiences greater deflection and hence a higher risk of fracture. This finding matches the results seen by Berlemann et al.¹⁸ who found lower failure loads to the adjacent vertebra with increased filling of PMMA cement.

Baroud et al.¹² and Polikeit et al.⁹⁶ had concluded in a connection between cement augmentation and adjacent vertebra fracture, while Villarraga et al.¹¹⁹ and Ananthakrishnan et al.⁶ interpreted no such link, even though all had reported similar results. The finite element models by Villarraga et al.¹¹⁹ and Polikeit et al.⁹⁶ showed larger areas of trabecular bone in the adjacent vertebra with high strains after treatment, especially near the endplate area closest to the treated vertebra. Additionally, the same magnitude increase in disc pressure after cement augmentation was seen in all the finite element models^{12,96,119}. The *in-vitro* study by Ananthakrishnan et al.⁶ that had actually measured the disc pressure after cement augmentation also observed a comparable increase for the same compression loading condition. Regardless, the 2 to 25% increases in disc pressure reported by all the studies maybe too small to have any contribution to the adjacent vertebral fracture mechanism. The slight changes in disc pressure maybe due to the differences in the material properties of the many components of the spinal segments.

Vertebroplasty is mainly used on fractured vertebrae, while its application as a prophylactic treatment is gaining popularity. The spinal segments tested in this study were not damaged prior to treatment in order to eliminate bone cement placement as a factor that may influence the results. Due to the different heterogeneous bone density

distribution within each vertebra, fracture location and severity will vary for each vertebra. In the study by Ananthakrishnan et al.⁶ where the middle vertebrae of three level spinal segments were fractured under flexion and compression prior to cement augmentation, various fracture patterns, locations and severity were observed. This variation will result in different cement placements, which according to the endplate deflection fracture mechanism - the closer the cement is to the endplates that share the intervertebral disc with the middle untreated vertebra of the segment, the greater is the deflection of the middle vertebral endplates inwards and higher its risk of fracture, will eventually lead to differences in adjacent vertebral fracture risks.

A limitation of this study is the unavailability of intervertebral disc quality data since disc degeneration affects the load distribution across the vertebral endplate and ultimately fracture strength and type^{1,22,49,97}. This added information may have helped to explain the aberrant results of the lone spinal segment, which showed an increase in fracture strength after vertebroplasty, as well as the one untreated segment that experienced a biconcave fracture rather than a wedge. Another limitation is the small number of spinal segments used. However, by performing paired comparisons between specimens of the same donor spine, biological variability is reduced as observed by the similar bone densities between the thoracic and lumbar segments of the same spine. Moreover, the purpose of this study was to show a trend of the effect of vertebroplasty treatment on the biomechanical properties of the spinal segments. The trends maybe less or more pronounced in other bone samples, but their tendencies would unlikely differ between specimens.

The uniqueness of this study is in the use of a 6 DOF robotic arm to apply unconstrained axial compression that closely duplicates physiological loading on the main loading axis of the vertebrae. The results are therefore the most realistic that can be obtained from an *in-vitro* cadaveric study. The treatment of both the top and bottom vertebrae of three level spinal segments magnifies the affect vertebroplasty had on the middle untreated vertebrae and helps to validate the endplate deflection fracture mechanism. It must be noted that even though the risk of fracture to the untreated adjacent vertebrae after vertebroplasty is higher, the amount it has increased depends on other factors like bone density, intervertebral disc quality, distribution and volume of the bone cement, and vertebral levels treated. The exact fracture mechanism has yet to be conclusively proven, but the hypothesized end affect of the stress concentrations observed in previous vertebroplasty-simulated models, including the ones in Chapter 4, on the fracture risk of adjacent vertebrae vertebral models is clearly demonstrated.

5.5 Conclusion

The distinct endplate fractures of the adjacent vertebrae after vertebroplasty observed experimentally concur with the hypothesized adjacent fracture mechanism from numerical studies where high stress concentrations within the treated vertebra are indicators of endplate deflection inwards into the adjacent vertebra, which increases their risk of fracture. Therefore, intravertebral stress concentrations must be minimized to reduce risk of adjacent vertebral fracture after vertebroplasty. The effect of distribution patterns of bone cements within the vertebra on the internal stresses was explored in the next chapter.

Chapter 6

EFFECTS OF CEMENT AUGMENTATION DISTRIBUTION AND MATERIAL PROPERTIES ON VERTEBRAL BIOMECHANICS

This study determines the effects of bone cement distribution patterns within the vertebral body as well as cement material properties on the intra- and extra-vertebral biomechanics. The compact distribution of poly(methylmethacrylate) (PMMA) within the vertebrae has been shown to cause stress concentrations in the bone tissue directly above and below the PMMA, which may lead to additional fractures of the already treated vertebrae and adjacent untreated ones. In order to minimize these stress concentrations, the differences in vertebral biomechanics after dispersed and compact cement filling were examined. A voxel-based finite element model of a L4 vertebral body was used to recreate the two fill patterns from two bone cements, CORTOSS and PMMA. The higher affinity of CORTOSS to bone tissue results in a more spatially dispersed distribution than PMMA. Greater vertebral stiffness reinforcement was observed with dispersed filling, which means that it requires a smaller volume of cement to achieve the same level of augmentation as with a compact fill, possibly reducing the risk of complications from cement leakages. The minimal intravertebral stress concentrations found with a dispersed cement fill may also indicate a lowered risk of subsequent fractures in the adjacent untreated vertebrae.

6.1 Introduction

The percutaneous application of a bone cement, specifically PMMA, to vertebral defects associated with osteoporotic vertebral compression fracture has proven clinical success in alleviating back pain ^{61,86}. Successful repair of the collapsed vertebrae was considered to have been achieved when strength is restored to pre-fractured values ¹⁶. Additional fractures could therefore be, theoretically, prevented if the spine was loaded to the same magnitude that caused the initial fracture. However, since 58% of osteoporotic vertebral fractures occur spontaneously during routine activities ²⁸, the loads experienced in subsequent fractures would easily equal or exceed that of the initial collapse. As a result, the fractured vertebrae need to be strengthened to “normal” or low fracture risk levels that enable sufficient support of weight-bearing dynamics ¹¹⁴. According to this improved success criterion, PMMA was unable to provide sufficient augmentation to reach low fracture risk levels without risking complications arising from cement extravasations (results from Chapter 3). Additionally, the compact distribution of PMMA within the vertebrae has been shown to cause stress concentrations in the bone tissue directly above and below the PMMA, which can lead to additional fractures of the already treated vertebrae and adjacent untreated ones (results from Chapters 4 and 5) ^{12,65,96}.

Conversely, a more dispersed filling of the vertebral body with cement is thought to be able to provide a more uniform structural reinforcement, alleviating the high stresses concentrations and their consequences. A new bone cement, CORTOSS (Orthovita, Inc., Malvern, PA) engineered specifically to mimic the strength characteristics of human cortical bone, has demonstrated greater dispersed fill within the

vertebral body than with PMMA (Figure 6-1). It is believed that the high affinity of the cement to bone is due to its synthetic combeite glass-ceramic particle composition, which makes the cement “spread itself out” in order to attain maximum contact with bone tissue. Similar to PMMA, CORTOSS is viscous and self-setting. However, unlike PMMA, CORTOSS allows direct bone apposition at the cement-bone interface, cures at temperatures 27°C lower than that for PMMA and is twice as strong and twice as stiff as PMMA⁹².

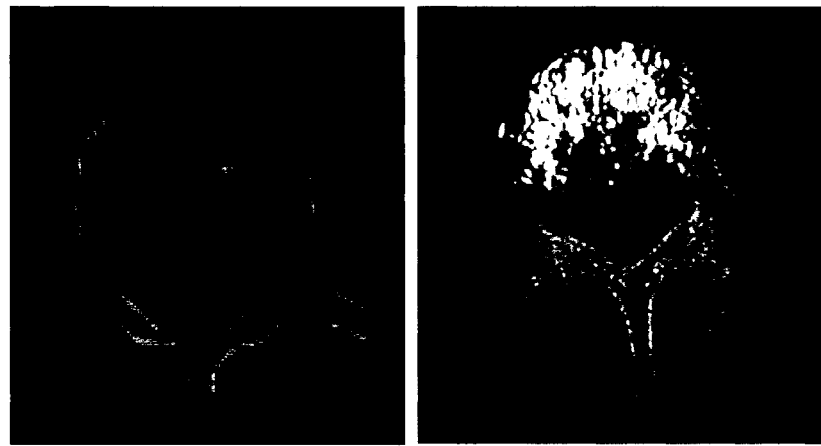


Figure 6-1: Quantitative computed tomography scans of vertebrae treated with PMMA and CORTOSS. The compact distribution of PMMA within vertebra (left) is distinctly different from the more dispersed distribution of CORTOSS (right).

The objective of this investigation was to determine the effects of cement distribution patterns within the vertebrae on the intra- and extra-vertebral mechanics. In order to study the natural distinct fill patterns of CORTOSS and PMMA, actual vertebrae treated individually with the two cements were used. However, since the material properties of the two cements are significantly different and vertebral specimen parameters like geometry, bone density and architecture all affect whole vertebral mechanics and intravertebral load distribution, computer models were employed to allow

cement properties to be equalized and to eliminate biological variability. Cement distribution patterns of both CORTOSS and PMMA were simulated on the same anatomically detailed, specimen-specific finite element model of a L4 human vertebral body. The benefit of repeated analyses also allowed additional studies into the sensitivity of bone cement material properties on the recovery of the biomechanical properties of the treated vertebra to be performed.

6.2 Methods

6.2.1. QCT Image Processing

A 90 year old female with compression fracture of the L4 vertebra was treated with bipedicular vertebroplasty using 3 cm³ of CORTOSS. Twenty-five post-treatment quantitative computed tomography (QCT) scans of 1.0 mm thick transverse cross-sections were obtained of the treated L4 vertebra using a clinical scanner (140 kV and 360 mAs). The QCT scans were rendered using the auto-thresholding feature in Analyze version 5.0 (AnalyzeDirect, Lenexa, KS) to remove the posterior elements and to set all non-bone tissues to zero pixel value (Figure 6-2). The removal of the posterior elements was done to duplicate *in-vitro* mechanical test settings where they are typically sawed off to allow plano-parallel ends for on-axis loading⁶⁸. The extraneous tissues were nullified for greater distinction between bone and non-bone tissue pixel values in order to ease automation of the voxel mesh generation process. Voxel-based finite element models were used in this study as higher mesh resolution is required to accurately simulate the different cement distributions and thereby evaluate their effects.

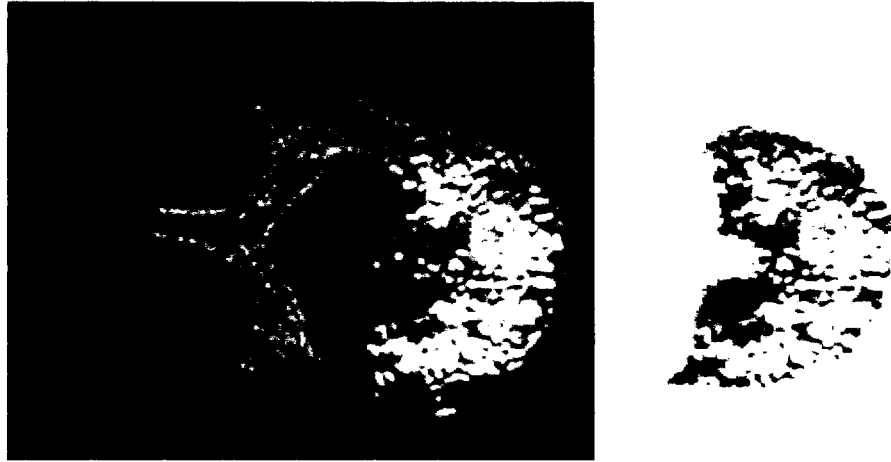


Figure 6-2: A quantitative computed tomography scan before (left) and after rendering (right) by auto-thresholding using Analyze to remove the posterior elements and to set the extraneous non-bone tissue to zero pixel value.

6.2.2. Voxel Model Generation

With the rendered QCT scans, 8-noded voxel based finite element models were generated automatically using custom C++ programs. Finite element solutions contain errors due to the idealization of geometry (discretization error) and displacement field (interpolation error) which had to be minimized⁹¹. To test the reliability of the model's predictions, a convergence study was performed to investigate the sensitivity of voxel model convergence characteristics on element size in terms of in-plane and axial (slice thickness) dimensions. Stiffness was selected as the output parameter to focus on since it has significant clinical relevance as an indicator of vertebral strength.

Based on the resolution of the original digitized QCT scans (0.3x0.3x1 mm), 5 different models of element size 0.9x0.9x1 mm, 1.2x1.2x1 mm, 1.5x1.5x1mm, 1.5x1.5x2 mm and 2.1x2.1x2 mm were developed by scaling the QCT slice images using regional averaging. For an example, the scaling for the 1.5x1.5x1 mm sized element was

performed such that within every 25 square pixels on the in-plane for each slice (5 pixels in the x and y axes), any pixel with value greater than zero were averaged. Similarly for the 1.5x1.5x2 mm sized element, only pixel values greater than zero within every 25 square pixels on the in-plane for every 2 slices for a total of 50 pixels were averaged. This criterion ensured that only bone tissue was averaged so that pixel values of the elements at the periphery of the vertebral body models would not be artificially lowered through the QCT image scaling process. The new averaged pixel values for each bone element in the 5 different element size models were subsequently used to determine the material properties of trabecular bone (see Material Properties section below).

PMMA casing cement with a modulus of 2,500 MPa and Poisson's ratio of 0.3, was virtually appended to the ends of the vertebral body model. A one element thick layer of the casting cement was added from the most protruding points at the top and bottom endplates. The spaces between those two layers and the concave contours of their respective endplates were also filled with casting cement elements. The flat and parallel outer surfaces of both casting cement layers ensured plano-parallel ends for on-axis loading. One element thick layer of metal, with modulus of 209 GPa and Poisson's ratio of 0.3, was also added after the casting cement following the *in-vitro* experimental conditions to ensure uniform displacement^{68,69} (Figure 6-3). The finite element solver ABAQUS version 6.4 (ABAQUS Inc., Pawtucket, RI) was used to simulate uniaxial compression under displacement control to predict the stiffness of the 5 different sized element vertebral body models.

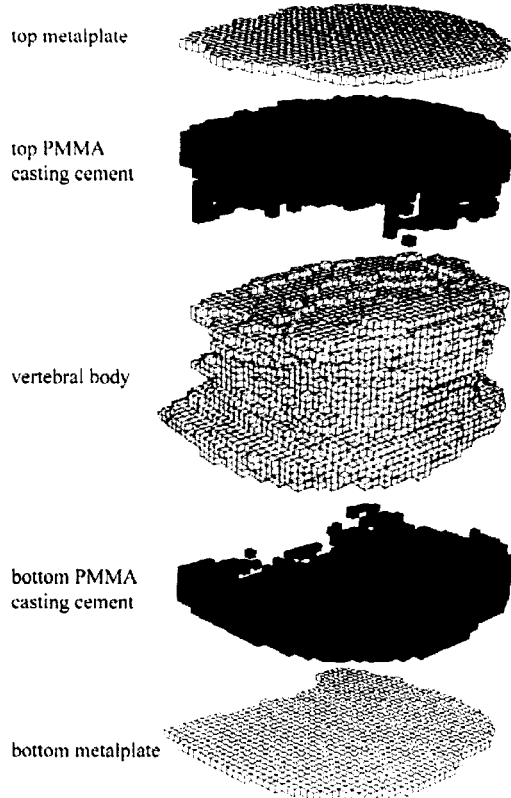


Figure 6-3: Voxel mesh of the vertebral potted with PMMA at the top and bottom endplates and finally attached to two metal plates.

The predicted vertebral stiffness decreased as the element size grew smaller (Figure 6-4). The sharpest decline was from the $1.5 \times 1.5 \times 2$ mm to $1.5 \times 1.5 \times 1$ mm sized element with a change in 5.59 N/mm per bone element. When the element size dropped to $1.2 \times 1.2 \times 1$ mm, the rate of change in stiffness had decreased to only 0.36 N/mm per bone element. Reducing the element size even further to $0.9 \times 0.9 \times 1$ mm added another 10,000 bone elements to model, but yielded a mere 7.26% change in predicted stiffness. Therefore, $1.2 \times 1.2 \times 1$ mm is the largest element dimensions that can be used to generate a voxel based finite element model of a human vertebra using the least number of elements and hence fastest computation time while still producing reliable results.

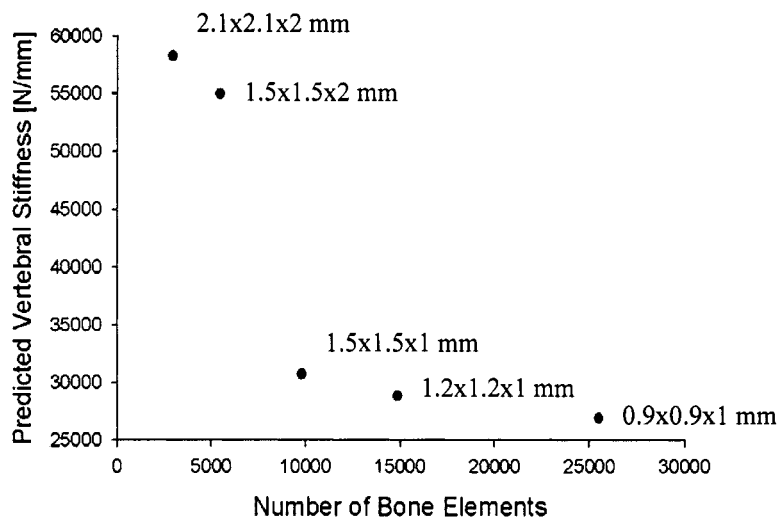


Figure 6-4: Effect of element size and hence mesh density on the predicted vertebra stiffness. Convergence is achieved with 14,886 bone elements with element size of 1.2x1.2x1 mm.

6.2.3. Material Properties

Material definition

One objective of the liquid K₂HPO₄ phantom in QCT images is to allow conversion of the computed tomography (CT) numbers in Hounsfield units to bone mineral density in g/cm³, which is then correlated to bone elastic modulus ⁶⁸. In the absence of the phantom, elastic moduli of bone elements were determined directly from their pixel values. Furthermore, only QCT scans of the vertebra already treated with CORTOSS was available, so the untreated and treated with PMMA models were generated based on the original scans. The original scans contained four material types, bone marrow, trabecular bone, cortical bone or highly dense trabecular bone and the bone cement CORTOSS, each with their distinct pixel values or range in the case of trabecular bone. Bone marrow consisting of mostly water and fat has pixel value of about 18,000,

while CORTOSS being radio-opaque has pixel value of over 65,534. Pixel values of trabecular bone lies between 18,000 and around 60,000. The 16 bit binary QCT images have pixel value limits between 0 ($2^0 - 1$) and 65,535 ($2^{16} - 1$).

The chosen 1.2x1.2x1 mm element size, though sufficiently small to minimize discretization and interpolation errors, is however large enough for three separate materials, bone marrow, trabecular bone and CORTOSS, to occupy the same element. As the pixel value of each element reflects the attenuation of the X-ray through the combination of the three materials, the exact fraction of each material contained within that element can not be ascertain given the limited information.

$$\begin{aligned} a PV_m + b PV_b + c PV_c &= PV_t \\ a + b + c &= 1 \end{aligned} \quad (6.1)$$

where a , b and c , and PV_m , PV_b and PV_c are the volume fractions and pixel values of bone marrow, trabecular bone and cement, respectively. PV_t is the total pixel value of the three materials in the element. With three unknowns, a , b and c , and only two equations, the system is undetermined and unsolvable.

On the other hand, if the assumption is made that each element can only be occupied by two different materials, either bone marrow and trabecular bone or trabecular bone and cement, then the system becomes solvable with two unknowns and two equations. The bone marrow and cement combination is omitted since CORTOSS possesses a high affinity to trabecular bone and therefore CORTOSS is assumed to be present either alone or with trabecular bone tissue. The set of equations is then reduced to,

$$\begin{aligned} a PV_m + b PV_b &= PV_t \\ a + b &= 1 \end{aligned} \quad (6.2)$$

for bone marrow and trabecular bone combination. While for bone and cement combination,

$$\begin{aligned} b \text{ PV}_b + c \text{ PV}_c &= \text{PV}_t \\ b + c &= 1 \end{aligned} \quad (6.3)$$

From the histogram of the pixel values of the original QCT scans, the minimum between 63,000 and 64,500 indicates the range where highest pixel value for trabecular bone lies. This minimum marks the separation between the trabecular-marrow and trabecular-cement composite, and is believed to be a result of CORTOSS being so radio-opaque that even a minute amount will boost the pixel value of bone to beyond the densest trabecular bone value. However, the minimum becomes less distinct and more like a plateau with scaling of the QCT scans due to averaging. For the 1.2x1.2x1 mm resolution scans, the highest pixel value for trabecular bone lies somewhere between 50,450 and 54,450. The exact pixel value of 53,043 was determined iteratively such that the total marrow space occupied by CORTOSS for all the bone elements in the model summed up to 3 cm³, the volume of cement injected into the vertebra. As a result, Equations 6.2 and 6.3 are represented graphically in Figure 6-5.

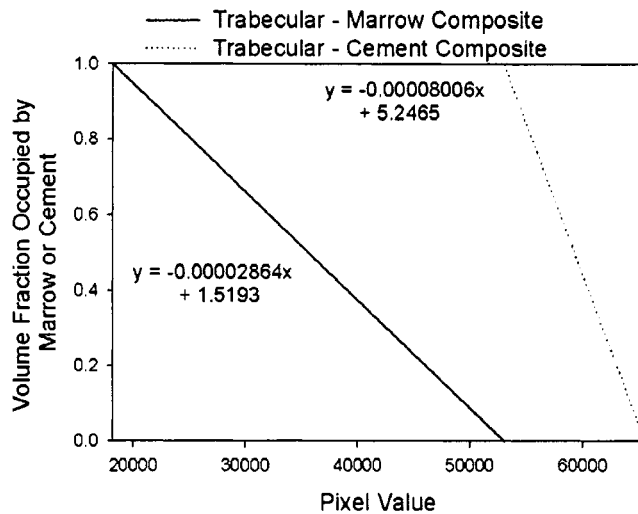


Figure 6-5: Material definitions of trabecular-marrow and trabecular-cement composites for 1.2x1.2x1 mm resolution QCT images. Elements with pixel value between 18,132 and 53,043 were defined as the trabecular-marrow composite where pixel value of 18,132 represented 100% bone marrow, while 53,043 pixel value represented densest trabecular bone. Trabecular-cement composite was defined with pixel values between 53,043 and 65,534 where 100% bone cement had a pixel value of 65,534.

Convergence study

The 5 different sized element finite element models were generated by scaling the original QCT scans, which creates a new pixel value for the densest trabecular bone in each case. The coarsest mesh (2.1x2.1x2 mm) has the lowest value while the finest mesh (0.9x0.9x1 mm) has the highest pixel value. The increasing densest trabecular bone pixel value with increasing mesh densities shifts the separation point between trabecular-marrow and trabecular-cement composites (Figure 6-6). The coarser meshes will then have more trabecular-cement composites and thus higher average elastic modulus compared to the finer meshes. Since the objective of the convergence study was to determine the effect of element size on predicted vertebral stiffness, the material properties assigned must be kept constant. Therefore, the material definitions from the

middle mesh density, $1.5 \times 1.5 \times 1$ mm sized element, were used in all 5 sized element models.

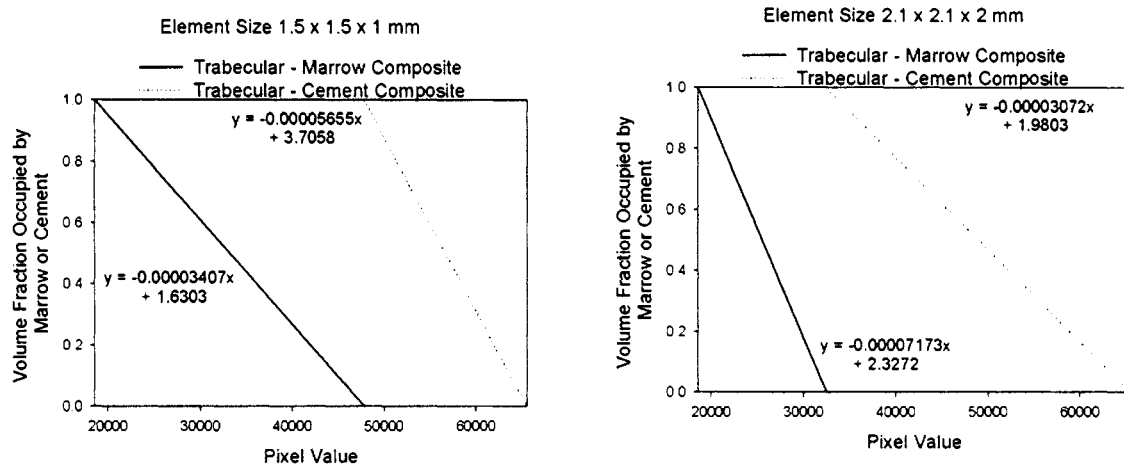


Figure 6-6: The material definitions of the trabecular-marrow and trabecular-cement composites for $1.5 \times 1.5 \times 1$ mm (left) and $2.1 \times 2.1 \times 2$ mm resolution QCT images (right). The pixel value for the densest trabecular bone that separated the trabecular-marrow and trabecular-cement composites was 47,850 for the $1.5 \times 1.5 \times 1$ mm image resolution. Reducing the resolution and hence the mesh density lowered the densest trabecular bone pixel value to 32,441, thereby enlarging the pixel spectrum for the trabecular-cement composite.

PMMA cement distribution

As each vertebra can only be treated only once, fluoroscopic X-rays of a second vertebra were used to obtain the filling pattern of PMMA after vertebroplasty. Using another L4 vertebra treated in the same manner with 10 cm^3 of PMMA, the geometry of the PMMA bolus was calculated through back-projection from fluoroscopic images. After injection, the vertebra was scanned at 12 known angles (every 15° starting at the anterior-posterior direction up to 180°). On each fluoroscopic image, the outline of the bolus was identified using Analyze software. Each of the silhouettes was then projected across a volume and the intersection of these projections was considered to be within the

bolus (Figure 6-7). Since the fringes of the bolus on the X-rays were difficult to separate from bone (the small contribution to the total absorbance at the edge lead to low contrast with bone), the tolerance for inclusion as PMMA was lowered to 10 projections. The new number of projections was found to produce the most accurate PMMA volume injected (10 cm^3). Therefore, the volume that was intersected by all 10 projections was designated as PMMA¹¹³. By using the reconstructed volume of the PMMA in conjunction with the pre-treatment QCT scans of the same vertebra, the position of the injected bolus within the second vertebral body was recreated.

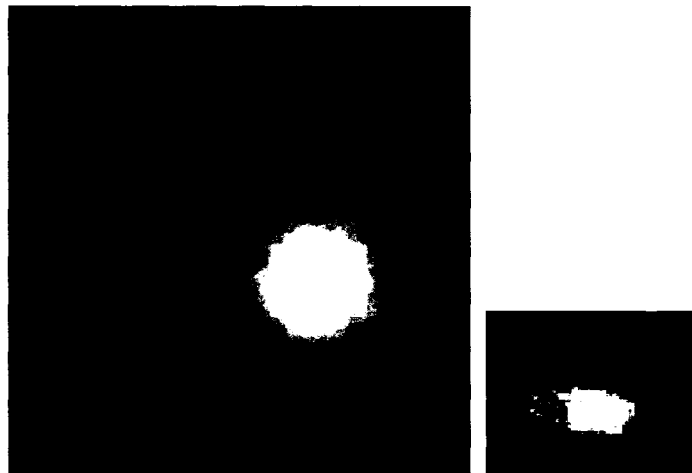


Figure 6-7: The intersection of the X-ray image projections (left) re-created the PMMA bolus injected into vertebra (right)¹¹³.

The isolated PMMA bolus image slices were assigned with an arbitrary pixel value of 100,000 and were overlaid onto the original QCT scans by simple addition. After scaling of the scans to $1.2 \times 1.2 \times 1 \text{ mm}$ resolution, any element with pixel value greater than the maximum CORTOSS value of 65,536 was identified to contain PMMA. Due to the differences in the resolution of the PMMA bolus slices ($0.6 \times 0.6 \times 1.25 \text{ mm}$) versus the original QCT scans ($0.3 \times 0.3 \times 1 \text{ mm}$) as well as the discrepancies in cement volumes (10

cm^3 of PMMA versus 3 cm^3 of CORTOSS), the size of the PMMA bolus images was adjusted. To meet the 3 cm^3 cement volume criterion, the PMMA bolus image was increased 1.5 times and positioned so that the PMMA bolus was contained within the vertebral body (Figure 6-8). Only the volume of the PMMA tagged elements occupied by either occupied by bone marrow or CORTOSS cement were added up. This created a second model of the first vertebral body with the same geometry and bone density distribution but with a different fill pattern of the same volume of cement (Figure 6-9). Therefore, a total of three vertebral body models were generated: the untreated, CORTOSS and PMMA filled models.

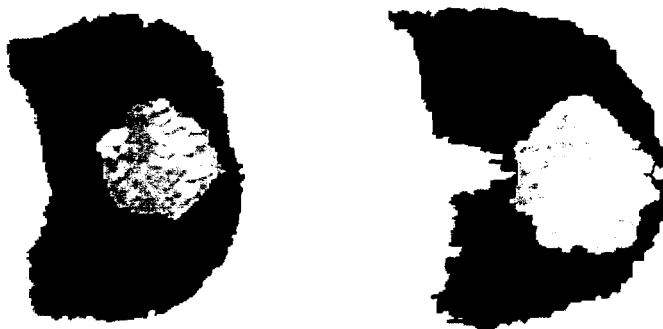


Figure 6-8: QCT slice numbers 7 (left) and 12 (right) overlaid with the transverse images of the PMMA bolus (brighter silhouette) that had been repositioned to fit within the CORTOSS treated vertebral body (duller silhouette) and resized so that the total volume of PMMA was the same as CORTOSS.

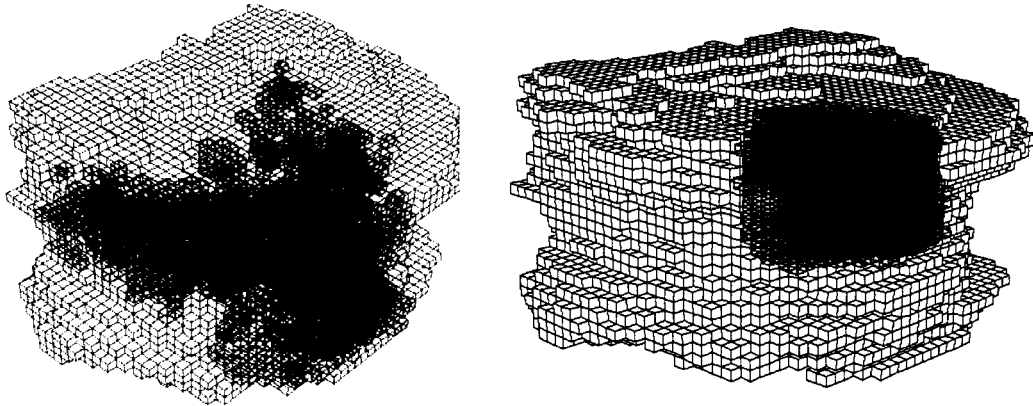


Figure 6-9: The compact fill pattern of CORTOSS (left) and PMMA (right) within the vertebral body model.

Material assignment

The correlation between bone element elastic modulus and volume fraction of bone tissue in the element was determined by calibrating stiffness predictions from voxel-based finite element models of 3 T9 and 2 L4 vertebrae to their respective experimental results in a side study. After QCT scanning, the vertebral bodies were prepared for testing by molding a layer of the casting cement to the concave endplates using a fixture that ensured plano-parallel ends⁶⁸. Compression tests of the vertebral bodies were performed between steel platens on a 20 kip MTS machine. Each vertebral body was preconditioned by cycling five times between 200 to 400 N and held for five minutes at 300 N, in order to reduce viscoelastic effects and allow proper seating between the platens, casting cement and vertebral endplates. After preconditioning, the specimens were loaded monotonically in displacement control at a rate of 5 mm/min to a 20% strain level. From the load deformation curve recorded, the vertebral stiffness derived was used in calibration of the finite element models.

Voxel-based finite element models of the 5 vertebral bodies were generated as described previously. The inclusion of the liquid K₂HPO₄ phantom in the QCT scans allowed for the conversion from CT numbers in Hounsfield units to bone mineral density in g/cm³. For each model the volume fraction of bone tissue in each bone element was determined by dividing the bone element density by the maximum element density. A first and a second order correlation between bone element elastic modulus and bone tissue volume fraction of the element were investigated,

$$\begin{aligned} E_{\text{elem}} &= C b + D \\ E_{\text{elem}} &= F b^2 + G \end{aligned} \quad (6.4)$$

where E_{elem} is the elastic modulus of the bone element, b is the volume fraction of bone tissue in the bone element, C and D , and F and G are the first and second order coefficients respectively. The coefficients were varied such that the error from the predicted vertebral stiffness when compared to the experimental results was minimized for all 5 models (Figure 6-10). The other elastic constants to describe the anisotropic bone elements (Young's modulus: E_{xx} , E_{yy} ; Poisson's ratio: ν_{xy} , ν_{xz} , ν_{yz} ; Shear modulus: G_{xy} , G_{xz} , G_{yz}) were derived from ratios obtained by Ulrich et al.¹¹⁶ (Table 3-2).

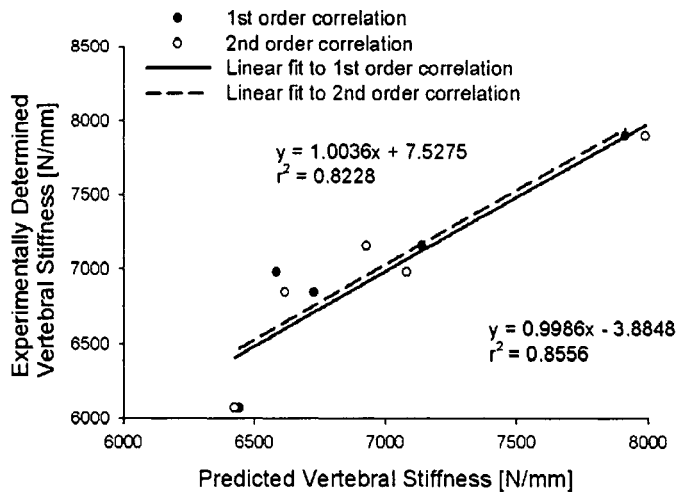


Figure 6-10: The accuracy of the calibrated coefficients for the first and second order correlations between bone element elastic modulus and bone tissue volume fraction to predict vertebral stiffness.

Both the calibrated first and second order correlations showed strong relationships to the experimental results ($r^2 = 0.8228$ for first order and $r^2 = 0.8556$ for second order). The relative errors for the calibrated first and second order correlations were also low at 7.3% and 5.7%, respectively. However, for a bone element that is totally occupied by bone tissue (volume fraction = 1.0), the elastic modulus of the densest bone element is only 570 MPa according to the first order correlation, while the second order correlation predicts 2,269 MPa, which is closer to literature values^{24,57} (Figure 6-11). Therefore, the second order correlations were selected for trabecular bone material assignment. A list of all the materials and their properties used in the models are summarized in Table 6-1.

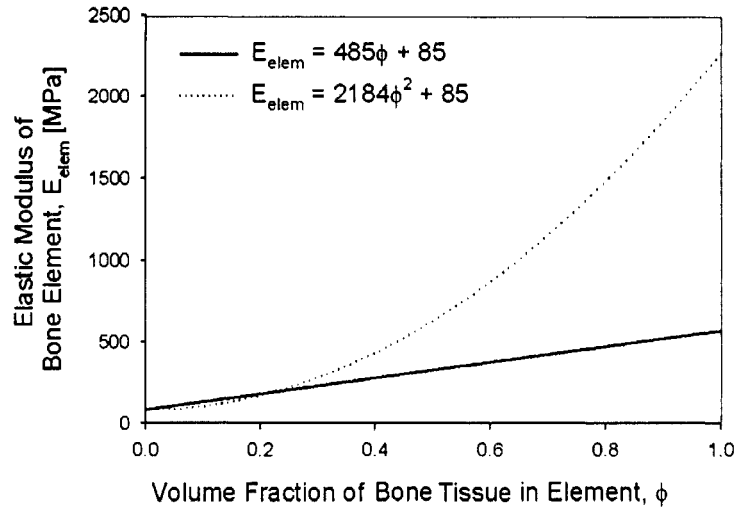


Figure 6-11: The range of bone element elastic modulus predicted using the calibrated first and second order correlations to bone tissue volume fraction. The elastic modulus derived from the second order correlation when $\phi = 1$ is closer to the experimentally determined values for cortical bone than for the first order correlation.

Table 6-1: Materials properties and element specifications.

Material	Number of elements	Elastic Modulus [MPa]	Poisson's ratio	Reference
Bone	14,886	$2184 \phi^2 + 85$	0.3	
PMMA layer	Top – 5,106 Bottom – 3,689	2,500	0.3	92
Cement				
CORTOSS	1,906	5,800	0.3	92
PMMA	2,133	2,500	0.3	92
Metal plate	Top – 973 Bottom – 1053	209,000	0.3	

ϕ is volume fraction of bone tissue in the bone element

All linear analyses to predict vertebral stiffness by simulating uniaxial compression under displacement control to a total displacement of 1 mm were performed using the commercially available finite element software ABAQUS version 6.4. For the two treated models, the cement moduli were varied (100, 500, 1000, 2500, 5800 MPa) in

order to observe their effect on the intra- and extra-vertebral biomechanics under different distribution patterns. Vertebral stiffness was predicted for a total of 11 different cases (2 cement distributions x 5 cement moduli + 1 untreated case).

6.3 Results

The addition of CORTOSS into the vertebral body model increased vertebral stiffness by 28.6% to 33,936 N/mm, while treatment with PMMA resulted in only a 4.54% increase from the untreated model to 27,598 N/mm (Figure 6-12). Even though the same volume of cements used, the degree of vertebral stiffness augmentation with CORTOSS was 6 times that with PMMA. The large difference is due to the CORTOSS being twice as stiff as PMMA and also the more dispersed distribution of CORTOSS within the vertebral body compared to PMMA. The PMMA filled elements are concentrated at the anterior of the vertebral body while the CORTOSS filled elements are distributed throughout the vertebral body.

High axial stresses were noticed at the bone elements directly above and below the PMMA filled elements due to the shift in the applied load towards the cemented area of the vertebral body with the stiffer PMMA filled elements. However, minimal high stress concentrations were found in the CORTOSS model as the CORTOSS filled elements were dispersed throughout the vertebral body and were unable to cause such major shifts in the applied load (Figures 6-13).

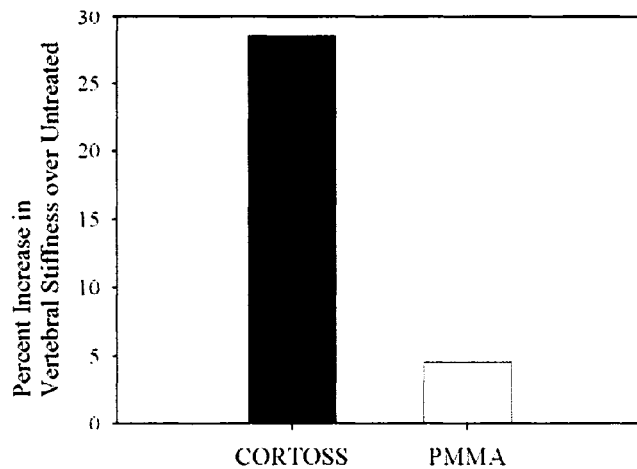


Figure 6-12: The increase in vertebral stiffness after treatment with CORTOSS was higher than with PMMA.

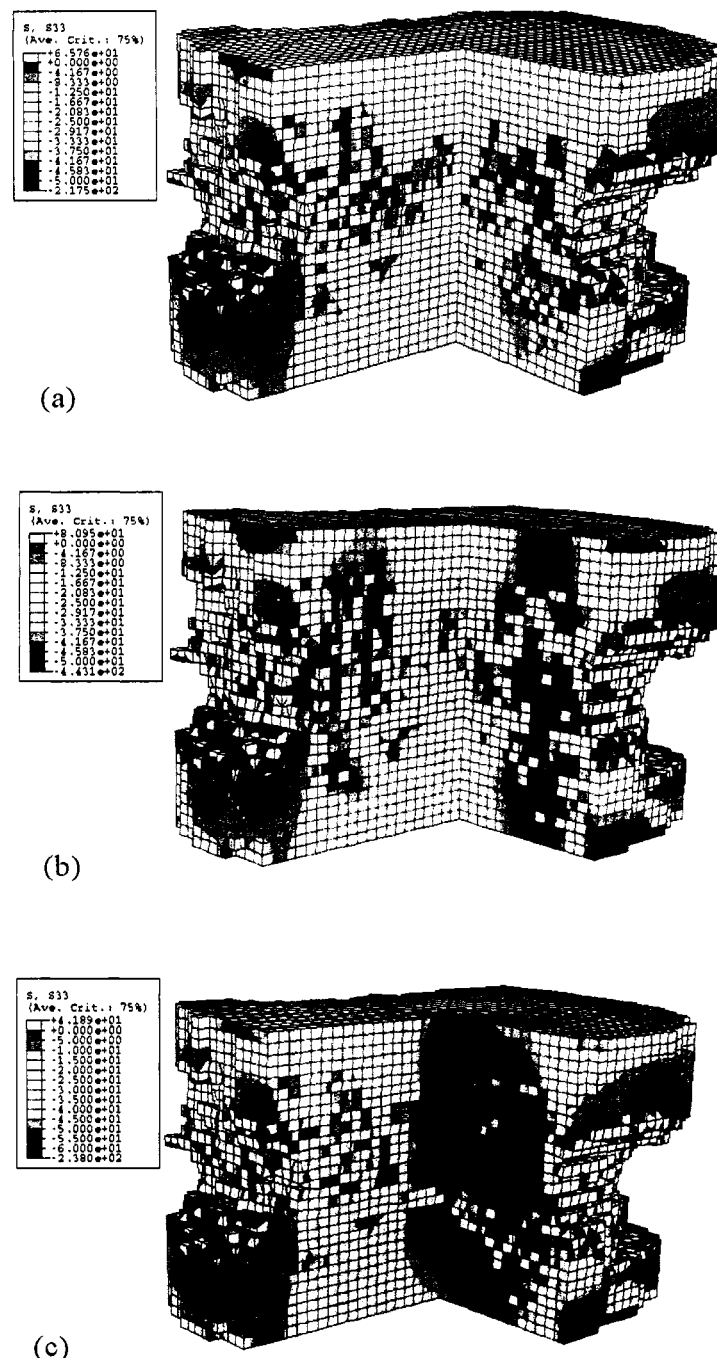


Figure 6-13: The distributions of axial stress in the (a) untreated, treated with (b) CORTOSS and (c) PMMA models. Large areas of high compressive stress (darkest areas) were observed in the PMMA models compared to the untreated, but were less prominent in the CORTOSS models.

To isolate the effect of cement distribution alone, the cement properties for both the CORTOSS and PMMA treated vertebral models were set equal. For the same cement volume and properties, the increase in vertebral stiffness was higher with a more dispersed cement distribution with CORTOSS than with a compact fill with PMMA. The difference in vertebral stiffness augmentation decreased with decreasing cement modulus (Figure 6-14).

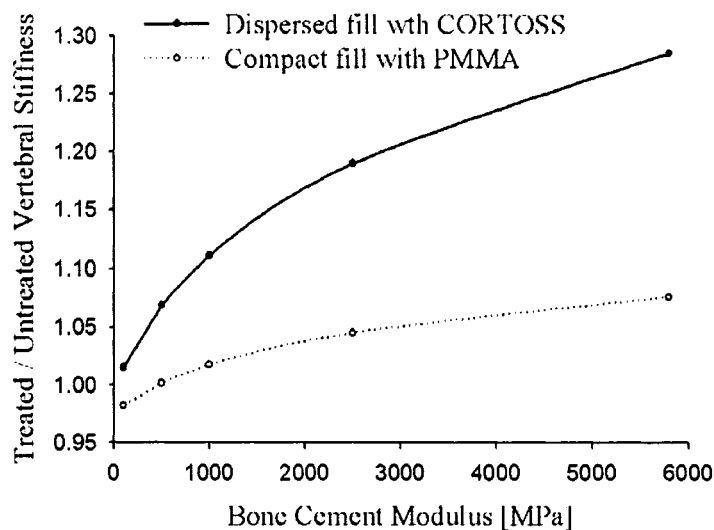


Figure 6-14: Higher vertebral stiffness increase achieved with dispersed cement fill than with a compact one.

The mechanism for vertebral reinforcement using the compact fill bone cement PMMA is load transfer as explained in Chapter 4 and it is also the cause of intravertebral stress concentrations as demonstrated in Chapter 5. However, this mechanism is not present for the CORTOSS treated model as the cement is dispersed within the vertebral body and therefore minimal stress concentrations were observed. Vertebral augmentation with a dispersed cement distribution works by reinforcing small areas of trabecular bone throughout the whole vertebral body rather than localized in one region. This way the

applied load is more uniformly carried by the entire augmented vertebral body instead of concentrating onto a small locale with compact cement fill. The compact PMMA cement fill only covers a maximum of 30% of the total cross-sectional area of the vertebral body. A larger cross-sectional area to resist the applied loads means more load can be withstood.

6.4 Discussion

The objective of this study was to determine the effect of cement distribution patterns within the vertebrae as well as cement material properties on the intra- and extra-vertebral biomechanics. The CORTOSS (dispersed fill) and PMMA (compact fill) treated vertebral body models showed significant differences in both the extra- and intra-vertebral biomechanics. The accumulation of PMMA filled elements at one locale focuses the shift in the applied load to that area, causing the bone elements above and below the PMMA to experience high axial stress. The CORTOSS filled elements dispersed throughout the vertebral body is unable to cause such major shifts in the applied load, and thus no additional high axial stress are present. Additionally, the spatially distributed reinforcement of small areas of trabecular bone within the entire vertebral body with CORTOSS enables the whole cross-sectional area of the vertebral body to bear the applied load, resulting in a higher increase in vertebral stiffness than with PMMA whose compact fill forces the applied load to act on a smaller area due to load transfer.

When the cement properties of CORTOSS and PMMA were equalized, thereby neutralizing the effect of cement properties, the dispersed cement fill pattern with

CORTOSS produced higher vertebral stiffness than with a compact cement fill pattern with PMMA using the same volume of cement. This result indicates that instead of injecting more cement into the vertebral body for added vertebral stiffness, a more dispersed cement distribution with less cement will produce the same level of augmentation. Thus, the risks of complications arising from cement leaks due to excessive filings can be reduced.

Although the vertebral body models were precisely replicated, the simulated monotonic, the uniaxial compressive loading conditions applied were, however, overly simplified. Vertebral bodies *in-vivo* experience more complex loading conditions including compression, shear and bending, which can lead to different types of fractures and damage behavior. Nonetheless, given the complexity of spine biomechanics and that almost all of the experimental studies performed on vertebroplasty tested the augmented vertebrae specimens under uniaxial compression, the uniform compressive loading condition simulated is considered adequate for the purpose of studying the effects of bone cement distribution and their material properties on vertebral reinforcement.

The vertebral stiffness predicted for all the models are higher than the typical vertebral stiffness of un-fractured L4 female vertebral body potted in casting cement. The stiffness of a fractured vertebra is lower than when un-fractured due to damage. The reason for the elevated prediction is that the QCT scans of the treated vertebra with CORTOSS used to create the models are those of an already fractured vertebra. The vertebra is so severely compressed that the concavities of the top and bottom endplates have depths of 10 mm and 7 mm, respectively, equivalent to over 25% of the height of the vertebra from the highest points. The reduction in height based on the initial height of

the un-fractured vertebra is even greater. The trabecular bone architecture within a compression fractured vertebral body is collapsed on itself due to the high porosity of the structure, resulting in densification at the fracture sites. Since the resolution of the QCT scanner is not high enough to visualize individual trabeculae, the fracture sites appear to consist of dense trabecular bone. Based on the material property assignment procedure, higher pixel values are assigned stronger bone material properties even though the trabecular bone is already structurally compromised. Although the predicted vertebral stiffness for all 3 models are higher than normal, the relative differences between the CORTOSS and PMMA treated model predictions versus the untreated model results are still valid.

The limitations to the study include the absence of the QCT scans of the vertebra before treatment with CORTOSS. If the pre-treatment scans were available, the exact volume fraction of trabecular bone and bone marrow occupying each bone element can be determined since only two materials are present. The exact position and volume fraction of CORTOSS occupying each element can also be calculated through simple subtraction of the pre- and post- treatment scans. However, without the pre-treatment scans, the untreated model had to be created from the scans taken after injection with CORTOSS. The limited information available compels the assumption that each element can only be occupied by two materials at once be made, bone-marrow and bone-cement, even thought there is a likelihood that it can contain all three materials. In light of this limitation, the bone material assignment regressions were calibrated to ensure that the volume fraction of the bone elements occupied by CORTOSS equaled that actually injected into the vertebral body.

Another limitation involves the unavailability of QCT scans of a second vertebra treated with PMMA. The distribution of PMMA within the vertebral body therefore had to be extracted from a series of fluoroscopic X-rays of a different vertebra treated with vertebroplasty. The procedure of extracting a three-dimensional geometry from 10 projections has two limitations. The most apparent one is that the resulting geometry is only an estimation of the actual shape of the bolus. The estimated shape will always be polyhedral, with a maximum of $n \times 2 + 2$ sides, where n is the number of projections taken. The superior and inferior faces are completely flat because X-ray images have to be in the sagittal plane in order to isolate the vertebrae from one another in the spinal segment. However, the estimated polyhedron is believed to represent the actual shape much more accurately than an assumed cylinder used in Chapters 3 and 4. The second difficulty is in accurately identifying the PMMA outline in each fluoroscopic image. With the typical amount of contrast agent, the X-ray density of PMMA is similar to that of dense bone, so it is difficult to render the edges, especially at the angles where it overlaps the posterior elements of the vertebrae. Also, small offshoots of the material (that fills the channel created by the insertion needle, for instance) are likely not be detected because of the low thickness. This difficulty can be partially overcome through expertise, and addition of extra contrast agent will make the PMMA appear denser in comparison to the surrounding bone.

The greater augmentation of the vertebral stiffness with a dispersed cement filling of the vertebral body means that a smaller volume of the filler material will still produce the same amount of stiffness augmentation achieved with a compact fill. The dispersed cement distribution also avoids intravertebral axial stress concentrations that are

generated as a consequence of load transfer and may lead to future fractures of the adjacent untreated vertebrae. As a result, a dispersed cement distribution pattern may result in a lower risk of complications due to cement leakages since smaller cement volume would be just as biomechanically effective as well as prevent subsequent fractures in the adjacent untreated vertebrae as intravertebral stress-risers are minimal.

6.5 Conclusion

Higher mechanical enhancements with lower risk of complications from cement leakages and adjacent vertebral fractures can be achieved with bone cements that result in dispersed distributions within the vertebrae and are ideal for use in vertebroplasty.

6.6 Acknowledgements

Financial support for this work was provided by the Orthovita, Inc. The authors thank Alistair Templeton for creating the PMMA bolus from X-ray.

Chapter 7

CONCLUSIONS

The ability of vertebroplasty to provide immediate mechanical reinforcement upon hardening of the injected bone cement along with the minimal invasiveness of the procedure make it a highly effective vertebral fracture prevention treatment, especially when current drug therapies are slow to act and when faced with the growing frequency of osteoporotic vertebral fractures as the population ages. However, before vertebroplasty can be implemented as a prophylaxis, the procedure's mechanical efficacy and patient safety issues must first be addressed. These concerns require deeper understanding of how the biochemistry and mechanics of the bone cement affects the vertebrae on both the tissue and whole bone level. This research focuses on evaluating the biomechanical efficacy of prophylactic vertebroplasty and optimizes the procedure by identifying aspects of bone cement properties that are critical to the biomechanical success of the treatment and that contribute to lower risk of complications which pose a threat to patient safety. In light of the many factors affecting the biomechanical outcome, including cement volume, placement, material properties and distribution patterns, as well as the bone densities of the vertebrae, computer models of human vertebral bodies were employed in this research, which allow for multiple analyses to be performed on the same specimen. The accuracy of the finite element vertebral models is assured as each model was generated from its specific QCT scans and also calibrated to its corresponding experimental results.

The definition of biomechanical success of vertebroplasty is introduced in this research as when vertebral strength is increased to beyond fracture risk levels (> 3.6 MPa). At this strength level, the vertebra is able to provide sufficient support for normal weight-bearing dynamics with low risk of fracture. The efficacy of the current bone cement, poly(methylmethacrylate) (PMMA), to achieve the new biomechanical goal of vertebroplasty was evaluated in Chapter 3. The study measured the varying degrees of mechanical enhancements at different PMMA volumes and placements within vertebrae at various severities of osteoporosis. Based on the results, guidelines as to the optimal PMMA volume and placement required to prevent any future fractures are established. For vertebrae at medium risk of fracture, prophylactic vertebroplasty is able to successfully offer reinforcement to the desired low fracture risk levels using small volumes of PMMA. However, for high fracture risk vertebrae, the volume of PMMA needed to reach low fracture risk levels is high enough to result in up to 67% chance of cement leakages^{37,73}. Large cement fills increase the risk of extravasations and subsequent complications that threaten the health and life of the patient. As a result, PMMA is ineffective for structural reinforcement of vertebrae at high risk of fractures.

Further increases in vertebral strength enhancements above what is achieved with PMMA would mean lesser cement volume and lower risk of leakages. Therefore in Chapter 4, the material properties of the bone cement were varied to determine the optimal properties that would achieve greater vertebral strength reinforcements. The results show that the maximum degree of vertebral strength increase achievable is the same amount reached with PMMA. Furthermore, the high cement modulus needed to reach the maximum vertebral strength increase triggers a shift in the applied load towards

the cement and away from the trabecular bone, forcing majority of the load to be carried by the stronger cement, causing high stress concentrations in the areas immediately above and below the cement. These stress concentrations increase the risk of subsequent fractures to the treated vertebrae and can also possibly lead to fractures in the adjacent untreated vertebrae according to the vertebroplasty-induced endplate fracture mechanism suggested by several numerical studies ^{12,96}. The mechanism proposes that the cement inhibits the inward deflection of the endplates of the treated vertebrae during compression, causing the incompressible discs to bulge inwards into the endplate of the adjacent vertebrae, which may increase its risk of fracture. The effect of the intravertebral stress concentrations on the adjacent vertebrae after vertebroplasty has to be proven in order to determine whether internal mechanical compatibility is an additional factor to consider when optimizing vertebroplasty.

The objective of Chapter 5 was to experimentally test the end-effect of intravertebral stress concentrations by examining the differences in fracture strengths and types to the adjacent vertebrae with and without vertebroplasty. A unique six degrees-of-freedom robotic arm was used to duplicate physiological loading conditions on treated and untreated three-level spinal segments. Of the six treated segments, five of them experienced reductions in fracture strengths after vertebroplasty. Additionally, the fractures in the treated segments were exclusively biconcave fractures, while mainly wedge type fractures were seen in the untreated segments. These results indicate that vertebroplasty does indeed weaken the adjacent untreated vertebrae and that the distinct biconcave fracture type observed after treatment concurs with the hypothesized

vertebroplasty-induced endplate failure mechanism. Therefore, internal stress concentrations within the vertebrae must be minimized.

In an attempt to achieve both maximum vertebral strength reinforcement and internal mechanical compatibility, the effect of different bone cement distribution patterns within the vertebrae on vertebral biomechanics was evaluated in Chapter 6. Dispersed and compact cement fill patterns, based on the actual spatial distributions of CORTOSS and PMMA bone cements respectively, were simulated on the same finite element vertebral model. In order to conclusively attribute any biomechanical discrepancies to the different fill patterns, the material properties of the bone cements in the two distribution cases were equaled to neutralize their effects. Higher vertebral stiffness increase and minimal intravertebral stress concentrations were observed for the dispersed cement fill compared to the compact one. The higher vertebral stiffness increase implies higher vertebral strength increase, which means lower cement volumes are needed and therefore lower risk of leakages. Fracture risks to the adjacent untreated vertebrae are also reduced due to the mitigated internal stress concentrations as shifts in load transfers are less intense with scattered cement positions. Therefore, bone cements that result in a dispersed distribution when injected into the vertebrae will offer the desired biomechanical reinforcement with minimal risk of complications.

This research analyzes the biomechanical effects of prophylactic vertebroplasty under different bone cement volumes, placements, material properties and distribution patterns. In the process of identifying key bone cement features that will result in maximum vertebral reinforcement and intravertebral mechanical compatibility, the procedure is optimized for maximum benefit with minimal risk to patient safety. The

biomechanically optimal bone cement is found to be one with high affinity to bone tissue such that upon injection into the vertebral body, the material “clings” onto the trabeculae to produce a spatially dispersed distribution within the vertebra. The disperse cement fill prevents major shifts in the applied load to one locale, resulting in minimal intravertebral stress concentrations, which lower the risk of adjacent vertebral fractures. The absence of load transfers also implies that applied loads are carried by the entire vertebral body rather than focused onto just the small area where the cement is concentrated. With a larger area to bear loads, more weight can be withstood.

Future research should be geared towards the development of materials with high affinity to bone tissue in addition to the other requirements for injectability, including high radio-opacity for visualization of potential leakages, sufficient setting time (~15 mins) and viscosity for ease of handling, and low curing temperature to prevent damage to bone tissue during hardening. More desirable material properties, such as biodegradability and osteoconductivity, can also be incorporated in light of the advances in biomaterials developed for tissue engineering. New prospective bioresorbable cements will be able to temporarily provide mechanical support, buying time for the new bone to grow to regain both bone mass and connectivity of the trabeculae lost due to osteoporosis. Current drug therapies can only increase bone mass and are unable to restore trabeculae interconnectivity. To this end, anabolic drugs, growth factors and other hormones can be integrated into the injected material, which are released as the material degrades to further stimulate bone formation. Moreover, since the cement eventually degrades, the procedure can be repeated if greater bone mass increase is desired. In addition to osteoinductive agents, the material can be laced with chemotherapeutic drugs

to fight cancer that has metastasized within the vertebra, which weakens it structurally, making it susceptible to fractures. In this case, the structural reinforcement feature of vertebroplasty doubles as a localized drug delivery vehicle. Now that the bone cements with spatially dispersed fill patterns is known to produce optimum biomechanical effects, the biochemistry of materials with this characteristic can be specifically tailored for different applications without any concerns for adverse affects to the treated and adjacent vertebrae from the dynamics of the weight-bearing spine.

REFERENCES

1. Adams MA, McNally DS, Dolan P. 'Stress' distributions inside intervertebral discs. The effects of age and degeneration. *J Bone Joint Surg Br* 1996;78:965-72.
2. Adventist Midwest Health. 2006. Available at: <http://www.keepingyouwell.com/services/radiology/vertebroplasty.asp>.
3. Ahmed AI, Blake GM, Rymer JM, et al. Screening for osteopenia and osteoporosis: do the accepted normal ranges lead to overdiagnosis? *Osteoporos Int* 1997;7:432-8.
4. Alonge L. FDA Public Health Web Notification: Complications Related to the Use of Bone Cement in Treating Compression Fractures of the Spine, 2003. Available at: <http://www.fda.gov/cdrh/safety/bonecement.pdf>.
5. Altkorn D, Vokes T. Treatment of postmenopausal osteoporosis. *Jama* 2001;285:1415-8.
6. Ananthakrishnan D, Berven S, Deviren V, et al. The effect on anterior column loading due to different vertebral augmentation techniques. *Clin Biomech (Bristol, Avon)* 2005;20:25-31.
7. Anonymous. Consensus development conference: diagnosis, prophylaxis, and treatment of osteoporosis. *Am J Med* 1993;94:646-50.
8. Anonymous. Osteoporosis prevention, diagnosis, and therapy. *Jama* 2001;285:785-95.
9. Asano S, Kaneda K, Umehara S, et al. The mechanical properties of the human L4-5 functional spinal unit during cyclic loading. The structural effects of the posterior elements. *Spine* 1992;17:1343-52.
10. Bai B, Jazrawi LM, Kummer FJ, et al. The use of an injectable, biodegradable calcium phosphate bone substitute for the prophylactic augmentation of osteoporotic vertebrae and the management of vertebral compression fractures. *Spine* 1999;24:1521-6.
11. Baran DT. Osteoporosis: which current treatments reduce fracture risk? *Cleve Clin J Med* 2000;67:701-3.

12. Baroud G, Nemes J, Heini P, et al. Load shift of the intervertebral disc after a vertebroplasty: a finite-element study. *Eur Spine J* 2003;12:421-6.
13. Belkoff SM, Maroney M, Fenton DC, et al. An in vitro biomechanical evaluation of bone cements used in percutaneous vertebroplasty. *Bone* 1999;25:23S-6S.
14. Belkoff SM, Mathis JM, Erbe EM, et al. Biomechanical evaluation of a new bone cement for use in vertebroplasty. *Spine* 2000;25:1061-4.
15. Belkoff SM, Mathis JM, Jasper LE. Ex vivo biomechanical comparison of hydroxyapatite and polymethylmethacrylate cements for use with vertebroplasty. *AJNR Am J Neuroradiol* 2002;23:1647-51.
16. Belkoff SM, Mathis JM, Jasper LE, et al. The biomechanics of vertebroplasty. The effect of cement volume on mechanical behavior. *Spine* 2001;26:1537-41.
17. Belkoff SM, Mathis JM, Jasper LE, et al. An ex vivo biomechanical evaluation of a hydroxyapatite cement for use with vertebroplasty. *Spine* 2001;26:1542-6.
18. Berlemann U, Ferguson SJ, Nolte LP, et al. Adjacent vertebral failure after vertebroplasty. A biomechanical investigation. *J Bone Joint Surg Br* 2002;84:748-52.
19. Biggemann M, Hilweg D, Seidel S, et al. Risk of vertebral insufficiency fractures in relation to compressive strength predicted by quantitative computed tomography. *Eur J Radiol* 1991;13:6-10.
20. Bostrom MP, Lane JM. Future directions. Augmentation of osteoporotic vertebral bodies. *Spine* 1997;22:38S-42S.
21. Brinckmann P, Biggemann M, Hilweg D. Prediction of the compressive strength of human lumbar vertebrae. *Spine* 1989;14:606-10.
22. Brinckmann P, Frobin W, Hierholzer E, et al. Deformation of the vertebral end-plate under axial loading of the spine. *Spine* 1983;8:851-6.
23. Chiras J, Depriester C, Weill A, et al. [Percutaneous vertebral surgery. Technics and indications]. *J Neuroradiol* 1997;24:45-59.
24. Choi K, Kuhn JL, Ciarelli MJ, et al. The elastic moduli of human subchondral, trabecular, and cortical bone tissue and the size-dependency of cortical bone modulus. *J Biomech* 1990;23:1103-13.
25. Christiansen C. Prevention and treatment of osteoporosis: a review of current modalities. *Bone* 1992;13:S35-9.

26. Clemente CD. Anatomy: A Regional Atlas of the Human Body. 4th ed. Baltimore, MD: Williams and Wilkins, 1997.
27. Cohen LD. Fractures of the osteoporotic spine. Orthop Clin North Am 1990;21:143-50.
28. Cooper C, Atkinson EJ, O'Fallon WM, et al. Incidence of clinically diagnosed vertebral fractures: a population- based study in Rochester, Minnesota, 1985- 1989. J Bone Miner Res 1992;7:221-7.
29. Cortet B, Cotten A, Boutry N, et al. Percutaneous vertebroplasty in patients with osteolytic metastases or multiple myeloma. Rev Rhum Engl Ed 1997;64:177-83.
30. Cotten A, Boutry N, Cortet B, et al. Percutaneous vertebroplasty: state of the art. Radiographics 1998;18:311-20; discussion 20-3.
31. Cotten A, Dewatre F, Cortet B, et al. Percutaneous vertebroplasty for osteolytic metastases and myeloma: effects of the percentage of lesion filling and the leakage of methyl methacrylate at clinical follow-up. Radiology 1996;200:525-30.
32. Cyteval C, Sarrabere MP, Roux JO, et al. Acute osteoporotic vertebral collapse: open study on percutaneous injection of acrylic surgical cement in 20 patients. AJR Am J Roentgenol 1999;173:1685-90.
33. Dahl OE, Garvik LJ, Lyberg T. Toxic effects of methylmethacrylate monomer on leukocytes and endothelial cells in vitro. Acta Orthop Scand 1994;65:147-53.
34. Danilewicz-Stysiak Z. Experimental investigations on the cytotoxic nature of methyl methacrylate. J Prosthet Dent 1980;44:13-6.
35. Dean JR, Ison KT, Gishen P. The strengthening effect of percutaneous vertebroplasty. Clin Radiol 2000;55:471-6.
36. Deramond H, Depriester C, Galibert P, et al. Percutaneous vertebroplasty with polymethylmethacrylate. Technique, indications, and results. Radiol Clin North Am 1998;36:533-46.
37. Deramond H, Depriester C, Toussaint P, et al. Percutaneous Vertebroplasty. Semin Musculoskelet Radiol 1997;1:285-96.
38. Deramond H, Wright NT, Belkoff SM. Temperature elevation caused by bone cement polymerization during vertebroplasty. Bone 1999;25:17S-21S.
39. Faulkner KG, Cann CE, Hasegawa BH. Effect of bone distribution on vertebral strength: assessment with patient-specific nonlinear finite element analysis. Radiology 1991;179:669-74.

40. Fleming LA. Osteoporosis: clinical features, prevention, and treatment. *J Gen Intern Med* 1992;7:554-62.
41. Fogelman I, Blake GM. Different approaches to bone densitometry. *J Nucl Med* 2000;41:2015-25.
42. Gangi A, Kastler BA, Dietemann JL. Percutaneous vertebroplasty guided by a combination of CT and fluoroscopy. *AJNR Am J Neuroradiol* 1994;15:83-6.
43. Genant HK, Majumdar S. High-resolution magnetic resonance imaging of trabecular bone structure. *Osteoporos Int* 1997;7:S135-9.
44. Glaser DL, Kaplan FS. Osteoporosis. Definition and clinical presentation. *Spine* 1997;22:12S-6S.
45. Goldstein SA, Goulet R, McCubrey D. Measurement and significance of three-dimensional architecture to the mechanical integrity of trabecular bone. *Calcif Tissue Int* 1993;53:S127-32; discussion S32-3.
46. Grados F, Depriester C, Cayrolle G, et al. Long-term observations of vertebral osteoporotic fractures treated by percutaneous vertebroplasty. *Rheumatology (Oxford)* 2000;39:1410-4.
47. Guglielmi G, Gluer CC, Majumdar S, et al. Current methods and advances in bone densitometry. *Eur Radiol* 1995;5:129-39.
48. Guzik DC, Keller TS, Szpalski M, et al. A biomechanical model of the lumbar spine during upright isometric flexion, extension, and lateral bending. *Spine* 1996;21:427-33.
49. Hansson T, Roos B. The relation between bone mineral content, experimental compression fractures, and disc degeneration in lumbar vertebrae. *Spine* 1981;6:147-53.
50. Hardouin P, Grados F, Cotten A, et al. Should percutaneous vertebroplasty be used to treat osteoporotic fractures? An update. *Joint Bone Spine* 2001;68:216-21.
51. Harrop JS, Prpa B, Reinhardt MK, et al. Primary and secondary osteoporosis' incidence of subsequent vertebral compression fractures after kyphoplasty. *Spine* 2004;29:2120-5.
52. Hayes WC, Bouxsein ML. Biomechanics of Cortical and Trabecular Bone: Implications for Assessment of Fracture Risk. In Mow VC, Hayes WC eds. *Basic Orthopaedic Biomechanics*. Second ed: Lippincott, Williams and Wilkins, 1997:69- 111.

53. Heini PF, Berlemann U, Kaufmann M, et al. Augmentation of mechanical properties in osteoporotic vertebral bones-- a biomechanical investigation of vertebroplasty efficacy with different bone cements. *Eur Spine J* 2001;10:164-71.
54. Higgins KB, Harten RD, Langrana NA, et al. Biomechanical effects of unipedicular vertebroplasty on intact vertebrae. *Spine* 2003;28:1540-8.
55. Hitchon PW, Goel V, Drake J, et al. Comparison of the biomechanics of hydroxyapatite and polymethylmethacrylate vertebroplasty in a cadaveric spinal compression fracture model. *J Neurosurg* 2001;95:215-20.
56. Homminga J, Weinans H, Gowin W, et al. Osteoporosis changes the amount of vertebral trabecular bone at risk of fracture but not the vertebral load distribution. *Spine* 2001;26:1555-61.
57. Hou FJ, Lang SM, Hoshaw SJ, et al. Human vertebral body apparent and hard tissue stiffness. *J Biomech* 1998;31:1009-15.
58. Ikeuchi M, Yamamoto H, Shibata T, et al. Mechanical augmentation of the vertebral body by calcium phosphate cement injection. *J Orthop Sci* 2001;6:39-45.
59. Ismail AA, Cooper C, Felsenberg D, et al. Number and type of vertebral deformities: epidemiological characteristics and relation to back pain and height loss. European Vertebral Osteoporosis Study Group. *Osteoporosis international* 1999;9:206-13.
60. Jensen ME, Dion JE. Percutaneous vertebroplasty in the treatment of osteoporotic compression fractures. *Neuroimaging Clin N Am* 2000;10:547-68.
61. Jensen ME, Dion JE. Vertebroplasty relieves osteoporosis pain. *Diagn Imaging (San Franc)* 1997;19:68, 71-2.
62. Jensen ME, Evans AJ, Mathis JM, et al. Percutaneous polymethylmethacrylate vertebroplasty in the treatment of osteoporotic vertebral body compression fractures: technical aspects. *AJNR Am J Neuroradiol* 1997;18:1897-904.
63. Kayanja MM, Togawa D, Lieberman IH. Biomechanical changes after the augmentation of experimental osteoporotic vertebral compression fractures in the cadaveric thoracic spine. *Spine J* 2005;5:55-63.
64. Keaveny TM, Pinilla TP, Crawford RP, et al. Systematic and random errors in compression testing of trabecular bone. *J Orthop Res* 1997;15:101-10.

65. Keller TS, Kosmopoulos V, Lieberman IH. Vertebroplasty and kyphoplasty affect vertebral motion segment stiffness and stress distributions: a microstructural finite-element study. *Spine* 2005;30:1258-65.
66. Kopperdahl DL. Structural consequences of damage on the mechanical behavior of the human vertebral body. *Mechanical Engineering*. Berkeley, CA.: University of California Berkeley, 1998.
67. Kopperdahl DL, Keaveny TM. Yield strain behavior of trabecular bone. *J Biomech* 1998;31:601-8.
68. Kopperdahl DL, Pearlman JL, Keaveny TM. Biomechanical consequences of an isolated overload on the human vertebral body. *J Orthop Res* 2000;18:685-90.
69. Liebschner MA, Kopperdahl DL, Rosenberg WS, et al. Finite element modeling of the human thoracolumbar spine. *Spine* 2003;28:559-65.
70. Liebschner MAK, Rosenberg WS, Keaveny TM. Effects of bone cement volume and distribution on vertebral stiffness after vertebroplasty. *Spine* 2001;26:1547-54.
71. Liebschner MAK, Sun K, Keaveny TM. Non-linear finite element modeling of human vertebral bodies. 10th Annual Symposium on Computational Methods in Orthopaedic Biomechanics. Dallas, TX, 2002.
72. Lim TH, Brebach GT, Renner SM, et al. Biomechanical evaluation of an injectable calcium phosphate cement for vertebroplasty. *Spine* 2002;27:1297-302.
73. Lin JT, Lane JM. Nonmedical management of osteoporosis. *Curr Opin Rheumatol* 2002;14:441-6.
74. Lindsay R, Nieves J, Formica C, et al. Randomised controlled study of effect of parathyroid hormone on vertebral-bone mass and fracture incidence among postmenopausal women on oestrogen with osteoporosis. *Lancet* 1997;350:550-5.
75. Lindsay R, Silverman SL, Cooper C, et al. Risk of new vertebral fracture in the year following a fracture. *Jama* 2001;285:320-3.
76. Lofman O, Larsson L, Toss G. Bone mineral density in diagnosis of osteoporosis: reference population, definition of peak bone mass, and measured site determine prevalence. *J Clin Densitom* 2000;3:177-86.
77. Martin H, Werner J, Andresen R, et al. Noninvasive assessment of stiffness and failure load of human vertebrae from CT-data. *Biomed. Technik* 1998;43:83-8.

78. Martin JB, Jean B, Sugi K, et al. Vertebroplasty: clinical experience and follow-up results. *Bone* 1999;25:11S-5S.
79. Mathis JM, Barr JD, Belkoff SM, et al. Percutaneous vertebroplasty: a developing standard of care for vertebral compression fractures. *AJNR Am J Neuroradiol* 2001;22:373-81.
80. Mathis JM, Petri M, Naff N. Percutaneous vertebroplasty treatment of steroid-induced osteoporotic compression fractures. *Arthritis Rheum* 1998;41:171-5.
81. Mazess RB, Barden, H.S., Drinka, P.J., Bauwens, S.F., Orwoll, E.S. and Bell, N.H. Influence of age and body weight on spine and femur bone mineral density in U.S. white men. *J. Bone Min. Res.* 1990;5:645-52.
82. Melick HGhv. Deformation and failure of polymer glasses. Eindhoven: Technische Universiteit Eindhoven, 2002.
83. Melton LJ, 3rd. How many women have osteoporosis now? *J Bone Miner Res* 1995;10:175-7.
84. Molloy S, Mathis JM, Belkoff SM. The effect of vertebral body percentage fill on mechanical behavior during percutaneous vertebroplasty. *Spine* 2003;28:1549-54.
85. Morgan EF, Yeh OC, Keaveny TM. Damage in trabecular bone at small strains. *Eur J Morphol* 2005;42:13-21.
86. Murphy KJ, Deramond H. Percutaneous vertebroplasty in benign and malignant disease. *Neuroimaging Clin N Am* 2000;10:535-45.
87. Murphy KJ, Lin DD. Vertebroplasty: a simple solution to a difficult problem. *J Clin Densitom* 2001;4:189-97.
88. National Institutes of Health: Osteoporosis and Related Bone Disease ~ National Resource Center. 2006. Available at: www.osteo.org.
89. National Osteoporosis Foundation. 2006. Available at: www.nof.org.
90. Newton-John HF, Morgan DB. The loss of bone with age, osteoporosis, and fractures. *Clin Orthop* 1970;71:229-52.
91. Niebur GL, Yuen JC, Hsia AC, et al. Convergence behavior of high-resolution finite element models of trabecular bone. *J Biomech Eng* 1999;121:629-35.
92. Orthovita. 2006. Available at: www.orthovita.com.

93. Patwardhan AG, Havey RM, Ghanayem AJ, et al. Load-carrying capacity of the human cervical spine in compression is increased under a follower load. *Spine* 2000;25:1548-54.
94. Patwardhan AG, Havey RM, Meade KP, et al. A follower load increases the load-carrying capacity of the lumbar spine in compression. *Spine* 1999;24:1003-9.
95. Patwardhan AG, Meade KP, Lee B. A frontal plane model of the lumbar spine subjected to a follower load: implications for the role of muscles. *J Biomech Eng* 2001;123:212-7.
96. Polikeit A, Nolte LP, Ferguson SJ. The effect of cement augmentation on the load transfer in an osteoporotic functional spinal unit: finite-element analysis. *Spine* 2003;28:991-6.
97. Pollintine P, Dolan P, Tobias JH, et al. Intervertebral disc degeneration can lead to "stress-shielding" of the anterior vertebral body: a cause of osteoporotic vertebral fracture? *Spine* 2004;29:774-82.
98. Rapado A. General management of vertebral fractures. *Bone* 1996;18:191S-6S.
99. Ray NF, Chan JK, Thamer M, et al. Medical expenditures for the treatment of osteoporotic fractures in the United States in 1995: report from the National Osteoporosis Foundation. *J Bone Miner Res* 1997;12:24-35.
100. Riggs BL, Melton LJ, 3rd. The worldwide problem of osteoporosis: insights afforded by epidemiology. *Bone* 1995;17:505S-11S.
101. Riggs BL, Wahner HW, Seeman E, et al. Changes in bone mineral density of the proximal femur and spine with aging. Differences between the postmenopausal and senile osteoporosis syndromes. *J Clin Invest* 1982;70:716-23.
102. Rosen CJ, Bilezikian JP. Clinical review 123: Anabolic therapy for osteoporosis. *J Clin Endocrinol Metab* 2001;86:957-64.
103. Ross PD, Davis, J.W., Epstein, R.S. and Wasnich, R.D. Pre-existing fractures and bone mass predict vertebral fracture incidence in women. *Ann. Intern. Med.* 1991;114:919-23.
104. San Millan Ruiz D, Burkhardt K, Jean B, et al. Pathology findings with acrylic implants. *Bone* 1999;25:85S-90S.
105. Shipman AJ, Guy GW, Smith I, et al. Vertebral bone mineral density, content and area in 8789 normal women aged 33-73 years who have never had hormone replacement therapy. *Osteoporos Int* 1999;9:420-6.

106. Silva MJ, Keaveny TM, Hayes WC. Computed tomography-based finite element analysis predicts failure loads and fracture patterns for vertebral sections. *J Orthop Res* 1998;16:300-8.
107. Silva MJ, Wang C, Keaveny TM, et al. Direct and computed tomography thickness measurements of the human, lumbar vertebral shell and endplate. *Bone* 1994;15:409-14.
108. Singer K, Edmondston S, Day R, et al. Prediction of thoracic and lumbar vertebral body compressive strength: correlations with bone mineral density and vertebral region. *Bone* 1995;17:167-74.
109. Sun K, Liebschner MA. Biomechanics of prophylactic vertebral reinforcement. *Spine* 2004;29:1428-35; discussssion 35.
110. Sun K, Liebschner MAK. Evolution of vertebroplasty: A biomechanical perspective. *Ann Biomed Engin* 2004;32:77-91.
111. Surgeon General. Bone health and osteoporosis: A report of the surgeon general., 2004.
112. Tawackoli W, Sun K, Liebschner M. Characterization of a human vertebral body collapse using a 6-DOF robotic system. American Society of Biomechanics 2004 Annual Meeting. Portland, Oregon, 2004.
113. Templeton A, Sun K, Fukshansky M, et al. Intra-operative inferior superior visualization of PMMA bolus in vertebroplasty. *Radiology* 2005;Submitted.
114. Tohmeh AG, Mathis JM, Fenton DC, et al. Biomechanical efficacy of unipedicular versus bipedicular vertebroplasty for the management of osteoporotic compression fractures. *Spine* 1999;24:1772-6.
115. Tosteson AN. Quality of life in the economic evaluation of osteoporosis prevention and treatment. *Spine* 1997;22:58S-62S.
116. Ulrich D, van Rietbergen B, Laib A, et al. The ability of three-dimensional structural indices to reflect mechanical aspects of trabecular bone. *Bone* 1999;25:55-60.
117. Uppin AA, Hirsch JA, Centenera LV, et al. Occurrence of new vertebral body fracture after percutaneous vertebroplasty in patients with osteoporosis. *Radiology* 2003;226:119-24.
118. Vesterby A, Mosekilde L, Gundersen HJ, et al. Biologically meaningful determinants of the in vitro strength of lumbar vertebrae. *Bone* 1991;12:219-24.

119. Villarraga ML, Bellezza AJ, Harrigan TP, et al. The biomechanical effects of kyphoplasty on treated and adjacent nontreated vertebral bodies. *J Spinal Disord Tech* 2005;18:84-91.
120. Visible Human Image Archiver and Viewer. 2006. Available at: <http://www.dhpc.adelaide.edu.au/projects/vishuman/>.
121. Watts NB, Harris ST, Genant HK. Treatment of painful osteoporotic vertebral fractures with percutaneous vertebroplasty or kyphoplasty. *Osteoporos Int* 2001;12:429-37.
122. Weill A, Chiras J, Simon JM, et al. Spinal metastases: indications for and results of percutaneous injection of acrylic surgical cement. *Radiology* 1996;199:241-7.
123. Wilson DR, Myers ER, Mathis JM, et al. Effect of augmentation on the mechanics of vertebral wedge fractures. *Spine* 2000;25:158-65.
124. Yang KH, King AI. Mechanism of facet load transmission as a hypothesis for low-back pain. *Spine* 1984;9:557-65.
125. Zoarski GH, Snow P, Olan WJ, et al. Percutaneous vertebroplasty for osteoporotic compression fractures: quantitative prospective evaluation of long-term outcomes. *J Vasc Interv Radiol* 2002;13:139-48.

APPENDIX

Vertebral reinforcement can be illustrated using a simplified block model of a sagittal cross-section of a vertebral body in order to explain the augmentation effect of vertebroplasty. Assuming symmetry with bipedicular vertebroplasty, only one side of the cross-section was analyzed, where the unshaded area represented trabecular bone while the shaded area is the introduced bone cement (Figure A-1).

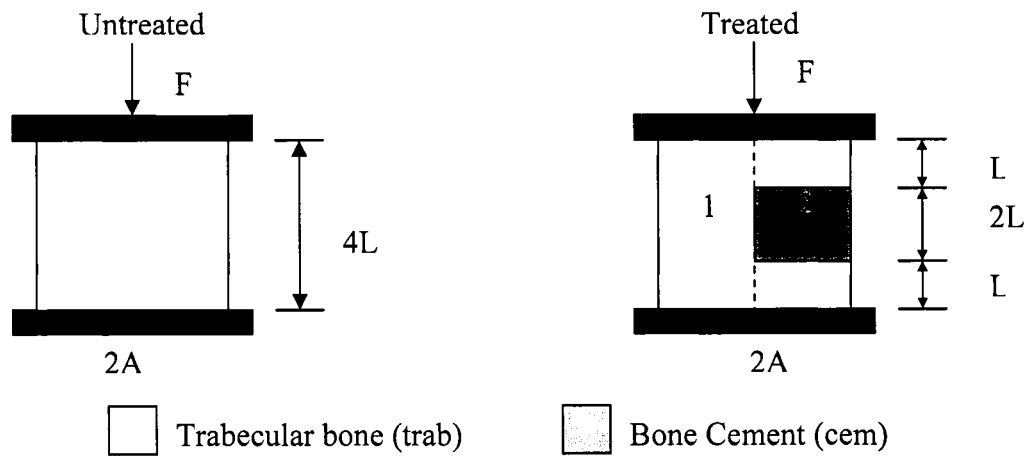


Figure A-1: Simplified block models of half of a sagittal cross-section of a vertebral body, with area $2A$ and total height $4L$, before and after implantation with a bone cement. A compression force of F was applied to both models.

For the untreated model, the overall stiffness of the vertebral body section is,

$$K_{T,\text{untreated}} = \frac{E_{\text{trab}} A}{2 L} \quad (\text{A.1})$$

where E_{trab} is the elastic modulus of the trabecular bone. For the treated model, the overall stiffness of the vertebral body section is,

$$\begin{aligned}
K_{T,\text{treated}} &= \frac{E_{\text{trab}} A}{4 L} + \frac{1}{\frac{L}{E_{\text{trab}} A} + \frac{2 L}{E_{\text{cem}} A} + \frac{L}{E_{\text{trab}} A}} \\
&= \frac{E_{\text{trab}} A}{4 L} \left(\frac{E_{\text{trab}} + 3 E_{\text{cem}}}{E_{\text{trab}} + E_{\text{cem}}} \right)
\end{aligned} \tag{A.2}$$

where E_{cem} is the elastic modulus of the bone cement. The overall stiffness of the treated vertebral body section can be expressed as a function of the overall stiffness of the untreated vertebral body,

$$\begin{aligned}
K_{T,\text{treated}} &= K_{T,\text{untreated}} \frac{1}{2} \left(\frac{E_{\text{trab}} + 3 E_{\text{cem}}}{E_{\text{trab}} + E_{\text{cem}}} \right) \\
\text{Or } \frac{K_{T,\text{treated}}}{K_{T,\text{untreated}}} &= \frac{\left(\frac{E_{\text{trab}}}{E_{\text{cem}}} + 3 \right)}{2 \left(\frac{E_{\text{trab}}}{E_{\text{cem}}} + 1 \right)}
\end{aligned} \tag{A.3}$$

With E_{trab} constant and by increasing the bone cement modulus, E_{cem} , the overall structural stiffness of the treated model also increased accordingly.

$$\begin{aligned}
E_{\text{cem}} < E_{\text{trab}}, \quad \frac{E_{\text{trab}}}{E_{\text{cem}}} > 1, \quad K_{T,\text{treated}} &< K_{T,\text{untreated}} \\
E_{\text{cem}} = E_{\text{trab}}, \quad \frac{E_{\text{trab}}}{E_{\text{cem}}} &= 1, \quad K_{T,\text{treated}} = K_{T,\text{untreated}} \\
E_{\text{cem}} > E_{\text{trab}}, \quad \frac{E_{\text{trab}}}{E_{\text{cem}}} &< 1, \quad K_{T,\text{treated}} > K_{T,\text{untreated}}
\end{aligned} \tag{A.4}$$

The mechanism behind vertebral reinforcement is load transfer, which can be proven mathematically. The loads applied to each medial-lateral half of the total area, σ_1 and σ_2 , can be expressed by their elastic moduli, E_1 and E_2 .

$$\begin{aligned}
 \sigma_1 &= E_1 \varepsilon_1 = E_1 \varepsilon_{\text{total}} \\
 \sigma_2 &= E_2 \varepsilon_2 = E_2 \varepsilon_{\text{total}} \\
 \frac{\sigma_1}{\sigma_2} &= \frac{E_1}{E_2}
 \end{aligned} \tag{A.5}$$

where the total strain, $\varepsilon_{\text{total}}$, are the same for both areas (ε_1 and ε_2) under uniaxial compression. E_1 and E_2 are related to E_{trab} and E_{cem} by,

$$\begin{aligned}
 E_1 &= E_{\text{trab}} \\
 E_2 &= \frac{2 E_{\text{trab}} E_{\text{cem}}}{E_{\text{trab}} + E_{\text{cem}}}
 \end{aligned} \tag{A.6}$$

Therefore, σ_1 and σ_2 in terms of E_{trab} and E_{cem} is,

$$\begin{aligned}
 \frac{\sigma_1}{\sigma_2} &= \frac{E_{\text{trab}} + E_{\text{cem}}}{2 E_{\text{cem}}} \\
 \text{Or } \frac{\sigma_1}{\sigma_2} &= \frac{1}{2} \left(\frac{E_{\text{trab}}}{E_{\text{cem}}} + 1 \right)
 \end{aligned} \tag{A.7}$$

With E_{trab} constant and by increasing the bone cement modulus, E_{cem} , more of the load applied is shifted towards area 2 where the stiffer and stronger bone cement is located and can carry higher loads. The trabecular bone immediately above and below the cement also bear the higher loads even though they are weaker than the bone cement. As a result, they experience higher stresses compared to trabecular bone in other areas.

$$\begin{aligned}
 E_{\text{cem}} < E_{\text{trab}}, \quad &\frac{E_{\text{trab}}}{E_{\text{cem}}} > 1, \quad \sigma_1 > \sigma_2 \\
 E_{\text{cem}} = E_{\text{trab}}, \quad &\frac{E_{\text{trab}}}{E_{\text{cem}}} = 1, \quad \sigma_1 = \sigma_2 \\
 E_{\text{cem}} > E_{\text{trab}}, \quad &\frac{E_{\text{trab}}}{E_{\text{cem}}} < 1, \quad \sigma_1 < \sigma_2
 \end{aligned} \tag{A.8}$$

Therefore, the mechanism behind the augmentation effect of the elastic modulus of the implanted bone cement on the overall stiffness and strength of the treated vertebral

body is the shift in the load distribution between the cement and the trabecular bone. The load transfer mechanism is also the cause of the high stress concentrations in the trabecular bone directly above and below the bone cement.